

An Advanced Model of Coal Devolatilization Based on Chemical Structure

A Thesis
Presented to the
Department of Chemical Engineering
Brigham Young University

In Partial Fulfillment
of the Requirement for the Degree
Master of Science

Dominic B. Genetti
April 1999

BRIGHAM YOUNG UNIVERSITY

GRADUATE COMMITTEE APPROVAL

of a thesis submitted by

Dominic B. Genetti

This thesis has been read by each member of the following committee and by majority vote has been found to be satisfactory.

Date

Thomas H. Fletcher, Chair

Date

Ronald J. Pugmire

Date

John N. Harb

BRIGHAM YOUNG UNIVERSITY

As chair of the candidate's graduate committee, I have read the thesis of Dominic B. Genetti in its final form and have found that (1) its format, citations, and bibliographical style are consistent and acceptable and fulfill the university and department style requirements; (2) its illustrative materials including figures, tables, and charts are in place; and (3) the final manuscript is satisfactory to the graduate committee and is ready for submission to the university library.

Date

Thomas H. Fletcher
Chair, Graduate Committee

Approved for the Department

Kenneth A. Solen
Department Chair

Approved for the College

Douglas M. Chabries
Dean, College of Engineering and Technology

ABSTRACT

An Advanced Model of Coal Devolatilization Based on Chemical Structure

Dominic B. Genetti

Department of Chemical Engineering

Master of Science

A model that predicts the quantity and form of nitrogen released during coal devolatilization has been developed and coupled with the Chemical Percolation Devolatilization (CPD) model. Based on the Chemical Structure of coal, the model predicts the fraction of coal nitrogen evolved with the tar and, subsequently, released as HCN at sufficiently high temperatures during primary devolatilization. The volatile nitrogen release model also predicts the nitrogen content of the char. This work represents the first time that a volatile nitrogen release model has been developed based on the chemical structure of coal as determined by ^{13}C NMR spectroscopy. It also represents the first time that a volatile nitrogen model has been validated by comparing model predictions with the chemical structure of char (as well as with light gas and tar yields). Predictions of nitrogen release during devolatilization compared well with nitrogen release measurements from various coals and pyrolysis conditions.

In order to make the CPD model more generally applicable, a *non-linear* correlation was developed that predicts the chemical structure parameters of both U.S. and non-U.S. coals generally measured by ^{13}C NMR spectroscopy. The chemical structure parameters correlated include: (i) the average molecular weight per side chain (M); (ii) the average molecular weight per aromatic cluster (M_{cl}); (iii) the ratio of bridges to total attachments (p_0); and (iv) the total attachments per cluster ($+I$). The correlation is based on ultimate and proximate analysis, which are generally known for most coals. ^{13}C NMR data from 30 coals were used to develop this correlation. The correlation was used to estimate the chemical structure parameters generally obtained directly from ^{13}C NMR measurements, and then applied to coal devolatilization predictions using the CPD model. The predicted tar and total volatiles yields compared well with measured yields for most coals.

In addition, a correlation of light gas pyrolysis product composition was developed based on coal type and the extent of light gas release. Estimations of light gas composition using the correlation compared well with measured light gas compositions from low and high heating rate pyrolysis experiments.

The nitrogen release model, ^{13}C NMR correlation, and light gas composition correlation have been coupled with the Chemical Percolation Devolatilization (CPD) model. These modifications enhance the industrial applicability of the CPD model. It is anticipated that the modified CPD model will be coupled with comprehensive combustion codes, and therefore may help screen new low NO_x technology.

ACKNOWLEDGMENTS

I would like to express gratitude to Dr. Thomas H. Fletcher for consistent and useful advice and support throughout my undergraduate and graduate career at Brigham Young University. I have learned a great deal from him academically and from his example. I would like to thank Dr. Ronald Pugmire and Dr. Mark Solum of the University of Utah for their contributions of NMR data and technical advice. I am also grateful for the funding that was received from the Advanced Combustion Engineering Research Center and from the Department of Energy, grant number DE-FG22-95PC95215.

I would like to thank Mary Goodman, Paul Goodman, and Michael Busse for their assistance in performing experiments and analyses. I would also like to thank Eric Hambly, Steve Perry, Alex Brown, and Josh Wong for many useful discussions about coal pyrolysis and other topics.

I would like to thank my Mother, Sandra L. Genetti, and my parents by marriage, Ross and Debbie Miller, for their support and encouragement. I would also like to thank my late Father, William E. Genetti, who was a professor of Chemical Engineering for 22 years. His memory has been a constant source of inspiration in my life. I would like to recognize as well each of my five siblings, Berlin, Opal, Andy, Vincent and Teresa, for their support. Particular thanks should be given to Berlin, who is also a Chemical Engineer, for many useful conversations about this project. Finally, I would like to express special gratitude to my wife, Mckenzie, for her love, support, and encouragement.

Table of Contents

List of Figures.....	xi
List of Tables.....	xvii
Nomenclature.....	xix
1. Introduction.....	1
2. Background.....	5
Coal Structure.....	5
Nitrogen in Coal.....	8
Coal Pyrolysis.....	8
Nitrogen Release During Pyrolysis.....	11
Modeling Devolatilization.....	15
The FG-DVC Model.....	16
The FLASHCHAIN Model.....	17
The CPD Model.....	17
Modeling Volatile Nitrogen Release.....	18
Summary.....	21
3. Objectives and Approach.....	23
4. ¹³ C NMR Correlation.....	25
Evaluation of Linear Correlations.....	26
Correlation Development.....	27
Experimental Data.....	27
Procedure.....	27
Example Case for p_0	31
Final NMR Correlation.....	32

Estimation of the Fraction of Stable Bridges.....	37
Implications of ¹³ C NMR Correlation.....	38
Application of Correlated Parameters in CPD Model.....	40
Discussion of NMR Correlation.....	43
5. Modeling Volatile Nitrogen Release.....	45
Evaluation of Nitrogen Release Data.....	45
Rank and Temperature Dependence.....	48
Time Dependence.....	50
Model Theory and Development.....	52
Light Gas Nitrogen.....	53
Nitrogen Released with Tar.....	56
Fraction of Stable Nitrogen.....	56
Nitrogen Model Parameters.....	57
Application of Nitrogen Model.....	59
Description of Test Cases.....	59
Comparisons with Data from Fletcher and Hardesty.....	60
Comparisons with Data Reported by Chen.....	64
Comparisons with Data Reported by Hambly and Genetti.....	66
Discussion of Volatile Nitrogen Release Model.....	70
6. Predicting Light Gas Composition.....	73
Background.....	73
Analysis of Light Gas Release Data.....	75
TG-FTIR Experiments.....	75
Light Gas Data From a Radiantly Heated Reactor.....	76
Pyrolysis Experiments at Various Heating Rates.....	76
Conclusions from Data Analysis.....	77
Correlation of Light Gas Composition.....	77

Interpolation for Coal Type.....	78
Interpolation for Extent of Light Gas Release.....	79
Application of Light Gas Correlation.....	81
Discussion of Light Gas Correlation.....	84
7. Conclusions.....	87
Correlations to Estimate Coal Structure.....	87
Volatile Nitrogen Release Model.....	88
Light Gas Submodel.....	89
Impact of this Work.....	90
8. Recommendations for Future Work.....	91
NMR Correlation.....	91
Volatile Nitrogen Modeling.....	91
Light Gas Correlations.....	92
References.....	93
Appendix A: Correlated Structural Parameters.....	99
Appendix B: Sample CPD Model Input Files.....	101
Appendix C: Sample CPD Model Input File.....	105
Appendix D: Tabulated Mass and Tar Release.....	107
Appendix E: Nitrogen Release Comparisons.....	109
N_{site} and N_{char} Comparisons.....	110
Mass and Nitrogen Release Comparisons.....	114
Appendix F: Particle Temperature Profiles of Radiantly Heated Reactor.....	123
Appendix G: Coal Pyrolyzed in BYU FFB.....	129
Appendix H: Velocity and Temperature Profiles of FFB.....	131
Appendix I: Analysis of Light Gas Data.....	133
Introduction.....	133
TG-FTIR Analysis of Pyrolysis Products.....	134

Light Gas Data from a Radiantly Heated Reactor.....	140
Light Gas Data from Currie Point Pyrolyzer.....	147
Conclusions.....	150
Appendix J: Light Gas Look-Up Table.....	151

List of Figures

Figure 2.1.	A hypothetical coal macromolecule.....	6
Figure 2.2.	Hypothetical coal pyrolysis reaction.....	9
Figure 2.3.	Tar and total volatile yields from devolatilization as a function of the carbon content of the parent coal.....	10
Figure 2.4.	Nitrogen volatiles release versus rank.....	13
Figure 2.5.	Distribution of nitrogen volatiles versus rank.....	14
Figure 4.1.	Coalification chart of 30 coals used in NMR correlation.....	31
Figure 4.2.	Plots of chemical structure parameters versus elemental composition and ASTM volatile matter content.....	33
Figure 4.3.	Plots of estimated chemical structure parameters versus the parameters derived from ^{13}C NMR analyses.....	36
Figure 4.4.	Comparison of model CPD predictions with measured mass release.....	41
Figure 4.5.	Comparison of CPD model predictions with measured mass and tar release	43
Figure 5.1.	Hypothetical nitrogen release steps.....	46
Figure 5.2.	Comparison of N_{site} decay in various chars during pyrolysis.....	49
Figure 5.3.	Comparison of N_{site} decay in various chars during pyrolysis.....	49
Figure 5.4.	Comparison of N_{site} decay in various chars during pyrolysis at two heating rates.....	51

Figure 5.5.	Comparison of total mass release from various coals during pyrolysis at two heating rates.....	51
Figure 5.6.	Comparison of predicted and measured N_{site} and N_{char} of versus time during pyrolysis.....	62
Figure 5.7.	Comparison of predicted and measured N_{site} and N_{char} of versus time during pyrolysis.....	62
Figure 5.8.	Comparison of predicted and measured mass and nitrogen release versus time during pyrolysis.....	63
Figure 5.9.	Comparison of predicted and measured mass and nitrogen release versus time during pyrolysis.....	63
Figure 5.10.	Comparison of predicted and measured mass and nitrogen release versus rank.....	64
Figure 5.11.	Comparison of predicted and measured tar nitrogen and light gas nitrogen release versus time.....	65
Figure 5.12.	Comparison of predicted and measured tar nitrogen and light gas nitrogen release versus time.....	66
Figure 5.13.	Predicted char nitrogen content versus measured char nitrogen content	67
Figure 5.14.	Comparison of predicted and measured mass and nitrogen release versus rank.....	67
Figure 5.15.	Comparison of predicted and measured mass release versus rank.....	69
Figure 5.16.	Comparison of predicted and measured nitrogen release versus rank.....	69
Figure 6.1.	Interpolation mesh on a coalification chart.....	80
Figure 6.2.	Comparison of predicted and measured light gas composition versus rank.....	82

Figure 6.3.	Comparison of predicted and measured light gas composition versus rank.....	83
Figure E.1.	Comparison of predicted and measured values of N_{char}	110
Figure E.2.	Comparison of predicted and measured values of N_{site} and N_{char}	110
Figure E.3.	Comparison of predicted and measured values of N_{char}	111
Figure E.4.	Comparison of predicted and measured values of N_{site} and N_{char}	111
Figure E.5.	Comparison of predicted and measured values of N_{char}	112
Figure E.6.	Comparison of predicted and measured values of N_{site} and N_{char}	112
Figure E.7.	Comparison of predicted and measured values of N_{site} and N_{char}	113
Figure E.8.	Comparison of predicted and measured values of N_{site} and N_{char}	113
Figure E.9.	Comparison of predicted and measured mass and nitrogen release.....	114
Figure E.10.	Comparison of predicted and measured mass and nitrogen release.....	114
Figure E.11.	Comparison of predicted and measured mass and nitrogen release.....	114
Figure E.12.	Comparison of predicted and measured mass and nitrogen release.....	114
Figure E.13.	Comparison of predicted and measured mass and nitrogen release.....	116
Figure E.14.	Comparison of predicted and measured mass and nitrogen release.....	116
Figure E.15.	Comparison of predicted and measured mass and nitrogen release.....	117
Figure E.16.	Comparison of predicted and measured mass and nitrogen release.....	117
Figure E.17.	Comparison of predicted and measured mass and nitrogen release versus rank.....	118
Figure E.18.	Comparison of predicted and measured mass and nitrogen release versus rank.....	119

Figure E.19.	Comparison of predicted and measured mass and tar release versus time.....	119
Figure E.20.	Comparison of predicted and measured mass and tar release versus time.....	120
Figure E.21.	Comparison of predicted and measured mass and tar release versus time.....	120
Figure E.22.	Comparison of predicted and measured mass and tar release versus time.....	121
Figure E.23.	Comparison of predicted and measured total and light gas nitrogen release versus time.....	121
Figure E.24.	Comparison of predicted and measured total and light gas nitrogen release versus time.....	122
Figure I.1.	Light gas release of Argonne Premium coals.....	135
Figure I.2.	H ₂ O content of light gas pyrolysis products.....	137
Figure I.3.	CO ₂ content of light gas pyrolysis products.....	137
Figure I.4.	CO content of light gas pyrolysis products.....	137
Figure I.5.	CH ₄ content of light gas pyrolysis products.....	138
Figure I.6.	C ₂ H ₄ content of light gas pyrolysis products.....	139
Figure I.7.	Light gas release of PETC coals.....	142
Figure I.8.	H ₂ O content of light gas pyrolysis products.....	143
Figure I.9.	CO ₂ content of light gas pyrolysis products.....	143
Figure I.10.	CO content of light gas pyrolysis products.....	144
Figure I.11.	CH ₄ content of light gas pyrolysis products.....	145
Figure I.12.	C ₂ H ₄ content of light gas pyrolysis products.....	146

Figure I.13.	Content of other light gas pyrolysis products.....	146
Figure I.14.	Light gas release of various coals versus rank.....	147
Figure I.15.	H ₂ O, CO ₂ , and CO content of light gas pyrolysis products.....	148
Figure I.16.	H ₂ and CH ₄ content of light gas pyrolysis products.....	148
Figure I.17.	C ₂ Hydrocarbon content of light gas pyrolysis products.....	149
Figure I.18.	C ₃ Hydrocarbon content of light gas pyrolysis products.....	149

List of Tables

Table 4.1.	List of Coals Used in ^{13}C NMR Correlation.....	28
Table 4.2.	Properties of Coals Used in ^{13}C NMR Correlation.....	29
Table 4.3.	^{13}C NMR Chemical Structure Parameters of Coals Used in Correlation.....	30
Table 4.4.	Outliers Removed From ^{13}C NMR Correlation.....	34
Table 4.5.	Coefficients of Modified Quadratic Correlations.....	35
Table 4.6.	Range of Values Used in ^{13}C NMR Correlations.....	39
Table 4.7.	Properties of Coals Studied by Xu and Tomita.....	42
Table 5.1.	List of Pyrolysis Experiments Examined for Nitrogen Release Trends....	48
Table 5.2.	Rate Parameters Used in Nitrogen Model.....	58
Table 5.3.	Description of Data Used to Validate Nitrogen Release Model.....	60
Table 6.1.	Kinetic Rate Coefficients in FG Submodel.....	74
Table 6.2.	Composition and Elemental Ratios of Coals Used to Create Triangular Interpolation Mesh.....	79
Table A.1.	Correlated Chemical Structure of Coals Used in ^{13}C NMR Correlation....	99
Table D.1.	Predicted and Measured Mass and Tar Yields.....	107
Table F.1.	Particle Temperature Profile of 56 ms Condition.....	123
Table F.2.	Particle Temperature Profile of 61 ms Condition.....	124
Table F.3.	Particle Temperature Profile of 66 ms Condition.....	124

Table F.4.	Particle Temperature Profile of 72 ms Condition.....	125
Table F.5.	Particle Temperature Profile of 77 ms Condition.....	125
Table F.6.	Particle Temperature Profile of 83 ms Condition.....	126
Table F.7.	Particle Temperature Profile of 87 ms Condition.....	126
Table F.8.	Particle Temperature Profile of 89 ms Condition.....	127
Table G.1.	Elemental Composition of Coals Pyrolyzed in FFB.....	129
Table H.1.	Gas Velocity Profile of 18 ms FFB Condition.....	131
Table H.2.	Gas Temperature Profile of 18 ms FFB Condition.....	131
Table H.3.	Gas Velocity Profile of 78 ms FFB Condition.....	132
Table H.4.	Gas Temperature Profile of 78 ms FFB Condition.....	132
Table I.1.	Moisture Content of Argonne Premium Coals.....	135
Table I.2.	Ultimate Analysis of Coals Studied by Chen.....	141
Table J.1.	Reference Coals Used in Look-Up Table.....	151
Table J.2.	Extent of Total Light Gas Release.....	152
Table J.3.	Mass Fraction H ₂ O.....	152
Table J.4.	Mass Fraction CO ₂	153
Table J.5.	Mass Fraction CH ₄	153
Table J.6.	Mass Fraction CO.....	154

Nomenclature

AFR	Advanced Fuel Research
ACERC	Advanced Combustion Engineering Research Center
ANL	Argonne National Laboratories
ASTM	American Society of Testing and Materials
an	anthracite coal
B.L.	bridges and loops per cluster
C_{Cl}	aromatic carbons per cluster
c_0	fraction of bridges that are stable
CPD	Chemical Percolation Devolatilization
daf	dry, ash free
DECS	Department of Energy Coal Sample
E	activation energy
f_a	total percent of sp^2 -hybridized carbon
f_a^A	percent of aromatic carbon
f_a^B	percent of bridgehead aromatic carbon
f_a^C	percent of carbonyl carbon
f_a^H	percent of aromatic carbon with proton attachment
f_a^N	percent of nonprotonated aromatic carbon
f_a^P	percent of phenolic or phenolic ether aromatic carbon
f_a^S	percent of alkylated aromatic carbon
f_{al}	total percent aliphatic carbon
f_{al}^*	percent aliphatic carbon that is nonprotonated or CH_3
f_{al}^H	percent aliphatic carbon that is CH or CH_2

f_{al}^O	percent aliphatic carbon that is bound to oxygen
FFB	methane air flat-flame burner
FG	functional group
FTIR	fourier transform infrared spectroscopy
f_{char}	char yield
f_{st}	fraction of stable nitrogen
gas_{nit}	fraction of coal nitrogen released as light gas
H/C	hydrogen to carbon molar ratio
HCN	hydrogen cyanide
hvAb	high volatile A bituminous coal
hvBb	high volatile B bituminous coal
hvCb	high volatile C bituminous coal
ICP	inductively coupled plasma
K	Kelvin
k_{HCN}	first order rate constant for HCN release in FLASHCHAIN
ligA	lignite A
lvb	low volatile bituminous coal
m_{coal}	mass of original coal
m_{char}	char yield
mvb	medium volatile bituminous coal
M_{Cl}	average molecular weight per cluster
M	average molecular weight of the cluster attachments
M_{site}	average molecular weight of the aromatic sites
	the change in the average moles of nitrogen per mole of aromatic clusters in FLASHCHAIN
N_{coal}	daf mass fraction of nitrogen in parent coal
N_{char}	daf mass fraction of nitrogen in char

N_{site}	daf mass fraction of nitrogen on an aromatic site basis
N_{tar}	daf mass fraction of nitrogen in tar
NCSS	Number Cruncher Statistical Software
NMR	nuclear magnetic resonance spectroscopy
NO _x	nitrogen oxides (NO, NO ₂ and N ₂ O)
NR	fraction of original nitrogen released during pyrolysis
O/C	oxygen to carbon molar ratio
p_0	fraction of attachments that are bridges
PCGC - 3	Pulverized Coal Gasification and Combustion code (3 dimensions)
PETC	Pittsburgh Energy and Technology Center
PSOC	Penn State Office of Coal Research
py-MS	pyrolysis mass spectroscopy
r^2	coefficient of determination
R	universal gas constant
s	second
sa	semi-anthracite coal
subA	subbituminous A coal
subB	subbituminous B coal
subC	subbituminous C coal
T	temperature
t	time
tar_{nit}	mass on nitrogen transported with tar
TG-FTIR	thermogravimetric fourier transform infrared spectroscopy
XPS	X-ray photoelectron spectroscopy
Y_{HCN}	molar yield of HCN
	refers to a differential change

$+1$	total attachments per cluster
	standard deviation
	fraction of initial attachments that are side chains
l	fraction of labile bridges
x	inverse of area under normal distribution curve
b	fraction of bridgehead carbons
X_C	daf percent carbon in parent coal
X_H	daf percent hydrogen in parent coal
X_N	daf percent nitrogen in parent coal
X_O	daf percent oxygen in parent coal
X_{VM}	ASTM volatile matter content of parent coal expressed as a percent
X_{gas}	the ratio of light gas released to the maximum light gas yield

1. Introduction

As environmental regulations on industrial emissions have increased, the focus of coal research has shifted more and more to understanding and reducing harmful pollutants such as nitrogen oxides (NO_x). During coal combustion, the majority of nitrogen oxide pollution comes from nitrogen found in the coal.^{1, 2} Nitrogen in the coal is released in two stages during the combustion of coal. During the first stage, known as devolatilization (or pyrolysis), nitrogen is released with tar or light gas. Tar is defined as the volatiles released that condense at room temperature. Nitrogen released during devolatilization is referred to as *volatile* nitrogen. As the tar and light gases combust in the presence of O_2 , the nitrogen may be oxidized to form NO_x pollutants. The second stage of nitrogen release occurs during char oxidation. Char is the solid portion of coal remaining after the tar and light gas species have been released during devolatilization. As the char combusts heterogeneously, nitrogen bound in the char is oxidized directly to NO_x . It has been shown that *volatile* nitrogen may contribute as much as 60 to 80 percent of the total NO_x produced during coal combustion.³

Common methods of reducing NO_x emissions during coal combustion include staged combustion and selective catalytic and selective non-catalytic reduction using ammonia or urea. The objective of these methods is to assure that nitrogen is emitted as N_2 rather than NO_x . Staged combustors have achieved moderate success in reducing the amount of *volatile* nitrogen that is converted to NO_x . However, because the nitrogen in the char is released by heterogeneous oxidation, staged combustion methods have little effect on NO_x formed from nitrogen in the char.² Although selective catalytic and non-catalytic reduction can be very effective in reducing NO_x species to N_2 , selective reduction is a relatively expensive alternative. Recently, advanced staged combustors,

known as low-NO_x burners, have been developed. Low-NO_x burners reduce NO_x emissions by creating locally fuel-rich regions with sufficient residence time and appropriate temperatures in which *volatile* nitrogen is converted to N₂ rather than NO_x. Low-NO_x burners have the potential to significantly reduce NO_x emissions from coal combustion facilities and are currently the most economically favorable alternative.

Current low-NO_x burners are designed with empirical relationships to describe nitrogen evolution during devolatilization. In order to design more efficient low-NO_x burners it is important to understand the chemistry and reaction mechanisms of devolatilization and *volatile* nitrogen release. Of equal importance is the development of accurate predictive models of devolatilization and nitrogen release that can be used in the design of more effective low-NO_x burners.

The primary objective of this study was to develop a model which predicts the amount and form of nitrogen released during primary devolatilization based on the chemical structure of coal, and to incorporate the model into a devolatilization model (the Chemical Percolation Devolatilization Model).⁴ Existing experimental data on nitrogen release and the chemical structure of coal, char, and tar were used in developing this nitrogen release model. This work represents the first volatile nitrogen release model based on the chemical structure of coal as measured directly by ¹³C NMR analyses. This research also represents the first time that nitrogen model predictions have been compared to the chemical structure of char.

This study also sought to enhance the industrial usefulness of the CPD model. The accuracy of predicted tar and total volatiles yields was improved by developing an empirical relationship between c_0 , the initial fraction of char bridges, and the oxygen and carbon content of coal. Before this work, the applicability of the CPD model was limited by the availability of ¹³C NMR data on parent coals. At the start of this project, such NMR data were only available for about 15 coals. Therefore, in order to increase the applicability of the CPD model to many coals, a correlation was developed between

chemical structural input parameters, normally obtained by ^{13}C NMR analysis, and the elemental composition and volatile matter content of coal. Also, an algorithm was developed and coupled with the CPD model that distributes the light gas released during devolatilization into CO , CO_2 , CH_4 , H_2O , and other light hydrocarbons. It is expected that with these additional features, the CPD model will be very useful in improving low- NO_x burner technology and in other coal combustion modeling applications.

2. Background

The background given here describes the current state of coal pyrolysis research. Special emphasis is given to coal pyrolysis modeling and the release of nitrogen during pyrolysis. First, a brief general description of the current understanding of the structure of coal will be given, including a discussion on the structure of nitrogen forms in coal. The process of coal pyrolysis will be addressed, and the composition of light gas released during pyrolysis will be examined. Several advanced pyrolysis models that have been developed in the past decade will be discussed, including approaches taken to predict nitrogen release. Finally, a summary of pyrolysis modeling will be given that addresses the industrial importance of this study.

Coal Structure

Coal is thought to consist of (i) a large matrix of aromatic clusters connected by aliphatic bridges, (ii) aliphatic and carbonyl side chain attachments to the aromatic clusters, and (iii) some weakly bonded components sometimes referred to as the mobile phase.^{5, 6} The aromatic clusters consist largely of carbon, but also contain heteroatoms such as oxygen, sulfur and nitrogen. The bridges which connect the aromatic clusters are believed to be almost exclusively composed of aliphatic functional groups, but may also contain atoms such as oxygen and sulfur.^{7, 8} Bridges containing oxygen as ethers have relatively weak bond strengths. Some bridges, known as char links, consist of a single bond between aromatic clusters. Char links are thought to be relatively stable. Because bridges are composed of a wide variety of functional groups, there is a large distribution in bond strengths. Attachments to the aromatic clusters that do not “bridge” to another aromatic cluster are called side chains. The mobile phase consists of smaller molecular

structures that are not strongly bonded to the matrix.^{9, 10} Figure 2.1 is a schematic illustrating these important structural components of coal.

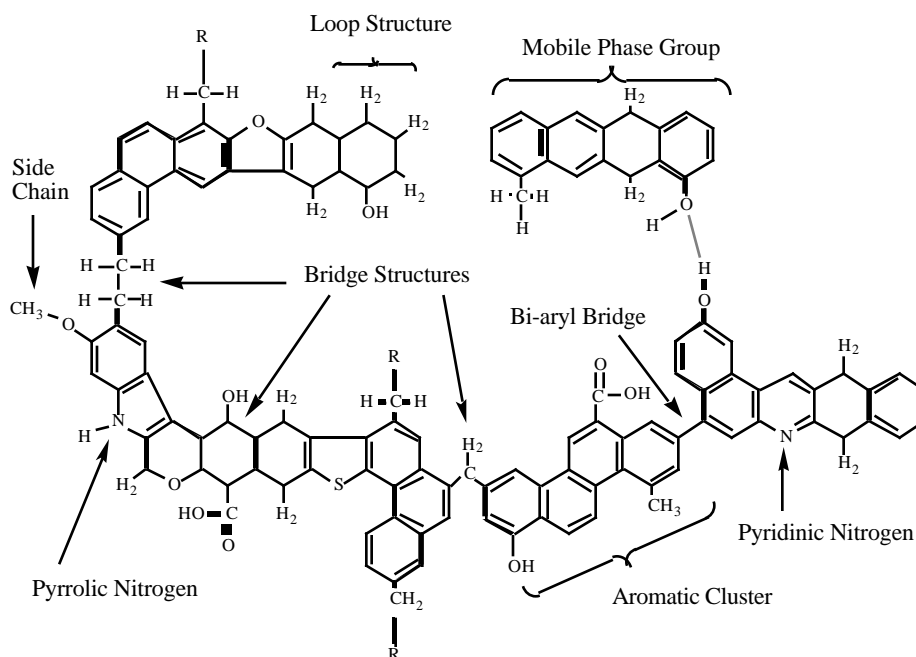


Figure 2.1. Schematic of hypothetical coal molecule. Modified from Solomon et al.¹¹

A fundamental knowledge of coal structure is important to fully understand and model the devolatilization and combustion behavior of coal. Due to the complex nature of coal, several different characterization techniques are commonly used to determine coal structure. Most coal characterization techniques, such as Pyrolysis Mass Spectroscopy and solvent extraction, either heat the coal or dissolve a portion of the coal with solvents, and then analyze the gas or liquid products. Since these techniques disrupt the network structure of the coal, the results are often a poor representation of the original coal structure. ¹³C NMR spectroscopy is one of the few non-destructive characterization techniques available to determine coal structure.

Solid-state ¹³C NMR spectroscopy has been shown to be an important tool in the characterization of coal structure. ¹³C NMR spectroscopy has been used to quantify the average carbon skeletal structure of a given coal with 12 parameters that describe the

aromatic and aliphatic regions of the coal matrix.^{12, 13} The value of f_a is the total fraction of aromatic, carboxyl and carbonyl carbons. This value is subdivided into f_a^C , which is the fraction of carbonyl and carboxyl carbons, and f_a' , which is the fraction of sp^2 -hybridized carbons present in aromatic rings. The value of f_a' is subdivided into protonated (f_a^H) and non-protonated (f_a^N) aromatic carbons. The non-protonated aromatic carbons are further subdivided into the fractions of phenolic (f_a^P), alkylated (f_a^S) and bridgehead (f_a^B) carbons. The fraction of aliphatic carbons is labeled f_{al} . This value is divided into the fraction of CH and CH₂ groups (f_{al}^H) and the fraction of CH₃ groups (f_{al}^*). The aliphatic carbons that are bonded to oxygen are labeled as f_{al}^O .

From the twelve structural parameters, combined with an empirical relationship between bridgehead carbons and aromatic carbons per cluster, a description of the lattice structure of coal can be obtained.¹² Some of the useful structural parameters determined from these analyses include: the number of carbons per cluster (C_{cl}), the number of attachments per cluster (coordination number, $+1$), the number of bridges and loops (B.L.), the ratio of bridges to total attachments (p_0), the average aromatic cluster molecular weight (M_{cl}), and the average side chain molecular weight (M).

¹³C NMR analyses of matching sets of coals, tars, and chars have been used to study the change in the chemical structure resulting from coal devolatilization.¹⁴ For example, Watt¹⁵ and Hambly¹⁶ performed pyrolysis experiments at a number of different conditions on six coals of various rank to provide matching sets of char and tar that were pyrolyzed to different degrees. ¹³C NMR analysis of these matching samples provided important data for comparison of the coals as a function of both rank and degree of pyrolysis. Coal lattice structure parameters derived from ¹³C NMR also provide important input parameters for coal conversion and combustion models.

¹³C NMR studies of coal are limited by the time and expense involved in performing the analyses. The fact that ¹³C NMR structural parameters have only been obtained for about 35 coals at the present time illustrates this weakness.

Nitrogen in Coal

Coal generally contains 1 to 2 percent nitrogen by weight.¹⁷ The nitrogen content is a weak function of coal type. Coals with about 85 wt % carbon seem to contain the largest amount of nitrogen.¹⁸ There seems to be a general consensus that nitrogen in coal is present primarily in two different heterocyclic forms: 5-membered (pyrrolic), and 6-membered (pyridinic) nitrogen functional groups (see Figure 2.1).^{15, 18-22} Some evidence also indicates the presence of a small amount of quaternary nitrogen functional groups.²⁰⁻²²

It has also been shown that 50 to 60% of the total coal nitrogen is in the form of pyrrolic nitrogen, while pyridinic nitrogen accounts for 30 to 40%.^{20, 21} Several studies have shown that the relative amounts of the different nitrogen functionalities found in coal vary slightly with rank.^{20, 21, 23} It appears that the relative amounts of pyridinic and pyrrolic nitrogen increase slightly with increasing coal rank corresponding to a decrease in the relative amount of quaternary nitrogen.

Coal Pyrolysis

The mechanisms and variables which control coal devolatilization are discussed in detail by Smith, et al.⁵ Only a brief description of coal devolatilization is given here. Devolatilization (or pyrolysis) is the first stage in coal combustion. Devolatilization occurs as the raw coal is heated in an inert or oxidizing atmosphere. As the temperature of the coal increases, the bridges linking the aromatic clusters break, resulting in finite-size fragments that are detached from the macromolecule.⁵

The bridges consist of a distribution of different types of functional groups, and the weakest bond strengths are broken first. The fragments are commonly referred to as metaplast. The metaplast then either (i) vaporizes and escapes the coal particle, or (ii) crosslinks back into the macromolecular structure. The metaplast which vaporizes consists mainly of the lower molecular weight fragments and becomes what is referred to

as tar. As stated earlier tar is defined as the gaseous pyrolysis products that condense at room temperature. The relationship between tar release and bridge scission is highly non-linear. Side chains and the broken bridge material are released as light gas in the form of light hydrocarbons and oxides. The portion of the coal particle remaining after devolatilization is called char. Figure 2.2 is a schematic of a hypothetical coal pyrolysis reaction.

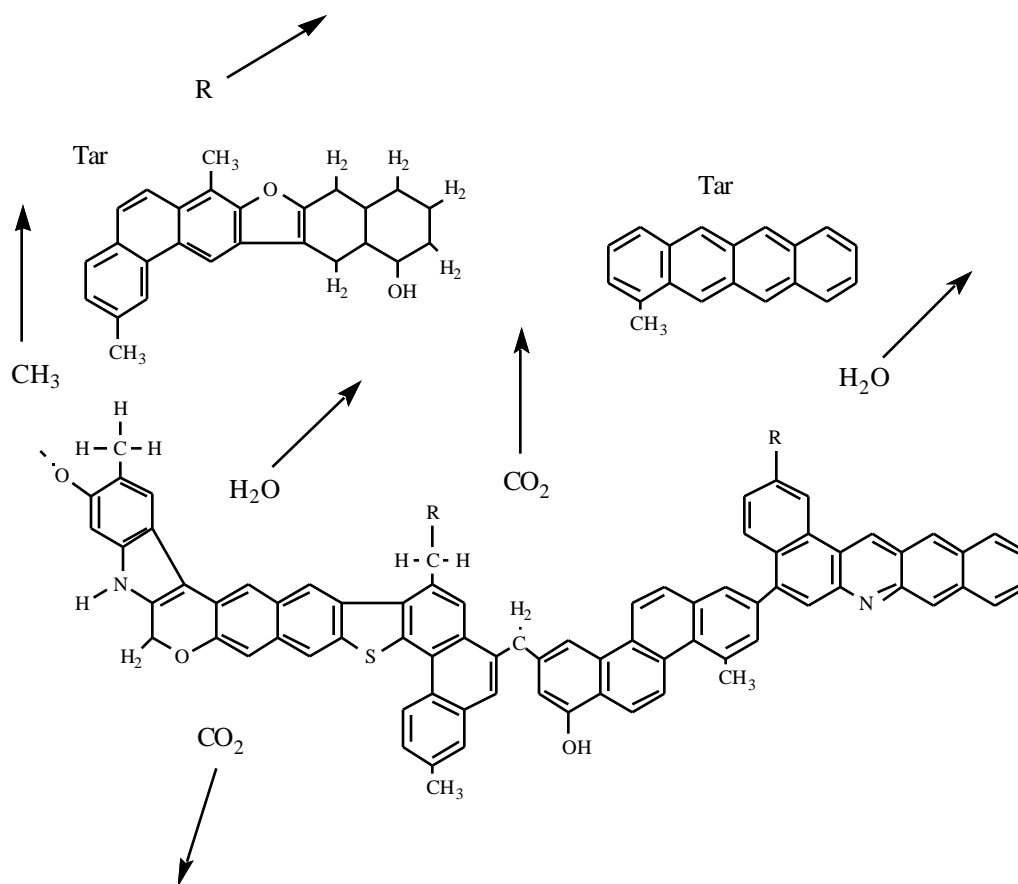


Figure 2.2. Schematic of pyrolysis reaction. Modified from Solomon et al.¹¹

The pyrolysis behavior of coal is affected by temperature, heating rate, pressure, particle size, and coal type among other variables.²⁴⁻²⁷ Higher mass release during devolatilization generally occurs at higher temperatures. As temperature increases, the

bridge and side chain breaking rates increase, more light gas is released, and more tar is released due to higher metaplast vapor pressures. The heating rate has the following two effects on devolatilization behavior: (i) as heating rate increases, the temperature at which volatiles are released increases; and (ii) generally, as heating rate increases, the overall volatiles yield increases.^{5, 26, 27} Higher pressures lead to lower overall mass release during devolatilization because of vapor pressure considerations.⁵

Devolatilization behavior is largely dependent on coal type.²⁸ Low rank coals (lignites and subbituminous coals) release a relatively large amount of light gases and less tar. Bituminous coals release much more tar than lower rank coals and moderate amounts of light gas. The highest rank coals release only small amounts of tar and even lower amounts of light gas. Figure 2.3 illustrates these trends where percent carbon in the coal is used as a rank indicator.

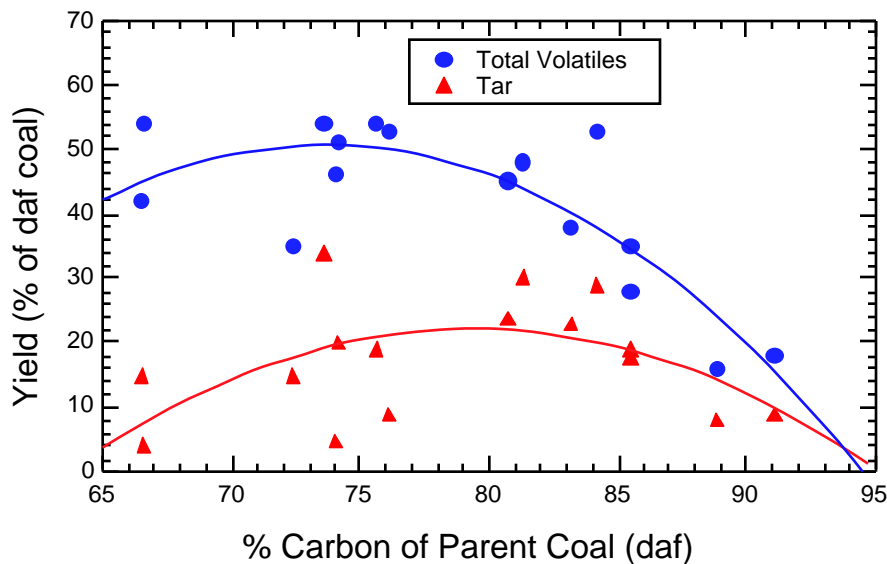


Figure 2.3. Volatiles yields from devolatilization experiments as a function of coal rank (adapted from Fletcher, et al.⁴) Solid lines are quadratic curve fits to the data, and are shown only for illustrative purposes.

Light gas released during devolatilization consists mainly of methane, carbon dioxide, carbon monoxide, and water.^{25, 27, 29-31} Other constituents include low

molecular weight hydrocarbons such as olefins, nitrogen species and sulfur species. Saxena studied light gas release at atmospheric pressures and low heating rates (1 K/sec).²⁷ Occluded carbon dioxide and methane were released at about 473 K. Above 473 K, condensation reactions resulted in the evolution of carbon dioxide and water. Between 473 K and 773 K, methane and small amounts of olefins began to evolve. Also in the range 473-773 K nitrogen structures and organic sulfur species began to decompose. Hydrogen began to evolve around 673 K. At higher temperatures (773-973 K) the volume of hydrogen, carbon dioxide, and methane increased relative to other hydrocarbon species.

In general, increasing the heating rate increases the temperature at which various gas species are evolved. Suuberg, et al.²⁵ studied the devolatilization behavior of a lignite at a heating rate of 1000 K/sec. Carbon dioxide evolution was observed to begin at about 723 K. Chemically formed water and carbon dioxide were evolved in the range of 773-973 K. Between 973 K and 1173 K, hydrogen and hydrocarbon gases were released. At higher temperatures the formation of additional carbon oxides were observed.

The composition of the light gas evolved during devolatilization is a function of coal rank.³¹ Light gas released from lignites contains a relatively large amount of carbon dioxide and carbon monoxide, but contains only a small amount of methane. Light gas evolved from bituminous coals during devolatilization contains a smaller fraction of carbon dioxide and carbon monoxide and a larger fraction of methane compared to light gas evolved from lignites. The variations in the species distribution of light gas as a function of rank is believed to be the result of variations in the composition of the aliphatic side chains.

Nitrogen Release During Pyrolysis

Baxter et al.¹ studied the relationship between N-release, carbon release, and total mass release during devolatilization and char oxidation of 15 coals. Baxter found that for

coals with low carbon content (or low rank coals) the rate of nitrogen release during early devolatilization is much less than the rate of total mass release. However, during late devolatilization and early oxidation, nitrogen is released at a faster rate than total mass is released. A similar, but more pronounced, trend was found when the rate of nitrogen release was compared to carbon release.

Coals with higher carbon content (higher rank) followed a different trend when compared with the release rates of carbon and total mass. Nitrogen release in high rank coals was faster compared to carbon and total mass release during devolatilization, with the ratios decreasing to about unity by the time oxidation began.¹

The observed trends of nitrogen release rates during devolatilization appear to be in good agreement with the nitrogen functional group studies mentioned earlier. Low rank coals generally have a large proportion of volatile, mostly aliphatic, attachments, bridges, and independent components.⁵ The aliphatic constituents are not believed to contain significant amounts of nitrogen. Higher rank coals, on the other hand, contain a relatively small amount of aliphatic material. This is in agreement with the relative nitrogen release trends for the low and higher rank coals. Since the aliphatic constituents are the most volatile part of the coal, they are released first with virtually no nitrogen. As the particles get hotter, the heterocyclic pyrrolic and pyridinic nitrogen functional groups begin to vaporize with the tar.

The nitrogen release rate trends in higher rank coals are similar to low rank coals, except that the high rank coals do not have an initial release of nitrogen-poor light gases (fewer aliphatics). The volatile matter in higher rank coals is dominated by aromatics, and this results in the preferential loss of nitrogen throughout devolatilization, since it is believed that the aromatic portion of coal contains the majority of the nitrogen found in coal.¹

Nitrogen release during coal devolatilization has also been observed to be a function of temperature. In an investigation conducted by Blair et al.³² it was shown that

as the pyrolysis temperature increased, nitrogen release increased proportionately and at a faster rate than total mass release. In heated grid devolatilization experiments using a subbituminous and two bituminous coals at temperatures of 570 and 1270 K, Solomon and Colket³³ found that initial nitrogen release was approximately proportional to the tar release. As mentioned previously, light gas release in most coals occurs before or concurrent with tar release. Since the light gas does not generally contain nitrogen, nitrogen release lags mass release early in devolatilization.

In general, the amount of nitrogen released during pyrolysis has been shown to be a function of coal rank.³⁴ Fractional nitrogen release seems to be relatively constant for low rank to high volatile bituminous coal. However, volatile nitrogen release drops dramatically with higher rank coals. The data in Figure 2.4 show the general volatile nitrogen release trend with coal type.

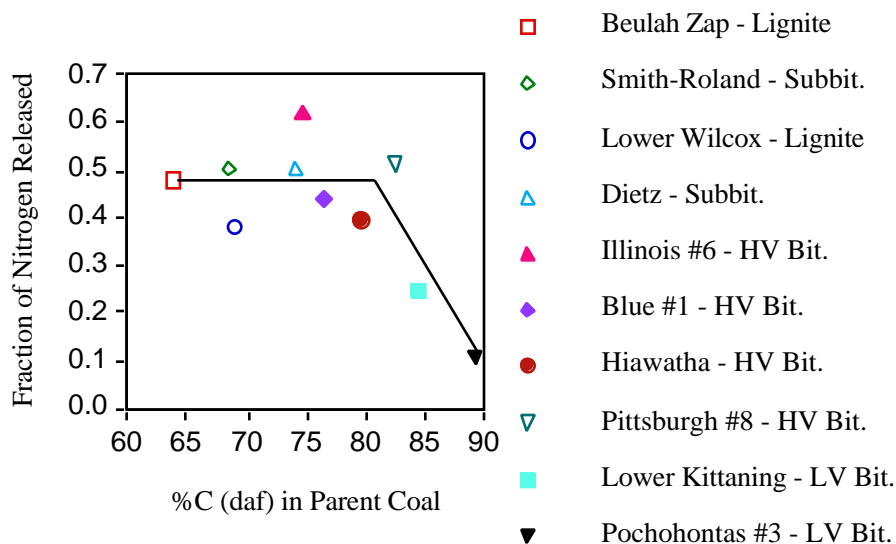


Figure 2.4. Nitrogen release a function of carbon content. Taken from Solomon and Fletcher.³⁴ Original data from Mitchell, et al.³⁵

It is thought that tar release is the primary, but not the only mechanism for nitrogen release. In heated grid pyrolysis experiments at heating rates of 500 K/s, Freihaut et al.³⁶ showed that the distribution of nitrogen between the volatiles and the

char, and hence the release mechanism, is a function of coal rank. Results indicated that at the moderate conditions of the experiments, low rank coals preferentially release nitrogen as HCN (or light gas nitrogen), while the bituminous coals release more nitrogen with the tar. High rank coals were shown to release only small amounts of nitrogen as tar and HCN. These results are summarized in Figure 2.5.

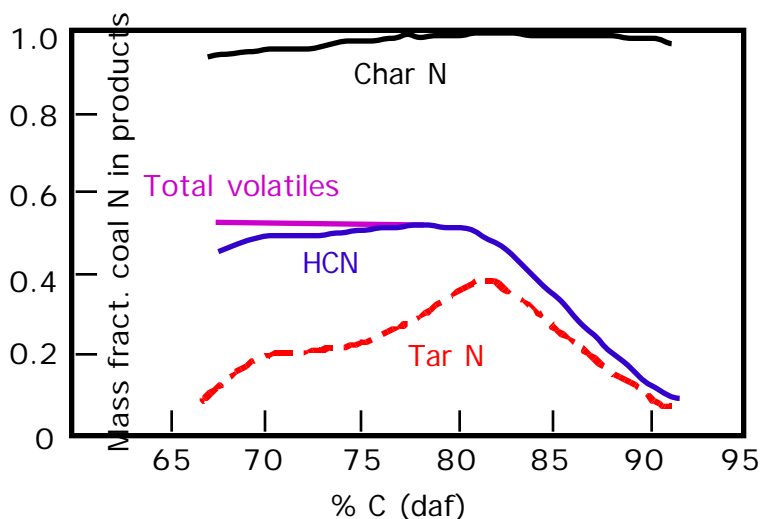


Figure 2.5. The distribution of nitrogen volatiles versus carbon content. Taken from Freihaut et al.³⁶

Light gas nitrogen release (believed to be HCN and NH_3) is thought to come from two sources: (i) ring opening reactions in the char and (ii) ring opening reactions in the tar. These two processes can occur simultaneously after the tar has been released. In a heated grid experiment conducted by Freihaut and coworkers at 500 K/s to 1243 K, it was shown that tar release occurred at 900-1100 K, followed by HCN release at temperatures above 1100 K.³⁷ It is thought that heterocyclic (i.e., pyrrolic and pyridinic) ring rupture in chars of low rank coals occurs more easily than in chars of higher rank coals.¹⁷ This would explain why nitrogen released as HCN is greater in low rank coals, and why nitrogen release generally follows total mass release instead of tar release.

Modeling Devolatilization

Early devolatilization models were based on simple single-reactions to describe total volatiles yields. Later, two-step models, which accounted for the competing effects of bridge-scission and cross-linking, emerged. These simple empirical models did not rely on the chemical structure of the original coal, and were generally based on empirical, rather than mechanistic, approaches.⁵ As a result, the predictive capabilities of such models are limited to the experimental range used to curve-fit the kinetic parameters of the particular model. Many of these early devolatilization models are reviewed extensively by Howard.³⁸

More recently, Ko et al.³⁹ presented a correlation relating maximum tar yield from rapid pyrolysis to coal type and pressure. Ko's correlation seems to accurately predict the maximum tar yield for many coals. The correlation, however, does not predict tar release as a function of time or temperature, nor does it treat light gas release.

In the last decade, as sophisticated coal characterization techniques have advanced the understanding of coal structure and devolatilization, network devolatilization models based on quantitative measurements of the chemical structure of coal have been developed. These models have been successful in predicting total volatiles and tar yields as a function of heating rate, temperature, pressure, and coal type.⁵ Three such devolatilization models are the FG-DVC model,⁴⁰ FLASHCHAIN,⁴¹ and the CPD model.⁴ These devolatilization models have the following features in common: (i) the parent coal is described using coal-dependent structural parameters, generally derived from NMR spectroscopy, TG-FTIR, py-MS, and/or other techniques; (ii) a statistical network model is used to describe the highly non-linear relationship between bridge scission and tar release; (iii) first order rate expressions with distributed activation energies are used to model the depolymerization of the infinite matrix, crosslinking of the metaplast with the matrix, and light gas formation; and (iv) a correlation of vapor pressure with tar molecular weight is used to help model tar vaporization. The network

devolatilization models are advantageous because they take a mechanistic approach, as opposed to a mere empirical curve-fitting approach, resulting in greater predictive capability and a wider range of applicability. A detailed summary of network devolatilization models is given by Smith, et al.⁵

Industrial interest in devolatilization of coals has led to a number of attempts to model structural input parameters (such as ¹³C NMR structural parameters) of coal based on simple linear correlations with the ultimate analysis of the coal. Only a brief description of the correlations between chemical structural features and the ultimate analysis used in the FG-DVC and FLASHCHAIN devolatilization models is given here. A brief summary of the CPD model is also included since it was used extensively in this project.

The FG-DVC Model

In the FG-DVC model⁴⁰ coal is represented as a two-dimensional Bethe lattice of aromatic clusters linked by aliphatic bridges. Various experimental techniques including TG-FTIR, solvent swelling and extraction, NMR, and FIMS must be employed to provide the needed input parameters for the FG-DVC which describe the coal structure and evolution kinetics. For coals where no such experimental data are available, Serio, et al.⁴² proposed a two-dimensional linear interpolation technique based on coal rank to estimate the input parameters for the FG-DVC model of coal devolatilization. The oxygen/carbon and hydrogen/carbon molar ratios were used as indicators of rank. The elemental ratios of nine well-studied reference coals (6 from the Argonne Premium Coal Sample Program and 3 from the Penn State Coal Sample Bank) were used to form a two-dimensional triangular mesh on a H/C vs. O/C coalification diagram. Each triangle was composed of three nodes (i.e. reference coals). For an unknown coal, the elemental composition determined the appropriate triangle, and the structural parameters of the unknown coal were interpolated from the parameters corresponding to the three nodes.

This triangular interpolation scheme was used for all of the model parameters for the FG-DVC model based only on the elemental composition of the coal.

FLASHCHAIN

FLASHCHAIN⁴¹ uses a linear chain model to represent coal structure, and several input parameters to describe the parent coal structure. Among these are the fraction of intact bridges (p_0) as determined through pyridine extract yields, carbon aromaticity (f_a), proton aromaticity (Hf_a), and aromatic carbons per cluster (AC/Cl). These last three parameters are tuned to empirically match devolatilization data, and then compared with solid-state ¹³C NMR spectroscopy of the coal (on those coals for which data exist). To extend FLASHCHAIN's ability to predict ultimate yields where only the ultimate analysis is available, simple (mainly linear) correlations were developed to estimate the input parameters as a function of the ultimate analysis alone (mainly percent carbon).⁴³ For example, in FLASHCHAIN, the carbon aromaticity, f_a , is estimated using a simple linear correlation. Data reported by Gerstein⁴⁴ were used to correlate f_a with the carbon content resulting in the following correlation:

$$f_a = 0.0159(\%C, \text{daf}) - 0.564. \quad (2.1)$$

In FLASHCHAIN p_0 , Hf_a , and AC/Cl are also estimated using simple linear correlations with the carbon content.⁴¹

The CPD Model

In the CPD (Chemical Percolation Devolatilization) model⁴ coal is represented as a two-dimensional Bethe lattice of aromatic clusters linked by aliphatic bridges. The CPD model distributes devolatilization products into char, tar, and light gas fractions. It does not distribute light gas into individual components such as CO₂, CO, H₂O, H₂, and light

hydrocarbons. Percolation statistics are used to describe the network decomposition. The CPD model is composed of five key elements: (i) a description of the parent coal based on quantitative ^{13}C NMR measurements of chemical structure; (ii) a bridge reaction mechanism with associated kinetics; (iii) percolation lattice statistics to determine the relationship between bridge breaking and detached fragments which are tar precursors; (iv) a vapor-liquid equilibrium mechanism to determine the fraction of liquids that vaporize; and (v) a cross-linking mechanism for high molecular weight tar precursors to reattach to the char.⁴ Four of the parameters derived from ^{13}C NMR analyses that describe the structure of the parent coal are used directly as input parameters to the CPD model.^{4, 12} These include M_{cl} (the average molecular weight per aromatic cluster), M (the average side-chain molecular weight), $+I$ (the average number of attachments per cluster), and p_0 (the fraction of intact bridges). The CPD model is unique because the majority of the model input parameters are taken directly from NMR data; other models use these parameters as empirical fitting coefficients. This helps justify the CPD model on a mechanistic rather than on an empirical basis.

Modeling Volatile Nitrogen Release

It is thought that nitrogen is released during primary devolatilization in two ways:^{17, 45} (i) nitrogen contained in the aromatic clusters is transported away as large aromatic tar molecules escape the coal matrix (this is often the primary mode of nitrogen release during devolatilization); and (ii) additional nitrogen can be released as HCN and NH_3 (light gas nitrogen) after the rupture of aromatic rings containing nitrogen heteroatoms. The detailed chemistry of HCN and NH_3 formation has not yet been determined. However, it is believed that nitrogen is first released as HCN. NH_3 is then formed from subsequent reactions with hydrogen.⁴⁵

Nitrogen release models have been developed and incorporated into the FG-DVC⁴⁵ and FLASHCHAIN¹⁷ devolatilization models. Several simplifying assumptions

are made in these models: (i) nitrogen atoms are randomly distributed throughout the aromatic clusters of the coal; (ii) nitrogen atoms contained in the aromatic clusters of the metaplast are transported from the coal matrix during tar evolution; and (iii) opening and condensation reactions of rings containing nitrogen heteroatoms do not significantly affect aromatic cluster molecular weight (since the nitrogen content is low). Both models use first order kinetics to describe the rate of release of nitrogen from the char.

Niksa¹⁷ extended the FLASHCHAIN model of devolatilization to predict nitrogen release by monitoring the change in the average moles of nitrogen per mole of aromatic clusters (). The rate of nitrogen evolution with the tar is directly proportional to the evolution rate of tar molecules, which accounts for the largest fraction of nitrogen release during devolatilization. Additional nitrogen is released as HCN. HCN release is modeled by a first order rate equation:

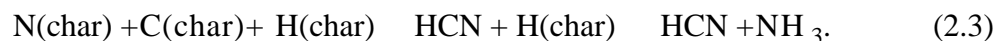
$$\frac{dY_{HCN}}{dt} = k_{HCN} \quad (2.2)$$

where Y_{HCN} is the molar yield of HCN, and k_{HCN} is the first-order rate constant which is calculated using a distributed activation energy function. This model partially accounts for the decrease in HCN production with larger aromatic clusters due to higher coal rank or cluster growth during devolatilization. In addition, the pre-exponential factor, A_{HCN} , is correlated with the O/N ratio to further account for lower HCN yields for high rank coals. The rate constants were empirically fit to match experimental nitrogen release data.

The nitrogen release model used by Bassilakis et al.⁴⁵ in the FG-DVC model is similar to that used in FLASHCHAIN. As in FLASHCHAIN, the primary mode of nitrogen release is through tar release, and further nitrogen release as HCN is described by first order kinetics with a distributed activation energy. The FG-DVC model, however, goes one step further by proposing a mechanism and kinetic model for the formation of

NH₃. Bassilakis, et al.⁴⁵ noted three important nitrogen release trends pertaining to HCN and NH₃ release during devolatilization: (i) lower rank coals release a larger fraction of their nitrogen as HCN and NH₃; (ii) in slow heating rate experiments (30 K/s) conducted on the Argonne premium coals, it was observed that HCN release generally preceded NH₃ release; and (iii) in a comparison of slow heating rate data with rapid heating rate nitrogen release data it was observed that only in the slow heating rate experiment was a significant amount of nitrogen released as NH₃.

Bassilakis proposed a simple mechanism to explain the second two observations. First, HCN evolves directly from the char.⁴⁵ Then, as the gas exits the particle through the pore structure of the char, gaseous HCN reacts heterogeneously with coal hydrogen to form NH₃, as depicted below:



Since residence times within the pore structure are much longer at slow heating rates, this mechanism could explain why NH₃ was only observed at slower heating rates. This phenomena was modeled in the FG-DVC model by using a simplified single cell structure to estimate residence time and a swelling model to estimate the swelling ratio. The HCN evolution rate was corrected to account for conversion to NH₃ based on the residence time in the pore.

The model developed in this thesis will differ from the volatile nitrogen release models developed for FLASHCHAIN and the FG-DVC model in that nitrogen release will be based on the chemical structure of coal as measured by ¹³C NMR spectroscopy. This will allow model predictions to be compared not only with nitrogen release data, but also with structural characteristics derived from available ¹³C NMR measurements of char structure.

Summary

Significant progress has been made during the last decade in understanding the structure and reaction processes of coal. Solid-state analysis techniques such as ^{13}C NMR spectroscopy have led to a better awareness of how the chemical structure of coal evolves during pyrolysis. Extensive devolatilization experiments have led to increased knowledge of the dependence of pyrolysis on temperature, heating rate, pressure, and coal type. Increased regulation of NO_x emissions in recent years has led to pyrolysis research that has substantially increased the understanding of the functionality of nitrogen in coal and the chemistry of nitrogen release. Increased understanding of coal structure and reaction processes has led to the development of advanced devolatilization models that predict tar and total volatiles yields and the composition of light gas as a function of coal type, temperature, pressure, and heating rate. The time and expense involved in performing coal specific analyses required to measure the input parameters for devolatilization models makes it difficult to apply the models to coals that have not already been well characterized. Therefore, correlations have been developed to estimate structural input parameters for the FG-DVC and FLASHCHAIN models of devolatilization based on more easily obtained data such as the elemental composition. Also, in just the last few years, submodels that predict the quantity of nitrogen released with the tar and as light gas have been incorporated into the FG-DVC and FLASHCHAIN models.

The following are several features that set the CPD model apart from other devolatilization models and attract a great deal of industrial interest: (i) the description of the coal structure is accurately determined from solid-state ^{13}C NMR analysis of the parent coal; (ii) the CPD model is truly predictive (based only on a given pressure, temperature profile, and parent coal structure, total volatiles and tar yields are predicted); (iii) the CPD model features very rapid convergence (low computer time requirements); (iv) the CPD model has been successfully implemented into comprehensive coal models

such as PCGC-3;³ and (v) the CPD model is available free of charge. The CPD model, however, does not currently treat nitrogen release or light gas composition. Furthermore, unlike the FG-DVC and FLASHCHAIN models, there is no alternative method to estimate the original structure of the parent coal when ¹³C NMR data are not available.

3. Objectives and Approach

The primary objective of this study is to develop a volatile nitrogen release model based on the chemical structure of coal, and to incorporate the nitrogen release model into the CPD model. This objective was accomplished by (1) evaluating the approaches used to model nitrogen release in the FG-DVC and FLASHCHAIN models, (2) developing a similar nitrogen release algorithm for the CPD model, (3) evaluating the model using a novel comparison with measured structures in char, and (4) evaluating the model by comparing model predictions of nitrogen release to experimental data not included in the development of the model (including nitrogen release data on 6 low volatile coals collected during pyrolysis experiments as part of this study).

A secondary, but important, objective of this study is to increase the industrial usefulness of the CPD model by (1) improving the accuracy of tar and light gas predictions, (2) developing a reasonable correlation between the chemical structural characteristics of coal as determined by ^{13}C NMR analyses (in order to estimate the chemical structural input parameters for the CPD model when NMR data are not available), and (3) developing a submodel for the CPD model that calculates the composition of light gas evolved during devolatilization. These objectives were accomplished by gathering, analyzing, and correlating data available in the literature from ^{13}C NMR analyses, ultimate and proximate analyses, and analyses of coal pyrolysis product composition. Also, as a result of this project, the literature data base was expanded by conducting ultimate, proximate, and ^{13}C NMR analyses on 12 coals from the Penn State Coal Data Bank.

The correlation of ^{13}C NMR parameters will be discussed first (Chapter 4) since that correlation was used to help evaluate the nitrogen release model. The nitrogen release model will then be discussed in Chapter 5, followed by the method to calculate the composition of light gas (Chapter 6).

Chapter 4. ^{13}C NMR Correlation

^{13}C NMR spectroscopy has been shown to be an important tool in the characterization of coal structure.⁵ Important quantitative information about the carbon skeletal structure is obtained through ^{13}C NMR spectral analysis of coal. Solid-state ^{13}C NMR analysis techniques have progressed beyond the mere determination of aromaticity, and can now describe features such as the number of aromatic carbons per cluster and the number of attachments per aromatic cluster. These ^{13}C NMR data have been used to better understand the complicated structure of coal, to compare structural differences in coal, tar, and char, and to model coal devolatilization.

Unfortunately, due to the expense of the process, extensive ^{13}C NMR data are not available for most coals. A *non-linear* correlation was therefore developed that predicts the chemical structure parameters of both U.S. and non-U.S. coals measured by ^{13}C NMR and often required for advanced devolatilization models. The chemical structure parameters correlated include: (i) the average molecular weight per side chain (M); (ii) the average molecular weight per aromatic cluster (M_c); (iii) the ratio of bridges to total attachments (p_0); and (iv) the total attachments per cluster ($+I$). The correlation is based on the elemental and volatile matter content, which are generally known for most coals. ^{13}C NMR data from 30 coals were used to develop this correlation. Before this project, ^{13}C NMR data of this type were only available for 18 coals. As part of this project, proximate, ultimate, and ^{13}C NMR analyses were conducted on 12 additional coals to expand the data set to 30 coals. The correlation was used to estimate the chemical structure parameters obtained from ^{13}C NMR measurements, and then applied to coal devolatilization predictions using the CPD model. It will be shown that the predicted yields compare well with measured yields for most coals.

Evaluation of Linear Correlations

An extensive statistical analysis was performed previously to determine the validity of linearly correlating the ^{13}C NMR structural parameters with the ultimate analysis and ASTM volatile matter content.⁴⁶ A data base including the elemental composition, ASTM volatile matter content, and the four ^{13}C NMR structural parameters for 30 coals of varying rank was used in the analysis (see Tables 4.1, 4.2 and 4.3). Preliminary results indicated that *linear* correlations of most ^{13}C NMR parameters versus elemental composition and/or volatiles content were not acceptable. This preliminary work suggested that *non-linear* correlations may prove to be of more value.

The previously mentioned database was re-examined using NCSS, a software package for statistical data analysis.⁴⁷ A linear correlation matrix was calculated between the ^{13}C NMR structural parameters and the ultimate analysis data. From the correlation matrix, the strengths of relationships between the individual elements and the derived parameters were easily determined. The ^{13}C NMR structural parameters were also examined for relationships among themselves. Multi-variate linear regression was then performed to derive the best possible linear combinations to predict each of the parameters as a function of the elemental composition and ASTM volatile matter content. The coefficient of determination, r^2 , which is an indication of the relative strength of correlation, was determined for each relationship ($r^2=1$ would be a perfect correlation).

The r^2 values for the linear correlations, as determined by NCSS, ranged from 0.12 for $+I$ to 0.60 for p_o ($r^2= 0.56$ and 0.13 for M and M_{cl} , respectively). With the possible exceptions of M and p_o , these are very weak correlations. As a result of this study, it was reaffirmed that correlations based on *linear* regressions of the ultimate analysis data are generally not suitable to accurately predict the structural parameters.

The purpose of the current investigation is to develop *non-linear* correlations that might be used to estimate the structural parameters for the network devolatilization models when ^{13}C NMR data are not available. Although one of the principal motives for

this study has been the estimation of the input parameters for the CPD model, the estimated structural parameters should be useful in other applications, and a similar approach could be used to develop predictive models for other structural parameters.

Correlation Development

Experimental Data

Tables 4.1, 4.2, and 4.3 show the database of 30 coals used in this study, including the ultimate analysis and the four chemical structure parameters derived from ^{13}C NMR analysis. The first eight coals are Argonne premium coals, coals 9-11 were studied at the Advanced Combustion Engineering Research Center (ACERC), coals 12-16 were studied at Sandia National Laboratories (selected from the Penn State Coal Bank), coals 17-18 were studied at Advanced Fuel Research, and coals 19-30 were selected from the Penn State Coal Bank to expand the database for this study. As part of this project coals 19-30 were ground and sieved, and the 53-75 μm size fraction was examined using solid-state ^{13}C NMR analyses.^{12, 48} A Leco CHNS-932 elemental analyzer was used to determine the elemental composition of coals 19-30 (oxygen was obtained by difference).⁴⁹ Also, for coals 19-30, proximate analysis was performed according to ASTM procedures to determine ash and volatile matter content. The 30 coals in Table 4.1 vary widely in rank as shown in the coalification chart in Figure 4.1

Procedure

As a first step, each of the ^{13}C NMR parameters was plotted versus each independent variable (i.e. elemental composition and ASTM volatile matter content). This permitted a first order screening to determine the relative dependence on each independent variable, and allowed a visual inspection of correlation patterns. Secondly, a separate non-linear (i.e., a polynomial) correlation was made for each independent variable, and a pseudo r^2 value was calculated to determine the strength of each

correlation. A variety of equation forms were examined, and experience showed that a cubic polynomial generally resulted in the best fit for most parameters. Finally, from the individual polynomial correlations, the form of the correlation was derived between each ^{13}C NMR parameter and the combination of all of the independent variables.

Table 4.1
List of Coals Used in ^{13}C NMR Correlation

#	Source	Seam	ASTM Rank	Location
1	PSOC 1507 (AR)	Beulah-Zap	ligA	Mercer Co., ND
2	PSOC-1520 (AR)	Wyodak	subC	Campbell Co., WY
3	PSOC-1502 (AR)	Blind Canyon	hvBb	Emery Co., UT
4	PSOC-1493 (AR)	Illinois #6	hvCb	St. Clair Co., IL
5	PSOC-1451 (AR)	Pittsburgh #8	hvAb	Green Co., PA
6	ANL (AR)	Stockton	hvAb	Kanawha Co., WV
7	ANL (AR)	Upper Freeport	mvb	Indiana Co., PA
8	PSOC-1508 (AR)	Pocahontas #3	lvb	McDowell Co., WV
9	PSOC-1443 (ACERC)	Lower Wilcox	ligA	Titus Co., TX
10	PSOC-1488 (ACERC)	Dietz	subB	Bighorn Co., WY
11	PSOC-1468 (ACERC)	Buck Mountain	an	Luzerne Co., PA
12	PSOC-1445D (Sandia)	Blue #1	hvCb	Mckinley Co., NM
13	PSOC-1451D (Sandia)	Pittsburg #8	hvAb	Green Co., PA
14	PSOC-1493D (Sandia)	Illinois #6	hvab	St. Clair Co., IL
15	PSOC-1507D (Sandia)	Beulah-Zap	ligA	Mercer Co., ND
16	PSOC-1508D (Sandia)	Pocahontas #3	mvb	McDowell Co., WV
17	Goudey A (AFR)	not named	hvb	-----
18	Goudey B (AFR)	not named	lvb	-----
19	DECS-1 (BYU)	Bottom	subC	Freestone Co., TX
20	DECS-7 (BYU)	Adaville #1	hvCb	Lincoln Co., WY
21	DECS-11 (BYU)	Beulah-Zap	ligA	Mercer Co., ND
22	DECS-13 (BYU)	Sewell	mvb	Greenbrier Co., WV
23	DECS-18 (BYU)	Kentucky #9	hvBb	Union Co., KY
24	DECS-20 (BYU)	Elkhorn #3	hvAb	Floyd Co., KY
25	DECS-21 (BYU)	Lykens Valley #2	an	Columbia Co., PA
26	DECS-27 (BYU)	Deadman	subA	Sweetwater Co., WY
27	PSOC-1515 (BYU)	Penna. Semian. C	sa	Sullivan Co., PA
28	PSOC-1516 (BYU)	Lower Kittanning	lvb	Somerset Co., PA
29	PSOC-1520 (BYU)	Smith-Roland	subC	Cambell Co., WY
30	PSOC-1521 (BYU)	Lower Hartshorne	lvb	Sebastian Co., AR

Table 4.2
Properties of Coals Used in ¹³C NMR Correlation

#	Source	% C (daf)	% H (daf)	% O (daf)	% N (daf)	% S (daf)	ASTM VM (daf)
1	PSOC 1507 (AR)	72.9	4.83	20.34	1.15	0.70	49.8
2	PSOC-1520 (AR)	75.0	5.35	18.02	1.12	0.47	49.0
3	PSOC-1502 (AR)	80.7	5.76	11.58	1.57	0.37	48.1
4	PSOC-1493 (AR)	77.7	5.00	13.51	1.37	2.38	47.4
5	PSOC-1451 (AR)	83.2	5.32	8.83	1.64	0.89	41.7
6	ANL (AR)	82.6	5.25	9.83	1.56	0.65	37.6
7	ANL (AR)	85.5	4.70	7.51	1.55	0.74	31.6
8	PSOC-1508 (AR)	91.1	4.44	2.47	1.33	0.50	19.5
9	PSOC-1443 (ACERC)	72.3	5.21	20.11	1.35	0.94	78.7
10	PSOC-1488 (ACERC)	76.0	5.23	17.27	0.94	0.53	44.2
11	PSOC-1468 (ACERC)	95.4	1.38	1.86	0.84	0.53	3.9
12	PSOC-1445D (Sandia)	75.6	5.26	17.33	1.32	0.49	48.2
13	PSOC-1451D (Sandia)	84.2	5.54	7.56	1.65	1.01	38.7
14	PSOC-1493D (Sandia)	74.1	4.96	13.18	1.45	6.29	43.4
15	PSOC-1507D (Sandia)	66.6	4.26	25.16	1.12	2.89	49.6
16	PSOC-1508D (Sandia)	88.8	4.37	5.14	1.06	0.60	17.2
17	Goudey A (AFR)	87.9	3.77	4.65	1.31	2.37	36.9
18	Goudey B (AFR)	88.5	4.94	1.40	na	1.75	19.3
19	DECS-1 (BYU)	70.7	5.83	20.83	1.47	1.18	53.6
20	DECS-7 (BYU)	72.5	5.22	20.09	1.17	1.04	45.6
21	DECS-11 (BYU)	68.5	4.94	24.96	1.00	0.64	61.7
22	DECS-13 (BYU)	85.5	4.91	7.12	1.72	0.72	33.2
23	DECS-18 (BYU)	79.4	5.62	8.57	1.74	4.71	44.6
24	DECS-20 (BYU)	82.7	5.73	8.76	1.78	0.99	40.5
25	DECS-21 (BYU)	93.8	2.72	1.96	0.92	0.62	5.1
26	DECS-27 (BYU)	76.5	5.24	15.95	1.53	0.76	40.6
27	PSOC-1515 (BYU)	88.4	4.02	5.47	1.24	0.86	11.8
28	PSOC-1516 (BYU)	86.2	4.86	4.64	1.81	2.45	21.6
29	PSOC-1520 (BYU)	67.4	5.37	24.39	1.00	1.84	53.4
30	PSOC-1521 (BYU)	91.2	4.56	1.53	1.82	0.89	23.5

Table 4.3 **^{13}C NMR Chemical Structure Parameters* of Coals Used in Correlation**

#	Source	M	M_{cl}	p_0	$+I$
1	PSOC 1507 (AR)	40	269	0.64	4.10
2	PSOC-1520 (AR)	42	408	0.55	5.60
3	PSOC-1502 (AR)	36	366	0.49	5.10
4	PSOC-1493 (AR)	27	322	0.63	5.00
5	PSOC-1451 (AR)	28	330	0.64	4.70
6	ANL (AR)	20	272	0.69	4.80
7	ANL (AR)	17	312	0.67	5.30
8	PSOC-1508 (AR)	13	307	0.74	4.40
9	PSOC-1443 (ACERC)	36	297	0.59	4.80
10	PSOC-1488 (ACERC)	37	310	0.54	4.70
11	PSOC-1468 (ACERC)	12	656	0.89	4.70
12	PSOC-1445D (Sandia)	45	384	0.48	5.00
13	PSOC-1451D (Sandia)	33	329	0.48	4.80
14	PSOC-1493D (Sandia)	39	402	0.52	5.50
15	PSOC-1507D (Sandia)	58	392	0.59	4.40
16	PSOC-1508D (Sandia)	18	285	0.70	4.20
17	Goudey A (AFR)	21	264	0.64	4.80
18	Goudey B (AFR)	19	295	0.65	5.00
19	DECS-1 (BYU)	55	505	0.42	5.80
20	DECS-7 (BYU)	43	381	0.55	5.10
21	DECS-11 (BYU)	42	329	0.68	4.60
22	DECS-13 (BYU)	72	483	0.72	4.50
23	DECS-18 (BYU)	35	370	0.48	5.30
24	DECS-20 (BYU)	21	247	0.64	4.70
25	DECS-21 (BYU)	13	216	1.00	3.80
26	DECS-27 (BYU)	34	361	0.55	5.20
27	PSOC-1515 (BYU)	4	231	1.00	6.00
28	PSOC-1516 (BYU)	21	354	0.35	4.50
29	PSOC-1520 (BYU)	46	282	0.64	3.70
30	PSOC-1521 (BYU)	14	225	0.69	4.40

* All ^{13}C NMR measurements were performed in the NMR Laboratory at the University of Utah under the direction of Professor Ronald J. Pugmire.

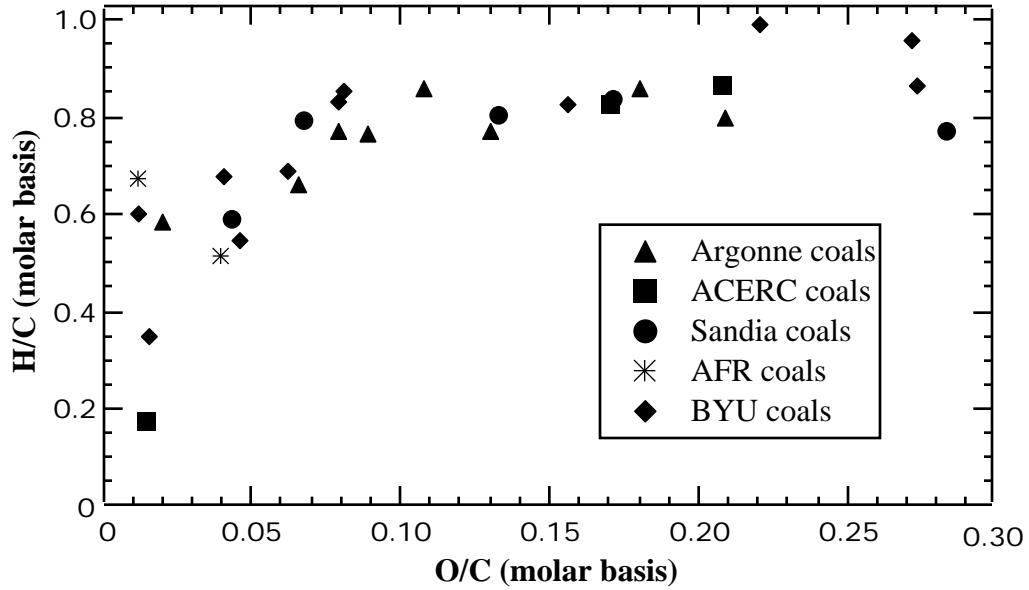


Figure 4.1. Coalification chart of 30 coals used in this research showing the diversity of rank of the selected coals.

Example Case for p_0

Plots of p_0 versus each independent variable are shown in Figure 4.2. It can be seen from this figure that the value of p_0 depends significantly on the relative content of carbon (X_C), hydrogen (X_H), oxygen (X_O), and ASTM volatile matter content (X_{VM}). Once it was determined that p_0 was dependent on the carbon, hydrogen, oxygen, and ASTM volatile matter content, the forms of the “best fit” equations from the four plots (p_0 versus X_C , p_0 versus X_H , etc.) were added together, resulting in Equation 4.1:

$$p_0 = c_1 + c_2 X_C + c_3 X_C^2 + c_4 X_C^3 + c_5 X_H + c_6 X_H^2 + c_7 X_H^3 + c_8 X_O + c_9 X_O^2 + c_{10} X_O^3 + c_{11} X_{VM} + c_{12} X_{VM}^2 + c_{13} X_{VM}^3 \quad (4.1)$$

where the c_i are empirical coefficients, and the elemental composition and ASTM volatile matter content are on a dry ash free basis. All of the “best fit” equations were third order polynomials which resulted in the modified cubic correlation of Equation 4.1. Initial guesses for the coefficients were usually a value of 1 or 0. The sum square error between the predicted values and the measured values of p_0 was minimized by optimizing the coefficients. This procedure was repeated for M , M_{cl} , and $+I$, resulting in similar

equations. Through this study it was determined that the chemical structural parameters have little dependence on the relative content of sulfur and nitrogen (see Figure 4.2). Therefore, sulfur and nitrogen were omitted from the correlations.

Final NMR Correlation

During the course of this research, while applying this modified cubic correlation to additional sets of NMR data for other coals, it was found that unrealistic values for M_{cl} and $+I$ were obtained for low rank coals ($X_O > 0.25$) and high rank coals ($VM < 0.10$). For example, some predicted values of M_{cl} were less than 100 daltons; the lowest NMR measurement for any coal was ~200 daltons. These unrealistic predicted values seemed to be the result of extrapolations of the cubic curve beyond the original data set. Therefore, the curve-fitting procedure was repeated for a quadratic set of equations, as shown below:

$$y = c_1 + c_2 X_C + c_3 X_C^2 + c_4 X_H + c_5 X_H^2 + c_6 X_O + c_7 X_O^2 + c_8 X_{VM} + c_9 X_{VM}^2 \quad (4.2)$$

where $y = M$, M_{cl} , $+I$, and p_0 . By using the quadratic correlation rather than the cubic, the number of coefficients were reduced, with a small corresponding penalty in the value of r^2 . The extrapolated values of the quadratic correlation seemed more reasonable for low and high rank coals.

To further improve the correlations, NCSS (Number Cruncher Statistical Software) was used to examine the data set for outliers and cross-correlations.⁴⁷ A factor analysis was performed to determine the optimum number of independent variables to be used in each correlation. Based on this analysis, it was determined that Equation 4.2 is a suitable correlation. The data set was screened with the aid of NCSS for outliers by examining the normal probability plots of the residuals (a plot of the inverse of the standard normal curve versus the ordered observations) of each dependent variable (M_{cl} , M , $+I$, and p_0). Stragglers at either end of the normal probability plot indicate outliers.

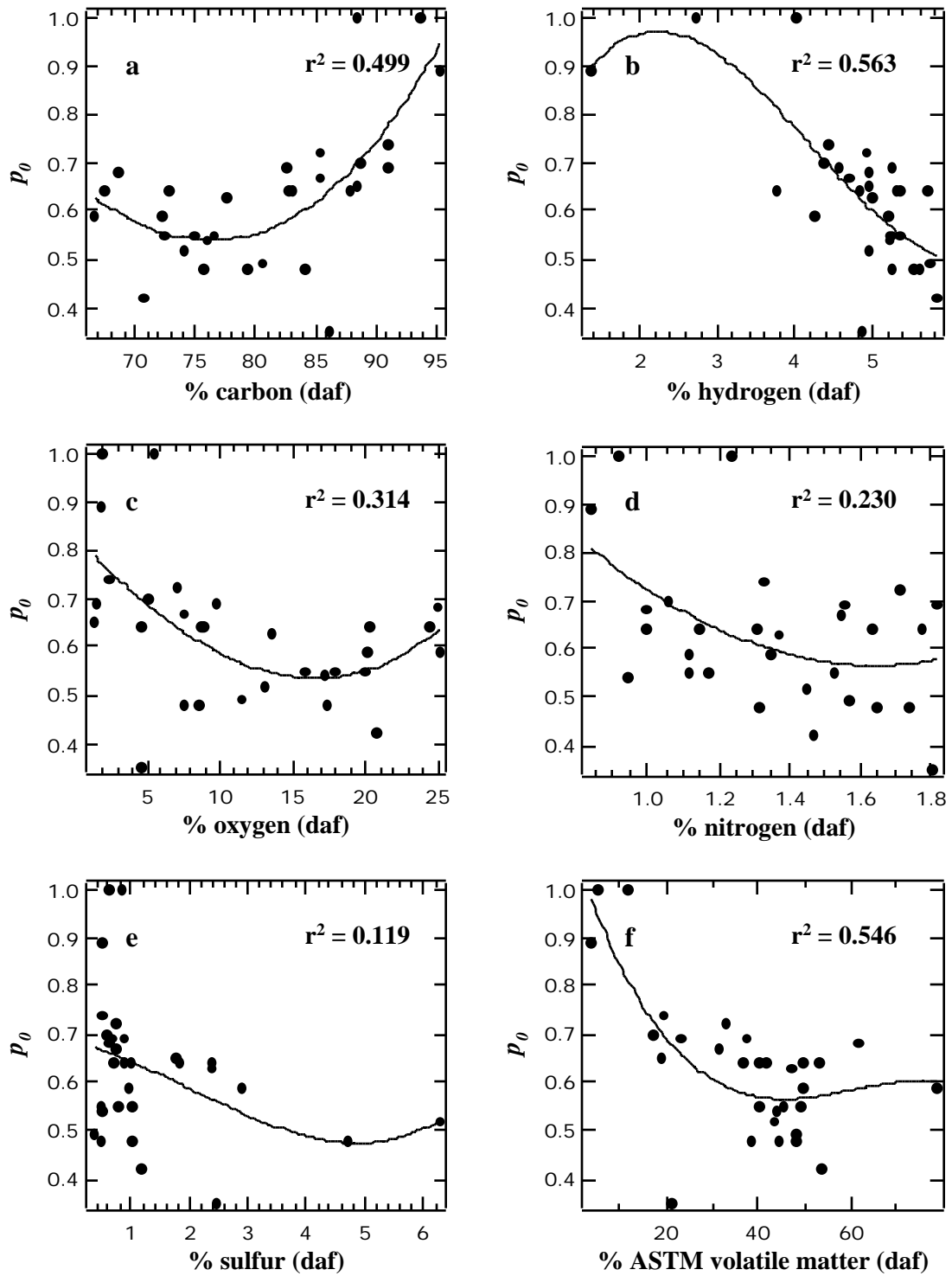


Figure 4.2. Plots of p_0 versus (a) % carbon (daf), (b) % hydrogen (daf), (c) % oxygen (daf), (d) % nitrogen, (e) % sulfur, and (f) % ASTM volatile matter content.

It was observed that the residuals of all of the dependent variables were normally distributed with the exception of a few stragglers. Further examination of the stragglers by comparing the stragglers with values of the same parameter from similar coals confirmed that some of these data were non-representative. These non-representative data points were removed from each correlation (see Table 4.4), which substantially increased the r^2 value in some cases.

Table 4.4

Outliers Removed from Correlations

NMR parameter	data points removed
<i>M</i>	6, 7, 22, 24, 27
<i>M_{cl}</i>	22, 24
<i>P₀</i>	6, 24, 27, 28
<i>+I</i>	1, 19, 27

During the course of this research, it was observed that the measured structural parameters, *M* and *p₀*, of the two separate Pittsburgh #8 and of the two separate Illinois #6 samples (*ANL* and *Sandia*) are remarkably different. Further examination of the ¹³C NMR data base revealed that the values of *M* of the *ANL* Pittsburgh #8, *ANL* Illinois #6, and *ANL* Stockton coals were small compared to other hv-bituminous coals of similar composition, and that the values of *p₀* for the same coals were large compared to other hv-bituminous coals. The unusual values of *M* and *p₀* of these three *ANL* coals are likely due to the fact that, unlike the other coals in the data base, the *ANL* coals have never been exposed to oxygen. Because these values of *M* and *p₀* appear to be non-representative of coals that have been exposed to oxygen, the values of *M* and *p₀* for the *ANL* Pittsburgh #8, *ANL* Illinois #6, and *ANL* Stockton coals were omitted when deriving the correlations. It is hoped that future research can be conducted to verify if the cause of the differences in these parameters is actually due to weathering.

The non-linear curve fitting package in NCSS was used to determine the coefficients corresponding to each equation. NCSS estimates the parameters of the non-linear models using the Levenberg-Marquardt non-linear least squares algorithm.⁵⁰ The coefficients resulting from this curve fit are listed in Table 4.5.

Table 4.5
Coefficients of Modified Quadratic Correlations

	<i>M</i>	<i>M_{cl}</i>	<i>P₀</i>	+1
<i>c</i> ₁	4.220E+2	1.301E+3	4.898E-1	-5.2105E+1
<i>c</i> ₂	-8.647E+0	1.639E+1	-9.816E-3	1.6387E+0
<i>c</i> ₃	4.639E-2	-1.875E-1	1.330E-4	-1.0755E-2
<i>c</i> ₄	-8.473E+0	-4.548E+2	1.555E-1	-1.2369E+0
<i>c</i> ₅	1.182E+0	5.171E+1	-2.439E-2	9.3194E-2
<i>c</i> ₆	1.154E+0	-1.007E+1	7.052E-3	-1.6567E-1
<i>c</i> ₇	-4.340E-2	7.608E-2	2.192E-4	4.0956E-3
<i>c</i> ₈	5.568E-1	1.360E+0	-1.105E-2	9.2610E-3
<i>c</i> ₉	-6.546E-3	-3.136E-2	1.009E-4	-8.2672E-5

The coefficients of determination, r^2 , were 0.94, 0.72, 0.88, and 0.62 for the quadratic correlations of *M*, *M_{cl}*, *p₀* and, +1, respectively. There is no direct r^2 defined for non-linear regression. The r^2 value calculated by NCSS and reported here is a pseudo r^2 value constructed to approximate the r^2 value used in multiple regression. The version of r^2 used for non-linear regression indicates how well the model performs after removing the influence of the mean of the dependent variable. For example, an r^2 value of 0.72 for *M_{cl}* means that approximately 72% of the variance of *M_{cl}* can be explained by the non-linear relationship between *M_{cl}* and the independent variables (i.e. elemental composition and ASTM volatile matter content). Only about 62%, however, of the variance of +1 is explained by the correlation. The chemical structure parameters estimated by the

correlations were also compared graphically with the chemical structure parameters derived from ^{13}C NMR analyses as shown in Figure 4.3.

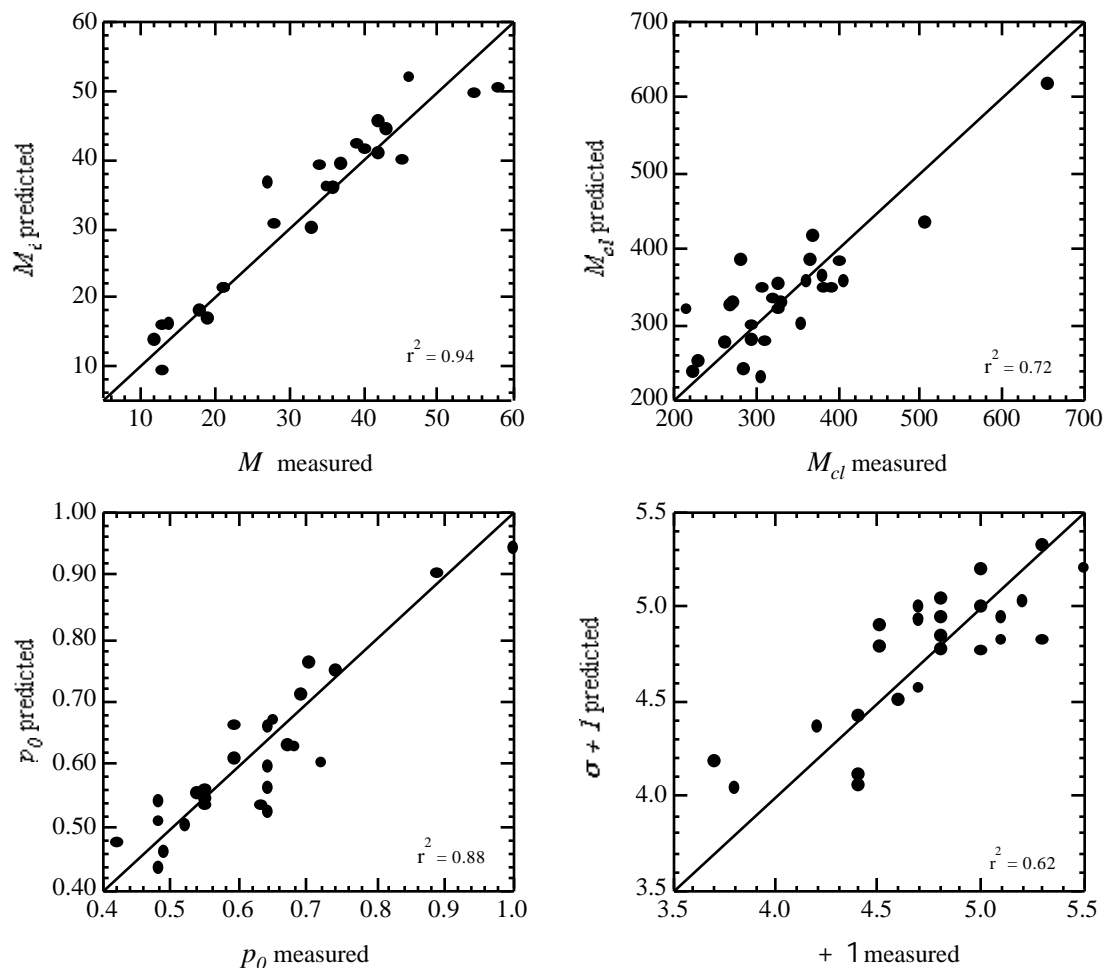


Figure 4.3. Plots of estimated chemical structure parameters versus the parameters derived from ^{13}C NMR analyses.

During the course of this research, the following question arose: after having removed the non-representative data, would more simple *linear* correlations adequately predict the four derived chemical structure parameters? In order to answer this question, multi-variate *linear* regression was performed on the data set using NCSS with the same non-representative data points being removed. The r^2 values of the correlations did increase substantially over those reported in the linear regression performed in the

preliminary studies where no data points were removed. The r^2 values of the new multi-variate *linear* correlations were 0.9, 0.22, 0.75, and 0.24 for M , M_{cl} , p_0 and $+I$, respectively. Further examination of the relationship between M and the elemental composition showed that with the non-representative data omitted, the value of r^2 for the linear correlation of M with the carbon content alone is 0.89. Experience in applying the simple linear correlation of M with carbon content resulted in consistent under-predictions of M for coals with carbon content between 82 and 86%. Even though the modified quadratic correlation of M only resulted in a slightly larger r^2 value (0.94), the under-prediction problem was partially alleviated by using the quadratic correlation. The r^2 values of the modified quadratic correlations of M_{cl} and $+I$ are much larger than are those of the corresponding multi-variate linear correlations. The r^2 value of the quadratic correlation of p_0 is also larger than that of the multi-variate linear correlation. In general, it appears that the *non-linear* correlations are more adequate in predicting the chemical structural parameters than multi-variate *linear* correlations.

Estimation of the Fraction of Stable Bridges

Each of the three devolatilization models mentioned previously require an estimation of the number of stable bridges existing in the parent coal or that are formed early in the pyrolysis process for low rank coals. In the CPD model, this parameter is c_0 . This parameter has generally been used to represent stable bridgehead and bi-aryl type linkages in low volatile bituminous coals, and to represent early crosslinking in lignites. In the past, c_0 has been used as a tuning parameter for these types of coals, and had to be changed as a function of heating rate, since crosslinking occurs at different rates as a function of heating rate. Based on drop tube and flat flame burner pyrolysis experiments performed by Watt¹⁵ at heating rates greater than 10^4 K/s, and pyrolysis experiments conducted by Fletcher and Hardesty⁴⁸ at Sandia National Laboratories, a rough correlation for c_0 was developed. For low rank coals, oxygen content in the parent coal

was used, since this correlates well with early crosslinking. For high rank coals, carbon content was used, since this may correlate well with the bi-aryl type linkages. The correlation for c_0 used for high heating rates was:

$$c_0 = \min[0.36, \max\{(0.118 X_C - 10.1), 0.0\}] \\ + \min[0.15, \max\{(0.014 X_O - 0.175), 0.0\}] \quad (4.3)$$

where X_C and X_O are the percent carbon and oxygen, respectively, on a dry ash free basis. Equation 4.3 was used in the CPD model for all predictions that used the correlated (and measured) chemical structure parameters.

Implications of ^{13}C NMR Correlation

The correlations work well for most coals, but significant discrepancies may occur for some unusual coals since the correlations only describe the average variance of the ^{13}C NMR parameters as a function of elemental composition and ASTM volatile matter content. It is important to emphasize that the correlations are not an adequate replacement of ^{13}C NMR analysis of coal, but are intended to give reasonable estimates of the structural parameters of most coals when ^{13}C NMR data are not available. The advantage of using the actual chemical structural parameters derived from ^{13}C NMR analysis is better accuracy of the structural parameters, particularly for unusual coals.

It is also important to note the boundaries of the correlation when applying the correlations to coals not included in the original data set. As mentioned previously, a broad variety of coals were included in the correlation. Of the coals included, X_C ranged from a minimum of 66.6 % to a maximum of 95.4 % (daf). A complete list of the boundaries for each independent variable is given in Table 4.6. Due to the quadratic nature of the correlations, extrapolation beyond the original data set may result in large discrepancies.

Table 4.6
Range of Values Used in Correlations

Constituent (daf)	Minimum	Maximum
X_C	66.6	95.4
X_H	1.38	5.84
X_O	1.40	24.16
X_N	0.84	3.42
X_S	0.37	6.29
ASTM VM	3.92	78.67

It is well documented that coal structure and reactivity are not only related to coal rank, but also to the origin and maceral content of coal.⁵ For example, a study conducted by Carr and Williamson on 130 coals showed that the aromaticity of coal, f_a , was not only related to coal rank (or degree of maturation) but also to the maceral/lithotype content of the coal.⁵¹ The carbon content of coal is often used as a rank indicator. Of the four chemical structural parameters derived from ^{13}C NMR analysis studied here, only M , the average molecular weight per side chain, correlates well with carbon content. This is further evidence that the chemical structure of coal is dependent on other factors besides coal rank. It is not possible to conclude from this study exactly why the non-linear correlations between elemental composition and the derived chemical structure parameters exist. Perhaps the correlations presented in this study exist because there is a relationship between the elemental composition, the ASTM volatile matter content of coal, and maceral/lithotype composition that the quadratic correlations are able to describe. A study examining the elemental composition and volatile matter content of macerals at various stages of maturation would be useful in confirming or discounting this hypothesis.

Application of Correlated Parameters in the CPD Model

Two sets of test cases were used to evaluate the reliability of using correlated structural parameters in the CPD model to predict total volatiles and tar yields. The first test case was a series of flat flame burner devolatilization experiments reported by Fletcher and Hardesty.⁴⁸ Predictions were made by the CPD model using (a) the actual NMR structural parameters and (b) the structural parameters estimated by the correlations (see Appendices B and C). The five coals used in this test case were part of the database used in the correlations. Predictions are compared with measurements in Figure 4.4. It can be seen that the use of the estimated structural parameters from the correlation gives predictions of total mass release that are as good as the actual NMR data in most cases. The average relative error between the predicted total volatiles yield and the measured total volatiles yield was 6.8% using the actual NMR structural parameters and 3.8% using the correlated parameters. For this set of test cases, using the correlated NMR parameters instead of the measured NMR parameters actually resulted in more accurate predictions of total mass release. It is anticipated, however, that for some unusual coals actual structural parameters derived from actual ¹³C NMR analysis will be needed to achieve reliable predictions of volatiles yields by the CPD model.

The second set of test cases consisted of total volatiles and tar yields for 17 coals used in devolatilization experiments by Xu and Tomita.²⁸ Xu and Tomita used a Curie-point pyrolyser to heat samples at 3000 K/s to 1037 K with a 4 second residence time at that temperature. NMR data are not available for this set of coals. Table 4.7 lists the coals used by Xu and Tomita, the corresponding ultimate analysis data, and the four structural parameters estimated by the correlations.

None of the structural parameters estimated by the correlations seem unreasonable (e.g., values of M_{cl} fell within known limits for all coals studied). Figure 4.5 shows the predicted and measured mass and tar release versus percent carbon in the parent coal. Appendix D lists the measured and predicted values of mass release and tar yields for the

17 coals used by Xu and Tomita. The predicted mass release and tar yields compare well with the values and trends of the corresponding measured yields for most of the coals tested. Average relative errors between the predicted values and the measured values were 13% for mass release and 20% for tar release. Overall, there does not appear to be a positive or negative bias in the error.

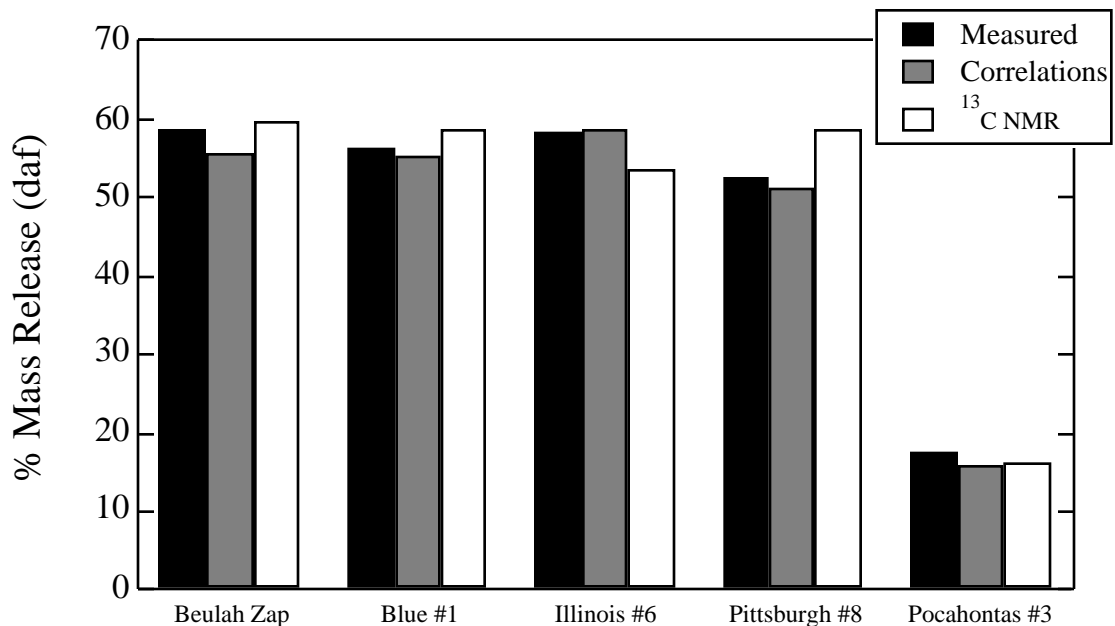


Figure 4.4. Comparison of CPD predictions with measured total mass release. The measured values refer to flat flame burner experiments conducted at Sandia, NMR values refer to CPD predictions of mass release using actual NMR structural parameters, and the correlation values correspond to CPD predictions of mass release using the correlated structural parameters.

The CPD model, however, over-predicted total mass release for coals in the range of 80 % to 84 % dry-ash free carbon content (Hunter Valley, Liddell, Newvale). The mass release measured by Xu and Tomita for the coals in this range seem low compared to total volatiles yields measured by other investigators for similar coals and similar conditions.^{1, 15, 16, 48, 52} This suggests that the Hunter Valley, Liddell, and Newvale samples are particularly unusual coals, or there was some error in the experimental

Table 4.7**Elemental Composition and Correlated Chemical Structure of Coals Used in Pyrolysis Experiments
Conducted by Xu and Tomita²⁸**

coal	% C (daf)	% H (daf)	% O (daf)	% N (daf)	% S (daf)	ASTM VM (daf)	<i>M</i>	<i>M_{cl}</i>	<i>P₀</i>	+ <i>I</i>
Yallourn	65.4	4.9	28.8	0.6	0.3	54	50	340	0.68	4.1
Rhein Braun	65.8	5.5	27.6	0.8	0.3	56	52	388	0.60	4.0
Morwell	67.4	5.0	26.8	0.5	0.3	53	48	343	0.64	4.4
Velva	69.1	4.8	23.9	1.4	0.6	52	47	335	0.62	4.6
Soyakoishi	70.2	5.2	22.4	1.8	0.2	46	47	369	0.58	4.6
South Beulah	71.8	4.7	19.2	1.4	2.9	45	44	349	0.59	4.9
Colowyo	74.0	5.0	18.6	1.9	0.4	39	41	351	0.59	5.0
Taiheiyo	76.0	6.5	16.0	1.2	0.3	56	46	529	0.36	4.9
Millmerran	76.9	6.6	15.4	0.5	0.6	55	45	547	0.34	4.9
Wandoan	78.5	5.8	14.4	0.9	0.4	50	39	395	0.47	4.9
Hunter Valley	80.3	5.0	12.2	2.0	0.4	37	33	323	0.57	5.1
Liddell	83.5	5.4	8.4	2.1	0.6	38	30	342	0.53	4.9
Newvale	84.2	5.0	8.9	1.4	0.5	34	28	297	0.59	4.8
Yubari Shinko	86.9	5.6	5.2	1.9	0.3	41	27	338	0.51	4.6
Vicary Creek	87.8	4.7	5.0	2.1	0.4	25	21	266	0.67	4.6
Keystone	89.4	4.4	3.2	2.2	0.8	17	16	251	0.76	4.4
Hongay	93.8	3.0	1.4	1.3	0.5	8	10	285	0.92	4.0

determination of the total volatiles yields for these coals in the study conducted by Xu and Tomita. Recently, an investigator conducted a pyrolysis experiment on a Hunter Valley coal at conditions similar to those used by Xu and Tomita, and measured a total volatiles yield of 48% (daf).⁵³

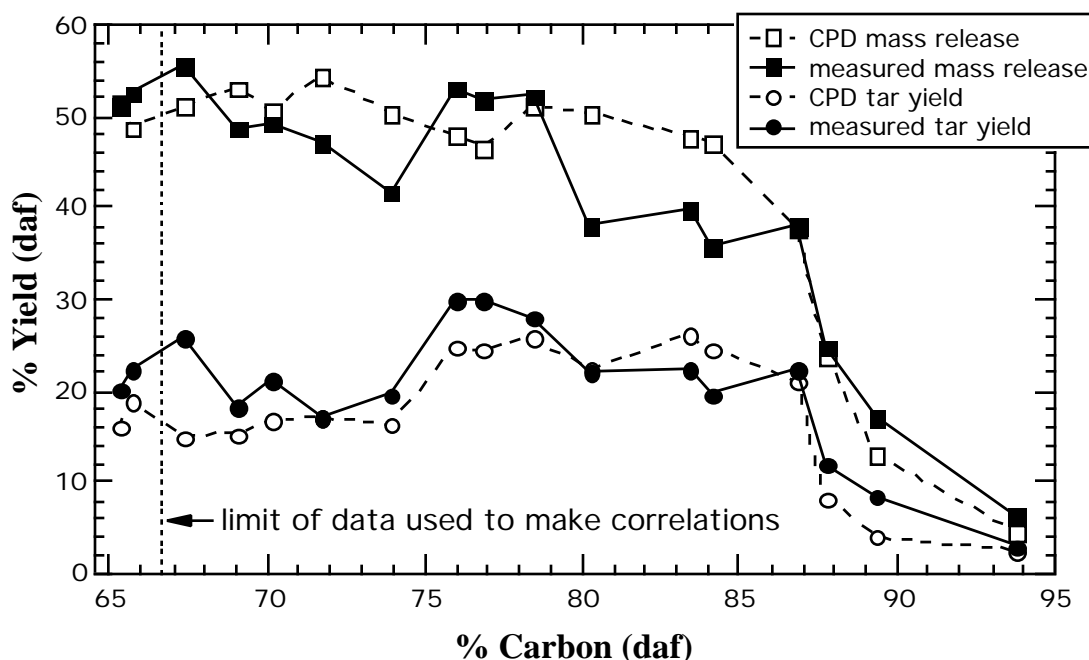


Figure 4.5 Comparison of CPD predictions with measured total mass release and tar yields. The measured values refer to the Curie-point pyrolyser experiments performed by Xu and Tomita.²⁸ CPD mass release and CPD tar yield refer to the CPD predictions using structural parameters estimated by the correlations developed in this research. The dotted line at 66.6 % C (daf) shows the lower boundary of the original data set. The upper bound is 95.4 % C (daf).

Discussion of NMR Correlation

Non-linear correlations were developed to model the average structural characteristics of coal as a function of elemental composition and ASTM volatile matter content. The coefficient of determination, r^2 , is a measure of how well the correlation explains the variation in the dependent variable as a function of the independent variables. The r^2 values for these correlations were 0.94, 0.72, 0.88, and 0.62 for M , M_{cl} , p_0 , and

+I, respectively. Reasonable estimations of ^{13}C NMR structural parameters for most coals can be expected using the correlation. However, it is expected that these correlations, just like any correlation, will not work well for some unusual coals.

The *non-linear* modified quadratic correlation of ^{13}C NMR measurements of coal structure with ultimate analysis and volatile matter content seems to be an appropriate method to estimate the coal structure input parameters for network devolatilization models, such as the CPD model. The correlation, combined with the CPD model, appears to work well in predicting total volatiles and tar yields for low to high rank coals. Although one of the principal motives for this study has been the estimation of the input parameters for the CPD model, the estimated structural parameters should be useful in other applications, and a similar approach could be used to develop predictive models for other structural parameters.

Chapter 5. Modeling Volatile Nitrogen Release

Currently, low-NO_x burners are designed using empirical relationships to describe the amount of nitrogen released during devolatilization. Comprehensive coal combustion models that calculate the amount of NO_x present during coal combustion, such as PCGC-3 (Pulverized Coal Gasification and Combustion, 3-dimensional), currently require the user to specify of the amount of nitrogen released during devolatilization.⁵⁴ In order to design more efficient low-NO_x burners and to improve the accuracy of the NO_x concentration predictions by comprehensive combustion codes, it will be necessary to accurately model the amount and form of nitrogen released during coal pyrolysis.

A model that predicts the amount and distribution between tar and light gas of nitrogen released during devolatilization has been developed and incorporated into the Chemical Percolation Devolatilization (CPD) model.⁴ The model is limited to nitrogen release during primary pyrolysis, and assumes that all light gas nitrogen is HCN. Model predictions of nitrogen release compared well with measured values for most coals and devolatilization conditions tested.

Evaluation of Nitrogen Release Data

A number of investigators have conducted pyrolysis experiments in an effort to characterize the temperature, time, and rank dependence of volatile nitrogen release. Of particular interest to this study are experiments in which the chemical structure of matching sets of coal and char were determined by ¹³C NMR spectral analyses. Studies examining the chemical structure of matching sets of coal and char samples using ¹³C NMR analyses have been conducted by Fletcher and Hardesty,⁴⁸ Watt,¹⁵ and Hambly.¹⁶

This study represents the first time that ^{13}C NMR analyses of the chemical structure of coal and char have been used to help evaluate a model of volatile nitrogen release.

Figure 5.1 is a diagram illustrating primary volatile nitrogen release. During pyrolysis, some of the nitrogen contained in the aromatic clusters of the metaplast are released with the tar. This is often the most significant form of nitrogen release. At higher temperatures ($> 1050\text{ K}$) additional nitrogen is released in the form of HCN due to the rupture of nitrogen containing aromatic rings in the char. Nitrogen released with the tar and nitrogen released from the char as HCN make up what is called primary volatile nitrogen release. Secondary nitrogen transformations in the tar can lead to additional HCN, but are not treated in this study.

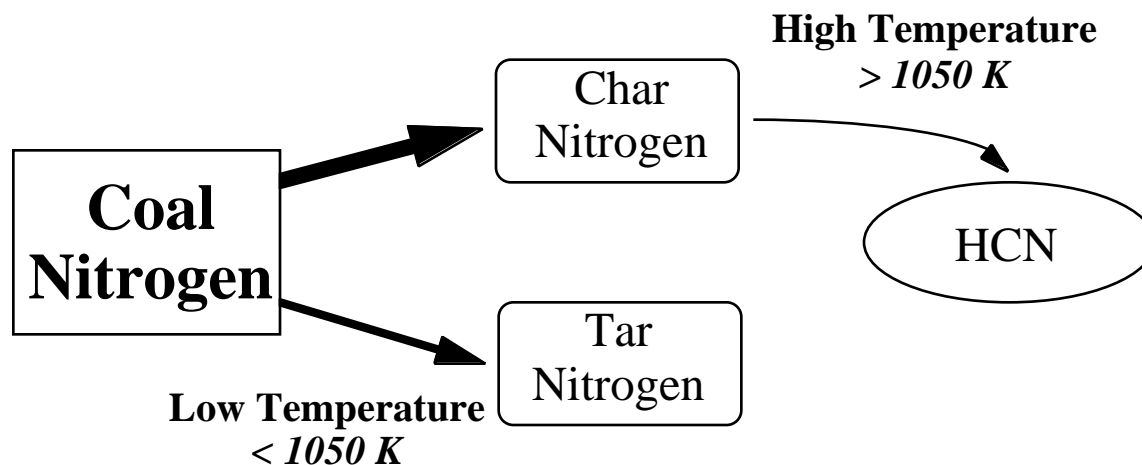


Figure 5.1. Diagram of hypothetical primary volatile nitrogen release steps

Total nitrogen release can be easily calculated from the measured char yield (m_{char}) and the mass fraction of nitrogen in the parent coal, N_{coal} , and in the char, N_{char} . The fraction of nitrogen released during pyrolysis, NR , is calculated as follows, where m_{coal} is the mass of the original coal sample (all of the parameters are on a dry-ash free basis):

$$NR = 1 - \frac{N_{char} m_{char}}{N_{coal} m_{coal}} \quad (5.1)$$

It is useful to define an aromatic site as an aromatic cluster minus the aliphatic side chains and bridge materials. By assuming that the molecular weight per aromatic site, M_{site} , is constant during pyrolysis, the amount of nitrogen released from the char as light gas can be determined. N_{site} is the average mass fraction of nitrogen per aromatic site, and is calculated from the mass fraction of nitrogen in the char (N_{char}) and ^{13}C NMR spectral analysis of the char :

$$N_{site} = N_{char} \frac{M_{cl}}{M_{site}} \quad (5.2)$$

where M_{cl} is the measured molecular weight per cluster in the char. M_{site} is calculated by subtracting the aliphatic material from the cluster as follows:

$$M_{site} = M_{cl} - (n + 1)M \quad (5.3)$$

where M is the average molecular weight per side chain in the char, and $n + 1$ is the number of attachments per cluster.

N_{site} decays during high temperature pyrolysis as nitrogen atoms are released from the char. By comparing the value of N_{site} in the coal and char, the mass of nitrogen released as light gas can be determined. The mass of nitrogen transported from the coal with the tar during primary pyrolysis is the difference between total nitrogen release and light gas nitrogen release. Secondary pyrolysis reactions of the tar make it difficult to determine directly the amount of nitrogen released with the tar.

Nitrogen release trends from pyrolysis experiments in which ^{13}C NMR analyses were conducted on matching sets of coal and char were analyzed in this study. Table 5.1 lists the investigators who have compared coal and char chemical structure using ^{13}C NMR spectroscopy. Table 5.1 also lists the coals that were pyrolyzed and the pyrolysis conditions.

Table 5.1

List of Pyrolysis Experiments Examined for Nitrogen Release Trends

Set	Investigator(s)	Coals (rank)	Reactor; residence time; peak gas temp; approximate heating rate
1	*Fletcher and Hardesty ⁴⁸	Beulah Zap (lig), Blue #1 (subB), Illinois #6 (hvbB), Pittsburgh #8 (hvaB), Pocahontas #3 (lvbB)	^a drop tube; 250 ms; 1050 K; 10 ⁴ K/s ^b drop tube; 240 ms; 1250 K; 10 ⁴ K/s ^c FFB (flat-flame burner); 47 ms; 1600 K; 10 ⁵ K/s
2	Hambly ¹⁶	Beulah Zap(lig), Blue #1 (subB), Illinois #6 (hvbB), Pittsburgh #8 (hvaB), Pocahontas #3 (lvbB)	drop tube; 280 ms; 1080 K; 10 ⁴ K/s

* A number of papers have been published on this set of data.^{1, 14, 55-57} The report published by Fletcher and Hardesty⁴⁸ represents a convenient compilation of this data set, and therefore was referenced throughout this project.

Rank and Temperature Dependence

Some investigators have reported a weak rank dependence of light gas nitrogen release.^{17, 30, 45} Low rank coals are thought to release nitrogen from the char as HCN more readily than high rank coals. Figure 5.2 compares the percent N_{site} decay that occurred in the chars during the pyrolysis experiments conducted by Fletcher and Hardesty in a drop-tube reactor (sets 1a & 1b). The percent decay of N_{site} is an indicator of the quantity of HCN (or light gas nitrogen) that has evolved during pyrolysis. The decay of N_{site} during the experiments of Fletcher and Hardesty does not seem to correlate with rank. Figure 5.3 Compares the percent decay of N_{site} in the chars pyrolyzed by Hambly (set 2). The decay of N_{site} in the chars collected by Hambly indicate that the decay of N_{site} is similar in lignites and bituminous coals. However, the decay of N_{site} in the Pocahontas #3 char, a low volatile bituminous coal, was significantly less than in the other chars.

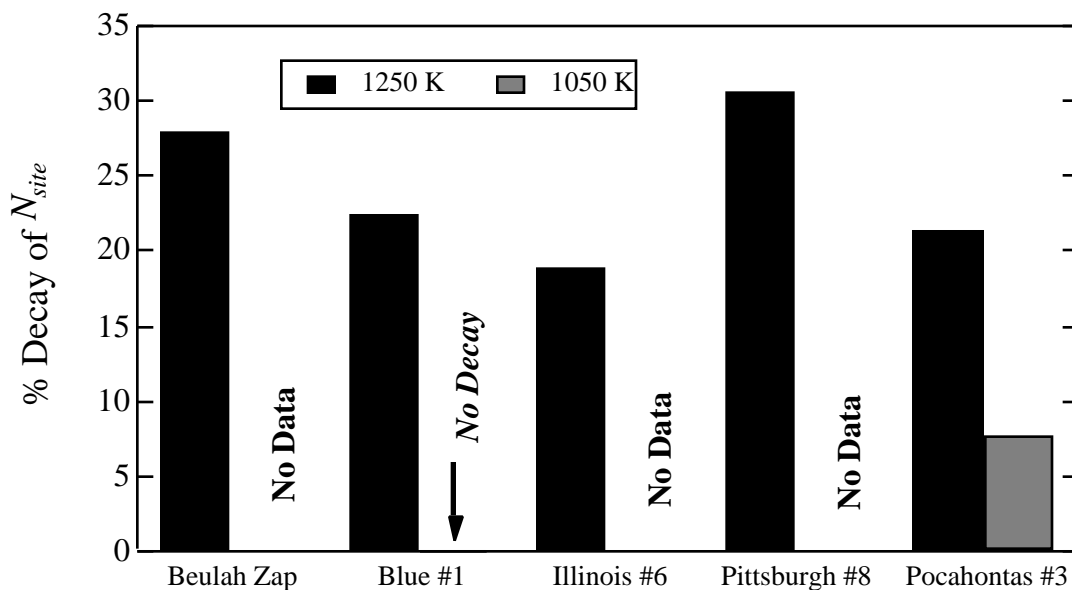


Figure 5.2. Comparison of the percent decay of N_{site} calculated from experimental pyrolysis data collected by Fletcher and Hardesty (sets 1a & 1b) and ^{13}C NMR analyses of the chemical structure of the matching sets of coals and chars. ^{13}C NMR analyses were not conducted on the Beulah Zap, Illinois #6, and Pittsburgh #8 chars. No change in N_{site} was observed in the Blue #1 char at the 1050 K condition.

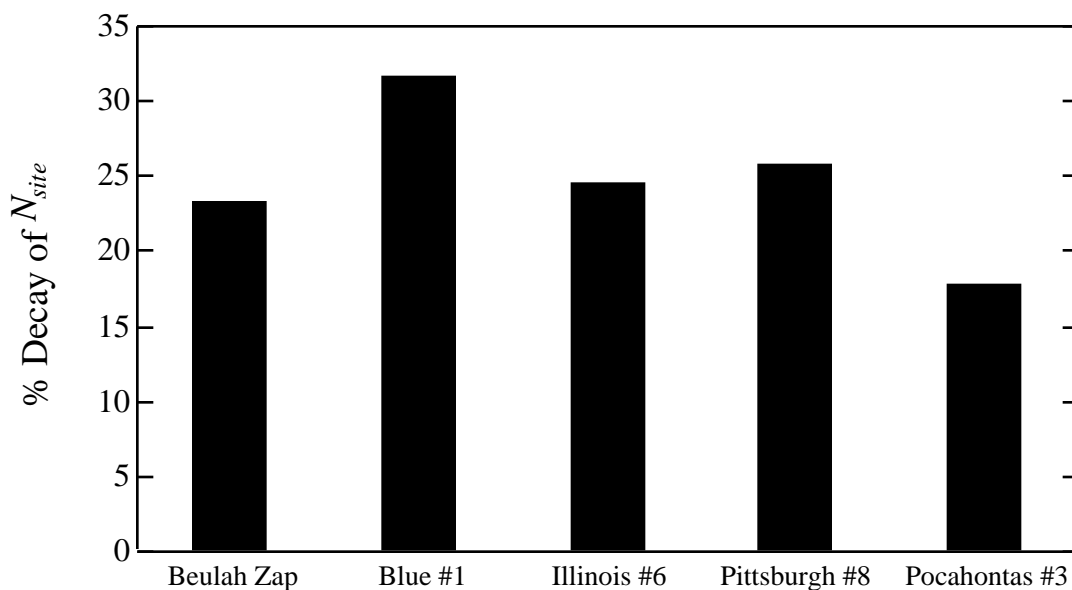


Figure 5.3. Comparison of the percent decay of N_{site} calculated from experimental pyrolysis data collected by Hambly (set 2) and ^{13}C NMR analyses of the chemical structure of the matching sets of coals and chars.

N_{site} decay trends in the chars produced by Fletcher and Hardesty (Figure 5.2) also indicate some temperature dependence. Unfortunately, ^{13}C NMR analysis was only performed on two of the char samples from the 1050 K drop tube condition. Regardless, the comparison of N_{site} decay in the two chars (Blue #1 and Pocahontas #3) from the 1050 K and 1250 K drop tube conditions is useful since both conditions had approximately the same residence time. Both chars produced at the 1050 K condition had much less N_{site} decay than at the 1250 K condition, indicating that as the temperature increases, N_{site} decay generally increases.

Time Dependence

Figure 5.4 compares N_{site} decay in the chars produced by Fletcher and Hardesty in a drop tube reactor at 1250 K (set 1a) and in a FFB with a peak gas temperature of about 1600 K (set 1c). Figure 5.5 compares the total mass release of the five coals pyrolyzed in the drop tube and FFB reactors. Total mass release was slightly higher in the FFB than in the drop tube reactor for all but one of the coals studied. It is interesting to note that in each case for which data exists, N_{site} decay was considerably lower in the FFB than in the drop tube reactor. This is puzzling since drop tube conditions are less severe than in the FFB. A possible explanation for this trend is the difference in residence times of the drop tube experiments (~240 ms) and the FFB experiment (~47 ms). It appears that at the temperatures being considered here (1250 K - 1600 K), N_{site} decay occurs on a much slower time scale than total mass release. It is reasonable to believe that if the residence time of the FFB experiment were increased, N_{site} decay would approach or surpass the levels attained in the 1250 K drop tube experiments.

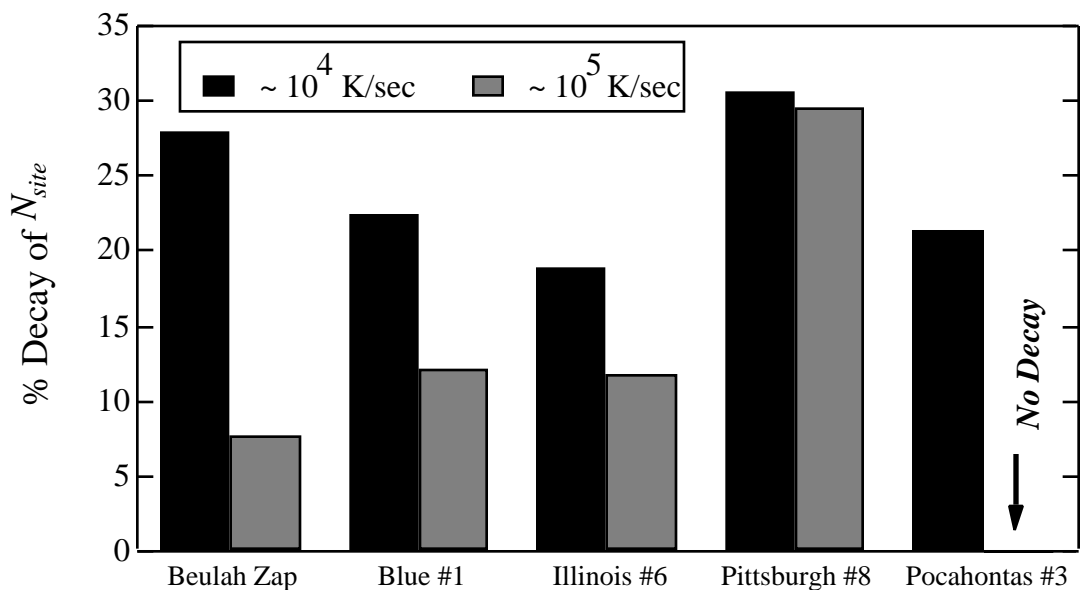


Figure 5.4. Comparison of the percent decay of N_{site} calculated from experimental pyrolysis data collected by Fletcher and Hardesty⁴⁸ in a drop tube reactor with a peak temperature of 1250 K and a FFB with a peak temperature of 1600 K (set 1).

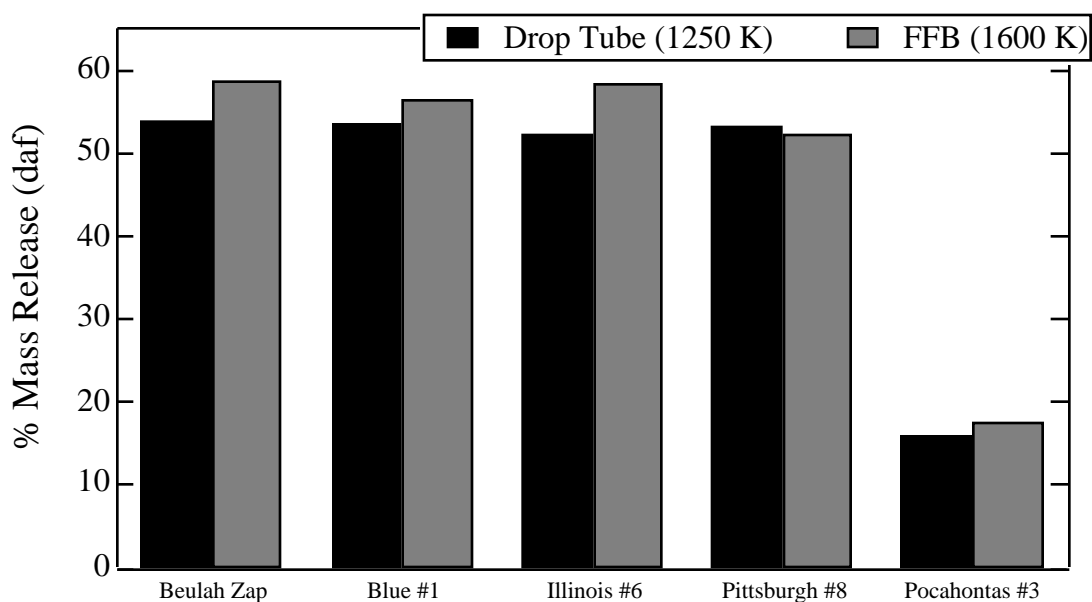


Figure 5.5. Comparison of total mass release from the five coals pyrolyzed by Fletcher and Hardesty⁴⁸ in a drop tube reactor with a peak temperature of 1250 K and a FFB with a peak temperature of 1600 K (set 1).

Model Theory and Development

It is thought that nitrogen is released during primary devolatilization in two ways (refer to Figure 5.1):^{17, 45} (i) nitrogen contained in the aromatic clusters is transported away as tar molecules escape the infinite matrix (this is often the primary mode of nitrogen release during devolatilization); and (ii) additional nitrogen can be released as light gas at high temperatures (thought to be primarily HCN) from the thermal rupture of aromatic rings containing nitrogen heteroatoms

In this work, a volatile nitrogen release model was developed and incorporated into the CPD model. The model developed in this study is based on the same assumptions used in the FG-DVC and FLASHCHAIN nitrogen release models as discussed in Chapter 2. This study, however, represents the first time that detailed chemical structural data produced by solid-state ¹³C NMR spectral analyses of the chemical structure of coal have been used to develop and evaluate a volatile nitrogen release model. The model predicts the amount of nitrogen released with tar, the amount of nitrogen released as light gas by the rupture of aromatic rings, and the nitrogen content of the char. Nitrogen which is released with tar was modeled by developing a simple scheme to account for the nitrogen transported from the coal matrix with the tar. Nitrogen released with the tar is the dominant mechanism of nitrogen release for many coals and devolatilization conditions. Additional nitrogen release, in the form of light gas, which results from the thermal rupture of aromatic rings containing nitrogen heteroatoms, was modeled by a first order Arrhenius rate equation with a distributed activation energy.

In addition to the assumptions already made in the CPD model, the following assumptions regarding the chemical structure of coal, char, and tar were made throughout the nitrogen release model development process:

1. Nitrogen atoms are randomly distributed throughout the aromatic sites in the coal.

2. Ring opening reactions have a negligible effect on average cluster size (aromatic site molecular weight is constant) since nitrogen content is small.
3. The average chemical structural parameters and composition of the tar released at a given time is identical in chemical structure and composition to the char.
4. At any instant, the mass of nitrogen per site, N_{site} , in the evolving tar is equal to the mass of nitrogen per cluster in the char. Combining assumptions 3 and 4 indicates that $N_{tar} = N_{char}$ at any instant in time.

The nitrogen release model developed in this study is limited to describing primary nitrogen release (refer to Figure 5.1). In this work, primary nitrogen release refers to (i) nitrogen transported from the macromolecule with the tar, and (ii) nitrogen released as light gas (HCN) from the char due to the thermal rupture of nitrogen containing aromatic rings. Secondary nitrogen transformations are not treated in the current study.

Light Gas Nitrogen

Nitrogen released as light gas originates from the thermal rupture of nitrogen-containing aromatic rings in the char. The exact mechanism by which thermal rupture of nitrogen containing rings occurs has not yet been established. It has been shown that there are a number of different nitrogen functional groups in coal.^{15, 18-22} Furthermore, the sizes of the aromatic clusters in a given coal vary greatly. The stability of a nitrogen atom is likely affected by the size of the cluster in which it is located, due to electron resonance structural considerations. Therefore, it is reasonable to assume that a distribution of activation energies will be necessary to describe light gas nitrogen release from the char. It is proposed that the decay of nitrogen contained in the aromatic sites of

the char (believed to result in HCN) at each time step can be described by a simple first order Arrhenius rate expression with a distributed activation energy:

$$\frac{dN_{site}}{dt} = A \exp \frac{-E}{RT} N_{site} \quad (5.4)$$

where N_{site} is the mass fraction of nitrogen in an aromatic site, E is the activation energy, R is the universal gas constant, and T the absolute temperature. E is distributed according to a normal distribution as follows:

$$E = E_o + x \sigma_E \quad (5.5)$$

where E_o is the mean activation energy and σ_E is the standard deviation of the activation energy. The term x is the inverse of the area under the normal distribution curve which is calculated using a tabulated error function solution based on the conversion of N_{site} .⁴ The kinetic parameters, A , E_o , and σ_E , were empirically fit to best match the experimental data on nitrogen release and N_{site} decay during pyrolysis as reported by Fletcher and Hardesty.⁴⁸

In order to model nitrogen release in the manner just described, it is critical that N_{site} be accurately calculated. Determination of the initial value of N_{site} is dependent on ¹³C NMR measurements of the chemical structure of coal according to:

$$N_{site_0} = N_{coal} \frac{M_{c_0}}{M_{site}} \quad (5.6)$$

where N_{coal} is the dry, ash, free nitrogen content of the coal, M_{site} is the molecular weight per site (which is constant), M_{c_0} is the initial average molecular weight per cluster in the coal as determined by ¹³C NMR analysis. M_{site} is calculated using measurements of coal structure as determined by ¹³C NMR data according to equation 5.3.

At sufficiently high pyrolysis temperatures, N_{site} begins to decay. N_{site} is calculated by integrating equation 5.4 over time in the CPD model using a modified Eulerian approach, including a predictor-corrector. Since aliphatic side chains and bridges are cleaved throughout devolatilization, a new M_{cl} must be calculated at each time step (specified below by the subscript i). The CPD model already keeps track of the number of side chains and bridges that still contain a significant amount of aliphatic material; therefore, M_{cl} can be calculated by the following simple equation:

$$M_{cl_i} = M_{site} + (c_0 + \ell_i + s_i)(N_{site} + 1)M \quad (5.7)$$

where c_0 is the fraction of initial attachments per cluster that are stable bridges, ℓ is the fraction of labile bridges, and s is the fraction of initial attachments that are side chains. The nitrogen content of the char can be calculated by converting N_{site} to a per cluster basis as follows:

$$N_{char_i} = N_{site} \frac{M_{site}}{M_{cl_i}}, \quad (5.8)$$

and since it is assumed that the nitrogen is evenly distributed among the aromatic sites and that the chemical structure of the metaplast and char are equal at any given moment during devolatilization, $N_{tar_i} = N_{char_i}$.

In order to determine the total amount of nitrogen released as light gas during devolatilization, the quantity of nitrogen released at each time step must be determined. The mass of nitrogen released from the char as light gas at each time step is proportional to the char yield, according to:

$$gas_{nit_i} = f_{char_i} N_{char_i} \quad (5.9)$$

where gas_{nit_i} is the differential fraction of coal nitrogen released as light gas during time step i , and f_{char} is char yield. The total fraction of coal nitrogen released as light gas up to time step i is determined by integrating equation 5.9 over time.

Nitrogen Released with Tar

The nitrogen transported away from the infinite matrix with the tar during time step i is calculated as follows:

$$tar_{nit_i} = N_{tar_i} tar_i \quad (5.10)$$

where tar_{nit_i} is the mass of nitrogen transported with the tar during time step i , N_{tar} equals N_{char} , and tar_i is the mass of tar released during time step i . The total mass of nitrogen transported with the tar is calculated by integrating equation 5.10 .

Fraction of Stable Nitrogen

During the course of this modeling effort, it became apparent that the temperature and time dependence of nitrogen release in the form of light gas would be difficult to model with simple first order kinetics as described above. A broad range of kinetic parameters (A , E_0 , and τ) was tested. It was easy to fit the kinetic parameters such that the nitrogen release model predictions matched the experimental data for one set of coals at one condition. However, it proved difficult, if not impossible, to adjust the kinetic parameters so that the model gave accurate predictions at different pyrolysis conditions, for example, heating rates of 10^4 K/s and 10^5 K/s.

The data on nitrogen release during devolatilization discussed previously suggest that the rate of light gas nitrogen release from the char has a slight rank dependence, which becomes more pronounced for high rank coals. Lignites seem to have a *slightly* greater propensity for light gas nitrogen release than bituminous coals. Low volatile bituminous

coals appear to have a much lower propensity for light gas nitrogen release than lignites or bituminous coals. A simple first order kinetic model is not adequate to simulate this trend.

The nitrogen release data examined in this study suggested that a fraction of nitrogen bound in the coal may be stable at the conditions of typical pyrolysis experiments. It is unclear whether this fraction of nitrogen atoms is already stable in the parent coal (perhaps due to the nitrogen bound in sites with a large number of rings), or becomes stable through some chemical reaction during devolatilization.

The hypothesis that a fraction of coal nitrogen is stable at common devolatilization conditions was tested in our nitrogen model as part of this research. It was determined that by assuming that a fraction of the nitrogen is stable, considerable improvement in the model predictions at various conditions could be achieved. Therefore, a rough correlation for the estimated fraction of stable nitrogen was developed based on coal rank.

Nitrogen Model Parameters

The kinetic parameters of the nitrogen model were determined empirically by adjusting A , E_0 , E , and f_{st} (the fraction of stable nitrogen) such that the model predictions of nitrogen release best fit experimental nitrogen release data from devolatilization experiments conducted by Fletcher and Hardesty in 1991 (set 1).⁴⁸ Because Fletcher and Hardesty performed devolatilization experiments on five coals of varying rank at two different heating rates ($\sim 10^4$ K/s and $\sim 10^5$ K/s) their results were useful in determining the appropriate rank and temperature dependence of the nitrogen release model. ^{13}C NMR analyses of matching sets of coal and char were performed for devolatilization experiments at many different residence times. Therefore, model predictions of N_{site} could be compared directly with the corresponding experimental values, which was very useful in evaluating the accuracy of the nitrogen release model.

The rate parameters which were determined to give a reasonable fit of the data are given in Table 5.2.

Table 5.2

Rate Parameters Used in Nitrogen Model

Parameter	Value	Description
E	100 kcal/mole	Ring rupture activation energy
A	$9 \times 10^{17} \text{ s}^{-1}$	Ring rupture frequency factor
	17 kcal/mole	Standard deviation for distributed E

The rate parameters listed in Table 5.2 represent one combination of values that seemed to adequately model the decay of N_{site} for a wide variety of conditions. Because an empirical approach was taken in determining these rate parameters, as opposed to a mechanistic approach, the absolute values of the rate parameters may have little physical significance. In fact, it is quite possible that a different combination of parameters would be equally adequate at simulating N_{site} decay. The high activation energy of 100 kcal/mole for N_{site} decay, however, is not unreasonable. The activation energy for bridge cleavage, for example, is 65 Kcal/mole in the CPD model. It seems appropriate that the activation energy for N_{site} decay would be significantly higher (100 kcal/mole) since N_{site} decay involves the thermal rupture of heteroaromatic rings at elevated temperatures.

It is interesting to compare the rate parameters for N_{site} decay resulting from this study to the rate parameters used in the FG-DVC model for HCN release. The mean activation energy, pre-exponential factor, and the standard deviation for the activation energy for HCN release in the FG-DVC model are 84.5 kcal/mole, $6.9 \times 10^{12} \text{ s}^{-1}$, and 9.4 kcal/mole, respectively. The differences between the rate parameters for N_{site} decay in the

CPD model and HCN release in the FG-DVC model do not seem unreasonable since the approaches used to model HCN release in the two devolatilization models are significantly different.

The fraction of stable nitrogen, f_{st} , was correlated with rank, using the dry, ash free carbon content as an indicator of rank resulting in Equation 5.12 where C is the dry,

$$f_{st} = \max\{0.5, 0.018(\%C, daf) - 1.062\} \quad (5.11)$$

ash, free percent carbon of the coal. For low and medium rank coals f_{st} is constant at 0.5. For higher rank coals, f_{st} increases linearly with carbon content. This is consistent with the experimental data on the decay of N_{site} , which suggests that N_{site} decays similarly in low and medium rank coals, but decays significantly less in high rank coals.

Application of Nitrogen Release Model

Description of Test Cases

The CPD model was used to predict the nitrogen release of several different coals during devolatilization at several different experimental conditions. Table 5.3 lists the researchers who conducted the experiments, the coals used, and the conditions of the experiments. CPD model predictions of total mass release, tar release, nitrogen release, N_{char} , and N_{site} were compared with experimental results for test sets 1 through 3. Due to the large number of test cases examined, only a brief summary of the most important results will be given here. Figures summarizing the results of test cases 1-3 that are not included in the main body are given in Appendix E.

Table 5.3.

Description of Sets of Test Cases Used in Model Evaluation

Set	Researcher(s)	Coals (rank)	Reactor; residence time; peak gas temp; approximate heating rate
1	Fletcher and Hardesty ⁴⁸	Beulah Zap (lig), Blue #1 (subB), Illinois #6 (hvbB), Pittsburgh #8 (hvaB), Pocahontas #3 (lvbB)	^a drop tube; 250 ms; 1050 K; 10 ⁴ K/s. ^b drop tube; 240 ms; 1250 K; 10 ⁴ K/s. ^c FFB (flat-flame burner); 47 ms; 1600 K; 10 ⁵ K/s.
2	Chen ⁵²	Dietz (subB), Illinois #6 (hvaB), Pittsburgh #8 (hvaB), Lower Kittanning (lvB)	drop tube; 56, 61, 66, 72, 77, 83, 86.5, and 89 ms; radiantly heated particles (1840 K wall temperature); 10 ⁴ K/s.
3	Hambly ¹⁶	Beulah Zap (lig), Blue #1 (subB), Illinois #6 (hvbB), Pittsburgh #8 (hvaB), Pocahontas #3 (lvbB)	^a drop tube; 170 ms; 820 K; 10 ⁴ K/s. ^b drop tube; 280 ms; 1080 K; 10 ⁴ K/s. ^c drop tube; 410 ms; 1220 K; 10 ⁴ K/s. ^d FFB; 18 ms; 1560 K, 10 ⁵ K/s.

Comparisons with Data From Fletcher and Hardesty⁴⁸

In general, the predictions of N_{site} and N_{char} compared well with the experimental data collected by Fletcher and Hardesty.⁴⁸ Figure 5.6 is an example of a Blue #1 coal pyrolyzed in a drop tube reactor by Fletcher and Hardesty with a peak temperature of 1050 K (set 1a). The experimental data suggest that there is little or no N_{site} decay at this condition. Only a small amount of N_{site} decay is predicted by the model. Predictions of N_{char} compare well with the measured values. The increase in N_{char} is due to the loss of aliphatic side chain material which does not contain nitrogen. Figure 5.7 is an example of a Blue #1 coal pyrolyzed in a drop tube reactor with a peak temperature of 1250 K (set

1b). Predictions of N_{site} and N_{char} compare well with the experimental values at this condition. Notice that by using a distributed activation energy function, the diminishing rate of N_{site} decay during late pyrolysis is accurately modeled. It is also important to note that the model is able to predict the trend of increasing N_{site} decay with increasing temperature. Similar agreement was achieved with data from other coals examined by Fletcher and Hardesty (see Appendix E, Figures E.1-E.8).

This work represents the first time that a nitrogen release model has been evaluated by comparing model predictions with the detailed chemical structure of char as determined by ^{13}C NMR analysis. As described previously, N_{site} is determined experimentally based on the nitrogen content of the char and the chemical structure of the char from ^{13}C NMR spectral analysis. By comparing predicted and measured N_{site} values, the ability of the model to predict HCN release is evaluated directly, and the ability of the model to accurately simulate changes in the chemical structure of the char during pyrolysis is implied.

Figures 5.8 and 5.9 compare model predictions of total mass and nitrogen release with experimental data for a Blue #1 coal pyrolyzed by Fletcher and Hardesty in a drop tube reactor with peak temperatures of 1050 K and 1250 K (sets 1a & 1b). Similar agreement was achieved with data from other coals examined by Fletcher and Hardesty (see Appendix E, Figures E.9-E.16).

It was observed that when the CPD model predictions of total mass release compared well with experimental data, model predictions of nitrogen release also compared well. When the CPD model over-predicted or under-predicted mass release, nitrogen release was also under or over-predicted by about the same amount. This is an indication that the model describing nitrogen release at the conditions of these experiments is mechanistically correct.

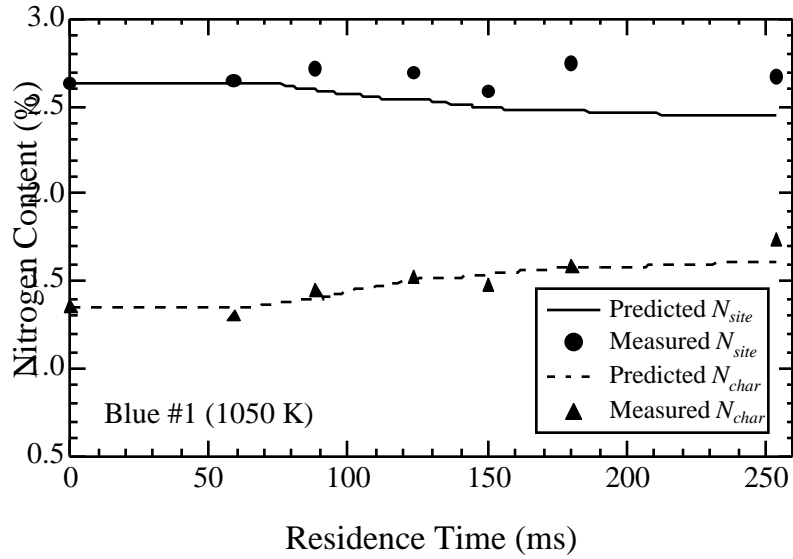


Figure 5.6. Comparison of predicted and measured N_{char} values of a Blue #1 subbituminous coal. Blue #1 was pyrolyzed in a drop tube reactor with a peak temperature of 1050 K and a residence time of 250 ms.⁴⁸

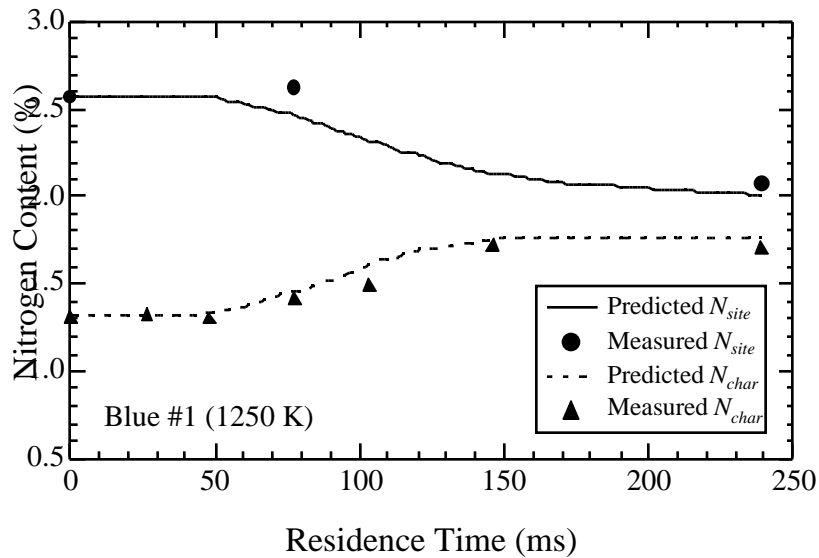


Figure 5.7. Comparison of predicted and measured N_{site} and N_{char} values of a Blue #1 subbituminous coal. Blue #1 was pyrolyzed in a drop tube reactor with a peak temperature of 1250 K and a residence time of 240 ms.⁴⁸

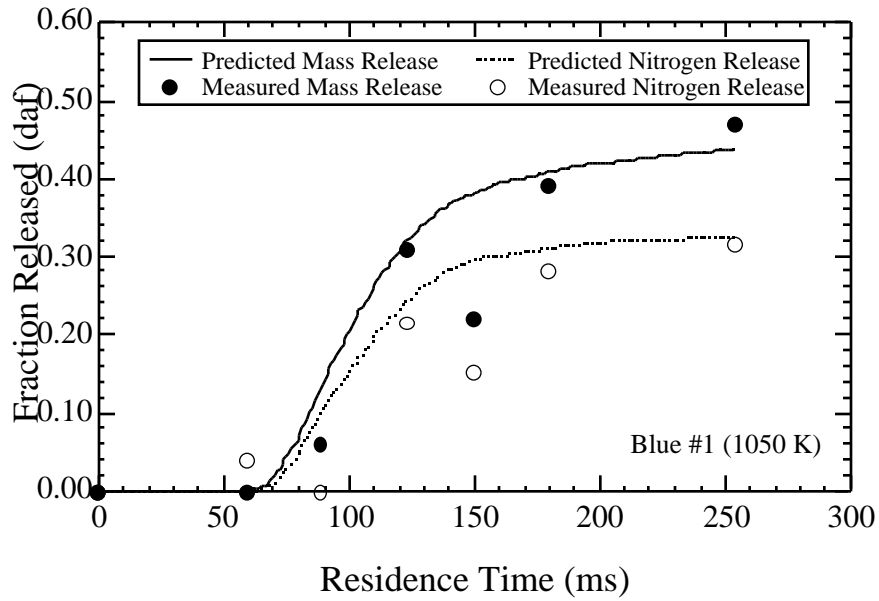


Figure 5.8. Comparison of predicted and measured fractional mass and nitrogen release of a Blue #1 high volatile bituminous coal. Blue #1 was pyrolyzed in a drop tube reactor with a peak temperature of 1050 K and a residence time of 250 ms.

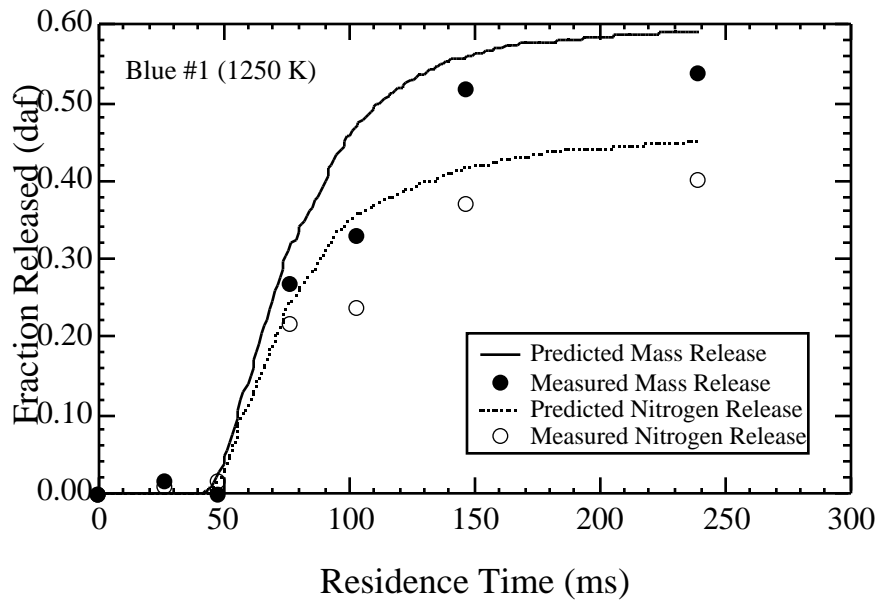


Figure 5.9. Comparison of predicted and measured fractional mass and nitrogen release of a Blue #1 high volatile bituminous coal. Blue #1 was pyrolyzed in a drop tube reactor with a peak temperature of 1250 K and a residence time of 240 ms.

Fletcher and Hardesty conducted pyrolysis experiments on five coals in a flat-flame burner with a heating rate of about 10^5 K/sec and a peak gas temperature of about 1600 K (set 1c). Figure 5.10 compares CPD model predictions of fractional mass and nitrogen release with experimental data obtained in the flat-flame burner. With the exception of Pocahontas #3, model predictions of mass and nitrogen release compared well with experimental data. Figure 5.10 is important because it shows the nitrogen model is able to pick up variations in nitrogen release due to differences in temperature and heating rate.

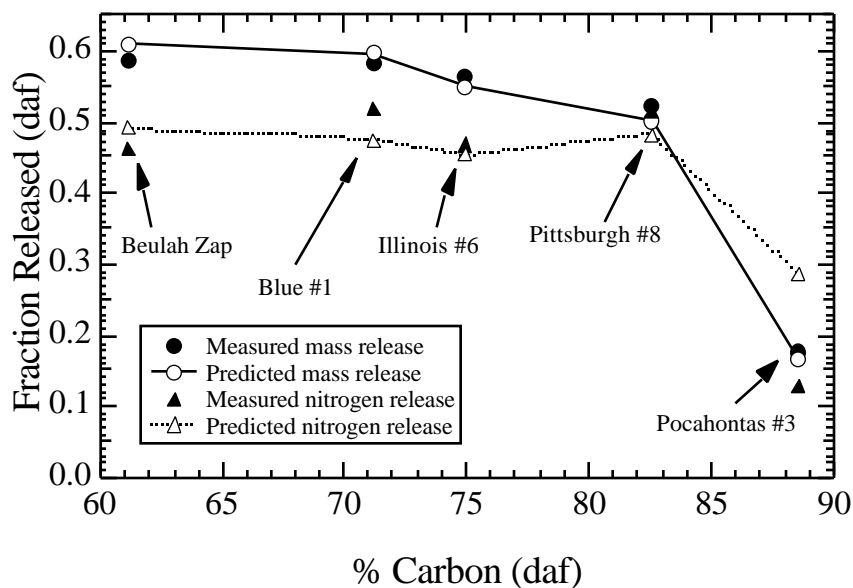


Figure 5.10. Comparison of CPD model predictions of mass and nitrogen release with experimental data for coals pyrolyzed in a flat-flame burner by Fletcher and Hardesty.⁴⁸ Carbon content is used as a rank indicator.

Comparisons with Data Reported by Chen

Chen⁵² pyrolyzed four coals to various degrees in a radiatively heated drop tube reactor (set 2). Since careful measurements of tar and light gas release were taken in Chen's experiments, CPD model predictions of tar and light gas nitrogen were compared directly with experimental data. This set of char data is particularly important in

evaluating this nitrogen model since it was not included in the regression of the model parameters. ^{13}C NMR data are not available for the coals studied by Chen. The NMR correlation described in Chapter 4 was used to estimate the chemical structure input parameters for the CPD model. Also, accurate particle temperature profiles were not available, since particles were heated radiantly. Therefore, CPD model predictions were performed by adjusting the temperature profile to match total mass release given for the Dietz coal and then using the same temperature profile for the remaining coals (see Appendix F). Figures 5.11 and 5.12 are comparisons of CPD model predictions of nitrogen released with the tar and light gas nitrogen with experimental data for Dietz and Pittsburgh #8 coals, respectively.

As shown in Figures 5.11 and 5.12, model predictions compared well with experimental measurements of total, tar, and light gas nitrogen release reported by Chen. Similar results were obtained for the other two coals studied by Chen (see Appendix E).

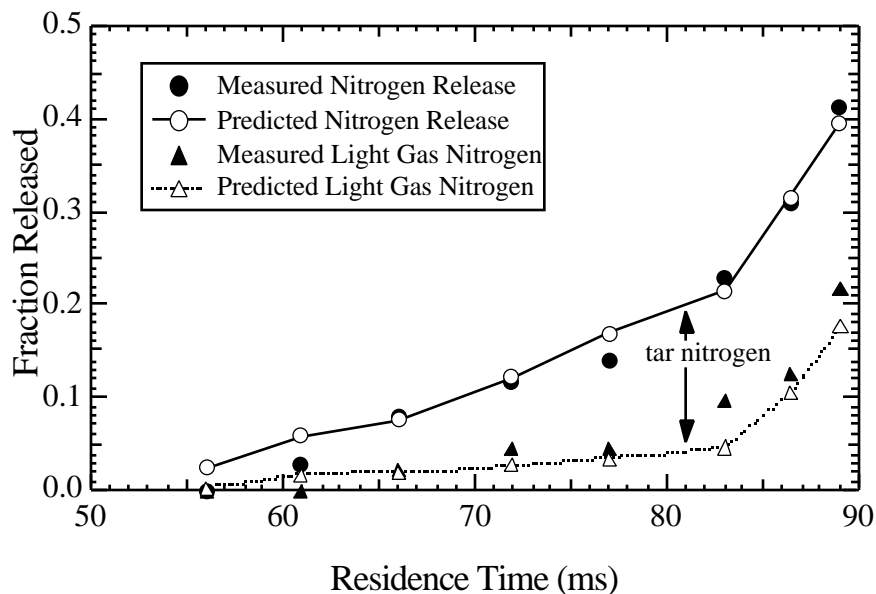


Figure 5.11. Comparison of predictions of total, tar, and light gas nitrogen with experimental data from experiments conducted by Chen⁵² on a Dietz subbituminous coal.

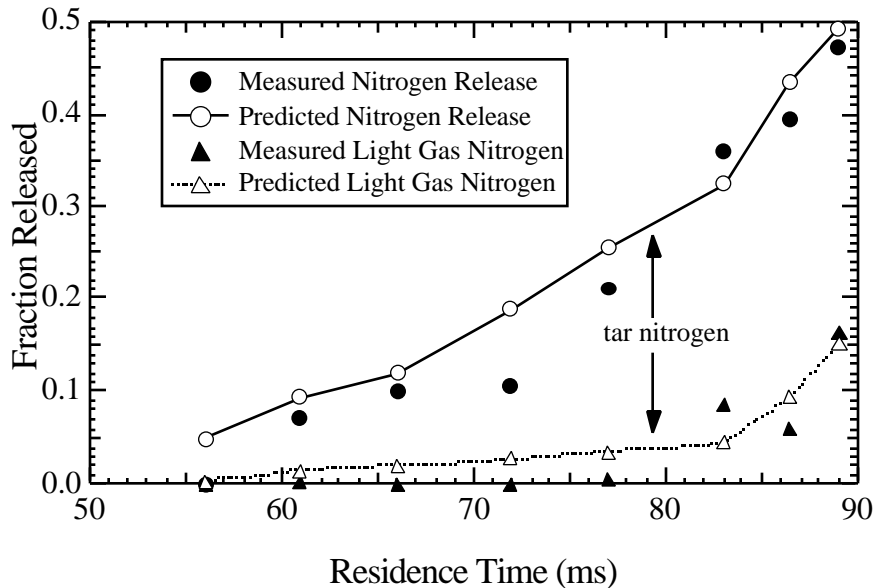


Figure 5.12. Comparison of predictions of total, tar, and light gas nitrogen with experimental data from experiments conducted by Chen⁵² on a Pittsburgh #8 high volatile A bituminous coal.

Comparisons with Data Reported by Hambly and Genetti

Hambly¹⁶ pyrolyzed five coals in a drop tube reactor at BYU at three different peak temperatures (sets 3a, 3b, & 3c). Figure 5.13 compares model predictions of N_{char} with the experimental N_{char} data from Hambly's experiments. The measured and predicted values of N_{char} compare well at all three conditions ($r^2 = 0.976$).

Figure 5.14 compares model predictions of mass and nitrogen with the experimental mass and nitrogen release data from Hambly's experiments with a peak gas temperature of 1220 K. The measured and predicted values of nitrogen release generally compare as well as the measured and predicted mass release. The largest disagreement seems to be for the lignite (Beulah Zap). Figures comparing model predictions with experimental mass and nitrogen release at the other two pyrolysis conditions used by Hambly are given in Appendix E.

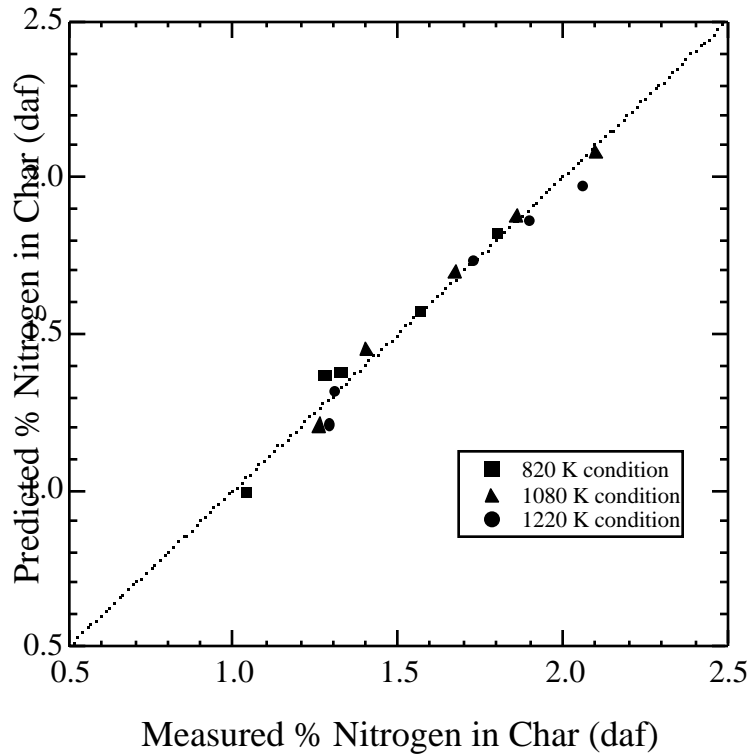


Figure 5.13. Comparison of predicted and measured N_{char} values of five coals pyrolyzed by Hambly in a drop tube reactor at Brigham Young University with peak temperatures of 820, 1080, and 1220 K ($r^2 = 0.976$).

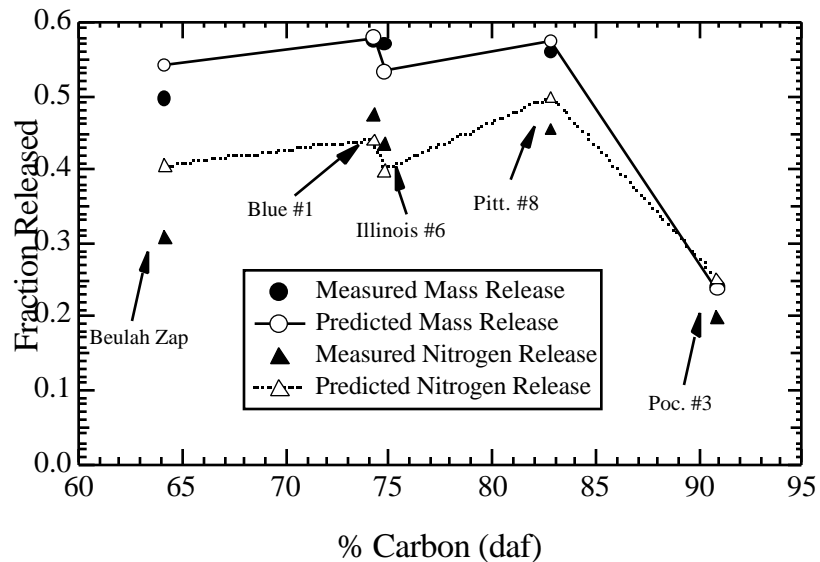


Figure 5.14. Comparison of predicted and measured mass and nitrogen release data of five coals pyrolyzed by Hambly in a drop tube reactor at Brigham Young University with peak temperature of 1220 K.

Hambly¹⁶ also conducted pyrolysis experiments on 11 coals in a flat-flame burner at Brigham Young University (set 3d). A list of the coals is given in Appendix G. The residence time was approximately 18 ms, and the peak gas temperature was about 1641 K. Mass release was determined by a mass balance on the char. The mass release of several of the coals pyrolyzed seemed unusually high for several low volatile coals. Therefore, as part of this thesis project, the experiments were repeated for the coals with suspiciously high mass release. It was discovered that a significant amount of char was being trapped in the separation system of the flat-flame burner apparatus. Therefore, the mass release calculated by Hambly using a mass balance on the char was too high. Care was taken in this study to collect the char trapped in the separation system after each coal was pyrolyzed. The new results seem to be consistent with the expected mass release based on coal type.

During the repeat experiments water flow problems in the collection probe of the flat-flame burner caused the probe tip to overheat at the 18 ms condition. To solve this problem, the repeat experiments were conducted at a condition which places the probe tip downstream of the hottest gases. The residence time of the experiments of this study was about 78 ms, and the peak gas temperature was the same as the 18 ms condition (1641 K). The flat-flame burner collection system and gas temperature and velocity profiles are described in detail by Ma.⁵⁸ Temperature and velocity profiles of the 18 ms and 78 ms conditions are given in Appendix H.

Figure 5.15 compares the CPD model predictions of total mass release with the measured mass release determined by Hambly and during the repeat experiments of this study. In general, the CPD model predictions of mass release compare well with the experiment data.

Figure 5.16 compares CPD model predictions of the total fraction of nitrogen release with the measured nitrogen release. Model predictions of nitrogen release for coals with carbon content between 67 and 80 percent compare well with the experimental data.

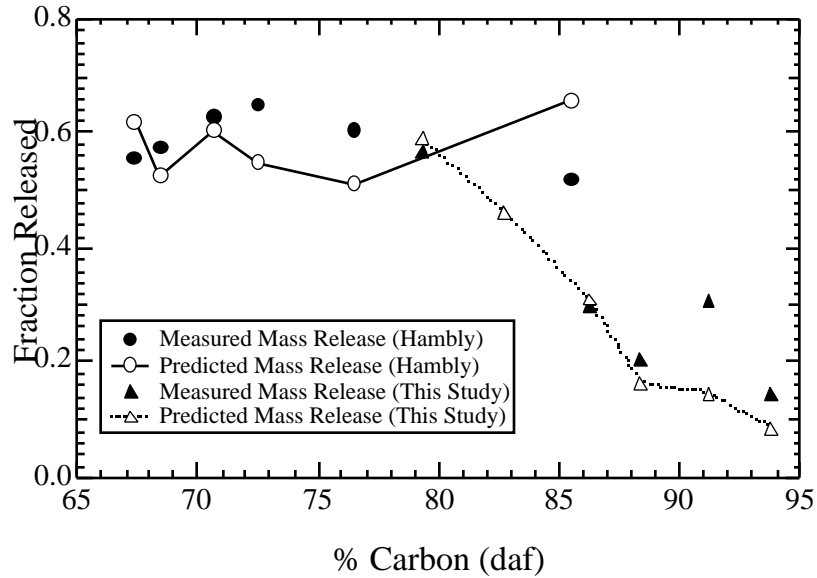


Figure 5.15. Comparison of CPD model predictions of mass release with experimental data for coals pyrolyzed in a flat-flame burner by Hambly¹⁶ and during this study. Carbon content is used as a rank indicator.

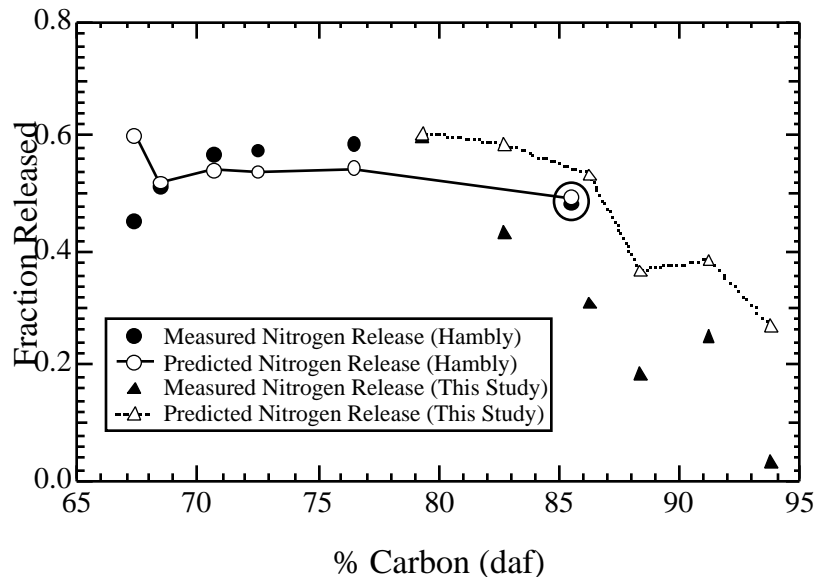


Figure 5.16. Comparison of CPD model predictions of nitrogen release with experimental data for coals pyrolyzed in a flat-flame burner by Hambly¹⁶ and during this study. Carbon content is used as a rank indicator.

For the higher rank coals (coals with greater than 80 % carbon) pyrolyzed in this study nitrogen release was over-predicted by the model by as much as 20 percent absolute. The model prediction of nitrogen release for the coal with 85.5 percent carbon

pyrolyzed by Hambly at the 18 ms condition, however, compares well with the experimental nitrogen release (designated with a circle in Figure 5.16). It appears that the nitrogen model developed in this study over-predicts nitrogen release that occurs at severe pyrolysis conditions (such as a methane flat-flame burner) and at extended residence times. The over-predictions for high rank coals result from over-predictions of light gas nitrogen, suggesting that a simple first order rate expression with a distributed activation energy may not be adequate to describe light gas nitrogen release at all pyrolysis conditions, particularly for high rank coals.

Discussion of Volatile Nitrogen Release Model

The volatile nitrogen release model developed in this study and incorporated into the CPD model appears to adequately model average nitrogen release behavior for a wide variety of coals and experimental conditions. This work represents the first volatile nitrogen release model developed based on ^{13}C NMR measurements of coal structure. This work also represents the first volatile nitrogen release model evaluated by comparing model predictions with chemical structural features of the char (determined by ^{13}C NMR spectral analyses).

Experimental conditions that have been simulated using the volatile nitrogen release model include high heating rates ranging from 10^4 K/s to 10^5 K/s, gas temperature ranging from 820 K to 1641 K, and residence times ranging from 18 to 400 ms. The model seems to accurately describe the volatile nitrogen release of many coals and pyrolysis conditions. Model predictions seemed particularly good for the four coals pyrolyzed by Chen at the 10^4 K/s heating rate condition.

It is apparent that the model over-predicted nitrogen release for some high rank coals pyrolyzed in the flat-flame burner (severe pyrolysis) at Brigham Young University with a residence time of 78 ms. This suggests that the simple first order kinetics used in this modeling effort may not be adequate to accurately describe nitrogen release at all

pyrolysis conditions. The correlation for the fraction of stable nitrogen, f_{st} , seems to adequately describe the decrease in N_{site} decay in high rank coals under most conditions. However, at severe pyrolysis conditions with relatively long residence times, N_{site} decay is still over-predicted. Further studies of the chemical structure of pyrolysis products from a wide variety of coals and conditions using solid-state ^{13}C NMR spectroscopy will be necessary to more fully understand the mechanism of light gas nitrogen release and develop a more robust model. For most pyrolysis conditions, however, reasonable predictions of volatile nitrogen release can be expected.

The nitrogen model developed in this study is similar to the nitrogen release models in the FG-DVC and FLASHCHAIN models in that (i) similar assumptions were made regarding the functionality of nitrogen in coal and how nitrogen is released during primary pyrolysis; and (ii) a first order rate expression with a distributed activation energy model was used to model nitrogen released from the char as HCN (N_{site} decay). However, unlike the other models, the nitrogen release model developed in this work is linked directly to the chemical structure of coal and the change in the chemical structure of char during pyrolysis. This is an important step towards developing a mechanistic model of nitrogen release to accurately determine the quantity of nitrogen released as HCN and tar.

Chapter 6. Predicting Light Gas Composition

Comprehensive coal combustion codes such as PCGC-3 are important tools in screening new technologies for improved combustion efficiency and emissions reduction strategies. In order to accurately model coal combustion, comprehensive combustion codes require that the quantity and product distribution of pyrolysis species be specified. The CPD model has been successfully used in PCGC-3 to calculate the quantity of char, tar, and light gas products during pyrolysis. Before this work, the distribution of light gas pyrolysis products (CH_4 , CO_2 , CO , H_2O , and other light gas species), however, had to be specified by the user.

A submodel has been developed in this work that efficiently predicts the distribution of light gas pyrolysis products. This model is based on coal type and a correlation between the light gas products and the extent of light gas release. Model predictions have been shown to compare well with measured quantities of water, methane, carbon dioxide, carbon monoxide, and other light gas species (calculated by difference) released during pyrolysis experiments conducted on a variety of coals at slow and high heating rates.

Background

The FG (functional group) submodel of the FG-DVC model of coal devolatilization describes the kinetics of individual species evolution at high-temperature and high-heating rate conditions.¹¹ The FG submodel solves 20 differential rate equations that are first order in individual functional group concentration. The functional group composition parameters (the initial fraction of the component in the parent coal) are generally determined from TG-FTIR pyrolysis experiments. In other words, the maximum yield of

each light gas component must be specified, and then each individual differential equation is solved to give the light gas composition as a function of time and temperature. In addition, distributed activation energies are used, which adds significant complexity. Table 6.1 lists the rank independent rate coefficients for the main light gas species of the FG submodel and species composition parameters for a bituminous coal and a lignite.

Table 6.1

Kinetic Rate Coefficients and Species Composition Parameters for FG Submodel

Gas	Functional Group Source	Rate Equation*	Pittsburgh hvAb coal	Beulah Zap lignite
CO ₂ extra loose	Carboxyl	$k = 0.81E + 13 \exp(-(22500 \pm 1500)/T)$	0.000	0.065
CO ₂ loose	Carboxyl	$k = 0.65E + 13 \exp(-(33850 \pm 1500)/T)$	0.007	0.030
CO ₂ light		$k = 0.11E + 13 \exp(-(38315 \pm 2000)/T)$	0.005	0.005
H ₂ O loose	Hydroxyl	$k = 0.22E + 13 \exp(-(30000 \pm 1500)/T)$	0.012	0.062
H ₂ O tight	Hydroxyl	$k = 0.17E + 13 \exp(-(32700 \pm 1500)/T)$	0.012	0.033
CO ether loose		$k = 0.14E + 13 \exp(-(40000 \pm 6000)/T)$	0.050	0.060
CO ether tight	Ether O	$k = 0.15E + 13 \exp(-(40500 \pm 1500)/T)$	0.021	0.038
CO extra tight	Ether O	$k = 0.20E + 13 \exp(-(45500 \pm 1500)/T)$	0.020	0.090
CH ₄ extra loose	Methoxy	$k = 0.84E + 13 \exp(-(30000 \pm 1500)/T)$	0.000	0.000
CH ₄ loose	Methyl	$k = 0.75E + 13 \exp(-(30000 \pm 2000)/T)$	0.020	0.017
CH ₄ tight	Methyl	$k = 0.34E + 13 \exp(-(30000 \pm 2000)/T)$	0.015	0.009

* The rate equation is of the form $k = k_0 \exp(-(E/R \pm \sigma/R)/T)$, with k_0 in s^{-1} , E/R in K, and σ/R in K. σ designates the spread in the activation energies in a Gaussian distribution. Adapted from Solomon.¹¹

For coals where TG-FTIR experimental data are unavailable, Serio, *et al.*⁴² proposed a two-dimensional linear interpolation technique based on coal rank to estimate the functional group parameters for the FG submodel. This interpolation scheme was discussed in Chapter 2. Since TG-FTIR data are not available for most coals, the interpolation method is used to estimate the functional group composition parameters for most coals.

In the current work, a submodel was developed that predicts the composition of light gas released during devolatilization without solving species continuity equations for each functional group. Using light gas evolution data reported by Solomon et al.³¹ and Chen⁵², a look-up table of light gas composition versus the extent of light gas release was created and used to develop a correlation to estimate the light gas pyrolysis product composition for any coal.

Analysis of Light Gas Release Data

A number of studies addressing the composition and kinetics of light gas species evolution have been conducted.^{25, 28, 29, 31, 52, 59, 60} The general implications of these studies are discussed in detail by Smith.⁵ Full analysis of the experimental light gas data conducted during this study is given in Appendix I; only a brief discussion of the conclusions is given here.

TG-FTIR Experiments

Solomon et al.³¹ developed a TG-FTIR instrument that combines thermogravimetric analysis with evolved gas product analysis by Fourier Transform infrared spectroscopy. This instrument was used to analyze the devolatilization products of the eight Argonne Premium Coals. The TG-FTIR analysis determined the relative amounts of H₂O, CO₂, CO, CH₄, and several other less significant gas species evolved during pyrolysis as a function of time. A correlation was developed to relate tar yield to the FTIR as well. The coal samples were heated to 900 °C at 30 °C/min, and then immediately cooled to 250 °C over a period of 20 minutes.

Analysis of the composition of light gas as measured by TG-FTIR analyses of the eight coals indicated that the quantity of light gas released during devolatilization at a given condition decreases with increasing coal rank.³¹ Furthermore, it was evident that the composition of light gas varies with rank. The light gas products of low rank coals

contain a larger fraction of CO and CO₂ relative to high rank coals. Light gas evolved from high rank coals appears to contain more CH₄ and other light hydrocarbons than light gas evolved from lower rank coals. The TG-FTIR study also indicated that the composition of light gas varies with the extent of light gas release. Finally, the TG-FTIR data suggested that the composition of light gas is similar for coals of similar rank.

Light Gas Data From a Radiantly-Heated Reactor

Chen³⁰ conducted pyrolysis experiments on four coals using a radiantly heated flow reactor. The coal particles were radiantly heated to temperatures of approximately 600 K to 1300 K at about 10⁴ K/s. The wall temperature of the reactor was 1840 K. The carrier gas remained relatively cool, minimizing secondary tar reactions, but complicating interpretation of particle temperatures. Each coal was pyrolyzed in the radiantly-heated reactor at eight different residence times. Peak particle temperature increased with increasing residence time. The effluent non-condensable gases were quantified using non-dispersive infrared (NDIR) analysis, chemiluminescence, and gas chromatography.

Careful inspection of the light gas data collected by Chen also indicated that the quantity and composition of light gas are rank dependent, and that the light gas pyrolysis products of coals of similar rank have similar compositions. Comparing the light gas data from the high heating rate experiments conducted by Chen to the TG-FTIR data (slow heating rate) suggested that the composition of light gas is mainly dependent on the extent of light gas release and is relatively insensitive to heating rate. However, light gas formed under high heating rate conditions does have a larger fraction of light hydrocarbon species such as C₂H₄ and C₂H₆. This may be due to high temperature secondary reactions

Pyrolysis Experiments at Various Heating Rates

Suuberg et al.²⁵ conducted pyrolysis experiments at various heating rates on a Montana lignite and a Pittsburgh no. 8 bituminous coal. Heating rates varied from about

300 K/s to 10^4 K/s. The results of his experiments indicated that the composition of light gas was insensitive to heating rate, but did vary with coal type and the extent of light gas release.

Conclusions from Data Analysis

The following important conclusions were drawn from these studies: (i) light gas from coal pyrolysis is primarily composed of water, carbon dioxide, carbon monoxide, and methane; (ii) other minor constituents include hydrogen, nitrogen and sulfur containing gases, and low molecular weight olefins and paraffins; (iii) the composition of light gas is a function of rank (low rank coals contain more carbon oxides while high rank coals contain more hydrocarbons); (iv) the evolution rates of individual species are relatively insensitive to coal type when normalized by the coal dependent yield; and (v) the composition of light gas seems to correlate well with the extent of light gas release, and is relatively insensitive to heating rate. Based on these conclusions, it appears that using a correlation based on coal type and the extent of light gas release to estimate light gas composition would be appropriate.

Correlation of Light Gas Composition

A correlation of light gas composition was developed in this study based on coal type and the extent of light gas release. A look-up table was created using light gas data collected on twelve coals studied by Solomon et al.³¹ and by Chen and Niksa.³⁰ The look-up table is given in Appendix J. The table gives the composition of light gas (H_2O , CO_2 , CO , CH_4 , and other light gases) as a function of the extent of total light gas release for each of the twelve coals. The extent of light gas release is defined as, X_{gas} , the ratio of the light gas yield to the maximum light gas yield.

One motivation in developing a model for light gas species release is to retain the tie to chemical structure through the CPD model. In the CPD model, a series of reactions

are used to model the cleavage of bridges and side chains to form light gas. The sum of aliphatic bridges (ℓ) and aliphatic side chains (s) represent the total quantity of light gas precursors. The initial distribution of attachments between bridges and side chains is determined by ^{13}C NMR spectral analysis of the parent coal. As light gas is evolved, ℓ and s approach zero in the CPD model, which represents the maximum light gas release possible. In this work, the composition of light gas was correlated with the extent of light gas release. The extent of light gas release (X_{gas}) was normalized in the CPD model by the initial amount of light gas precursors and ranges from 0 (no light gas release) to 1 (complete light gas release), as follows:

$$X_{\text{gas}} = 1 - \frac{\ell/2 + s}{(\ell/2 + s)_0} \quad (6.1)$$

where the “0” represents the structure of the parent coal. ℓ is divided by 2 because in the CPD model it is assumed that side chains are half the molecular weight of bridges.

In order to estimate the composition of the light gas pyrolysis products of any coal as a function of the extent of devolatilization, a submodel was developed for the CPD model that uses a double interpolation correlation. One interpolation is used for coal type, and the other for the extent of total light gas release based on three reference coals.

Interpolation for Coal Type

As discussed in Chapter 2, Serio et al.⁴² proposed a two-dimensional method based on coal rank to estimate the input parameters for the FG-DVC model. The O/C and H/C molar ratios were used as indicators of rank. The elemental ratios of several well studied coals were used to form a two-dimensional triangular mesh on a H/C vs. O/C coalification diagram. Each triangle was composed of three nodes (i.e. reference coals). For an unknown coal, the elemental composition determined the appropriate triangle, and the structural parameters of the unknown coal were interpolated from the parameters

corresponding to the three nodes. The numerical details of this interpolation technique are described by Serio et al.⁴²

In the submodel developed in this work for the CPD model, the interpolation technique described by Serio and coworkers was used to estimate the composition of light gas for any coal. Twelve coals studied by Solomon et al.³¹ and by Chen and Niksa³⁰ were used as the reference coals (Table 6.2). Figure 6.1 is a coalification diagram of the 12 reference coals which shows the triangular interpolation mesh created in this study.

Table 6.2
Elemental Composition and Elemental Ratios Used as Rank Indicators

Coal	Rank	% C (daf)	% H (daf)	% O (daf)	O/C (molar)	H/C (molar)
<i>PETC* coals studied by Chen and Niksa³⁰</i>						
Dietz	subB	69.50	5.00	24.10	0.260	0.857
Illinois #6	hvAb	74.10	5.30	13.40	0.136	0.852
Pittsburgh #8	hvAb	82.50	5.60	8.50	0.077	0.809
Lower Kittaning	lvb	88.70	5.00	2.10	0.018	0.672
<i>Argonne Premium Coals Studied by Solomon et al.³¹</i>						
Beulah Zap	ligA	72.94	4.83	20.34	0.209	0.789
Wyodak	subC	75.01	5.35	18.02	0.180	0.850
Illinois no. 6	hvCb	77.67	5.00	13.51	0.131	0.767
Utah Blind Canyon	hvBb	80.69	5.76	11.58	0.108	0.851
Lewis Stockton	hvAb	82.58	5.25	9.83	0.089	0.758
Pittsburgh	hvAb	83.20	5.32	8.83	0.080	0.762
Upper Freeport	mvb	85.50	4.70	7.51	0.066	0.655
Pocahontas no. 3	lvb	91.05	4.44	2.47	0.020	0.581
York Canyon**	hvAb	na	na	na	0.069	0.863

* Pittsburgh Energy Technology Center. ** York Canyon is not an Argonne Premium coal. It was obtained by Serio et al.⁴² from the Penn State Coal Sample Bank and studied with TG-FTIR analysis.

Interpolation for Extent of Light Gas Release

Once the appropriate triangle of reference coals is determined by the elemental composition of the unknown coal, the light gas composition of each reference node must

be calculated. This is accomplished by linearly interpolating between the data in the look-up table of reference coals based on the current value of X_{gas} of the unknown coal. Determination of the light gas composition, therefore, requires double interpolation. Linear interpolation is used to determine the light gas composition of each reference node corresponding to X_{gas} of the unknown coal. Then, the two dimensional triangular interpolation technique is used to determine the light gas composition of the unknown coal.

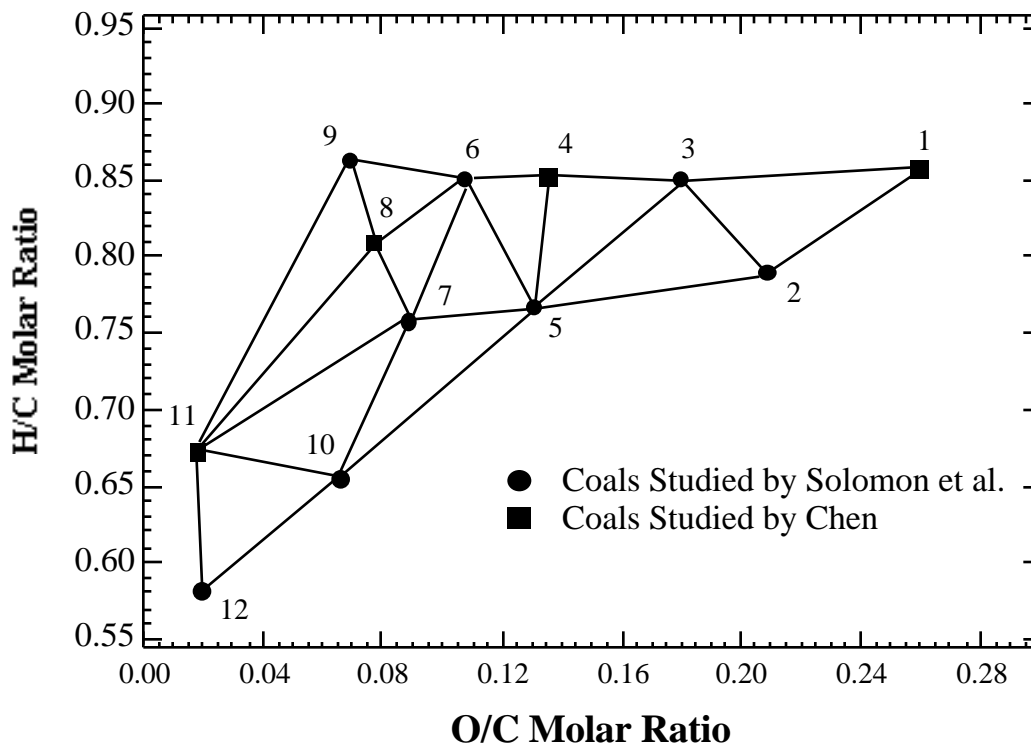


Figure 6.1. The interpolation mesh in the coalification diagram used to develop the light gas correlation. (1) Dietz, (2) Beulah Zap, (3) Wyodak, (4) Illinois no. 6, (5) Illinois no. 6, (6) Utah Blind Canyon, (7) Lewis Stockton, (8) Pittsburgh no. 8, (9) York Canyon, (10) Upper Freeport, (11) Lower Kittanning, (12) Pocahontas no. 3.

The CPD model calls the light gas submodel at each time step so that the light gas yield and composition are determined as a function of time and the extent of light gas release. The fraction of light gas consisting of “other” gases is calculated by difference.

$$y_{other} = 1 - y_i \quad (6.2)$$

The fractions of original coal mass released as H₂O, CO₂, CO, CH₄, and other light gases are also calculated.

During the course of the development of this submodel, while applying the light gas correlation to unknown coals, it was determined that a small fraction of coals do not fall within the triangular mesh of reference nodes. A crude method of estimating the light gas composition of such coals was developed. For most coals whose elemental composition does not correspond to a triangle within the mesh, the light gas distribution is estimated by the nearest node on the coalification diagram. The light gas composition of extremely high rank coals was estimated based on the measured light gas composition of the pyrolysis products of an anthracite coal, known as Hongay, reported by Xu and Tomita.²⁸ The light gas composition of extremely low rank coals was estimated based on data on a lignite, known as Rhein Braun, also reported by Xu and Tomita.

Application of Light Gas Correlation

CPD model predictions of light gas composition determined using the light gas composition correlation were compared with measured light gas data from low and high heating rate pyrolysis experiments on coals not used to develop the correlation. The correlated light gas compositions compared well with the measured data for most of the coals tested.

As previously discussed, Xu and Tomita²⁸ conducted devolatilization experiments on 17 coals in a Curie-point pyrolyzer which heated samples to 1037 K at 3000 K/s (see Table 4.7). CPD model predictions (see Appendix C) of light gas composition and the measured composition are compared in Figure 6.2. X_{gas} was about 0.87 in each case. For several individual cases large discrepancies between model predictions and the

experimental data exist (such as at 77% C). However, the general trends of the variation in light gas composition with coal type are well predicted.

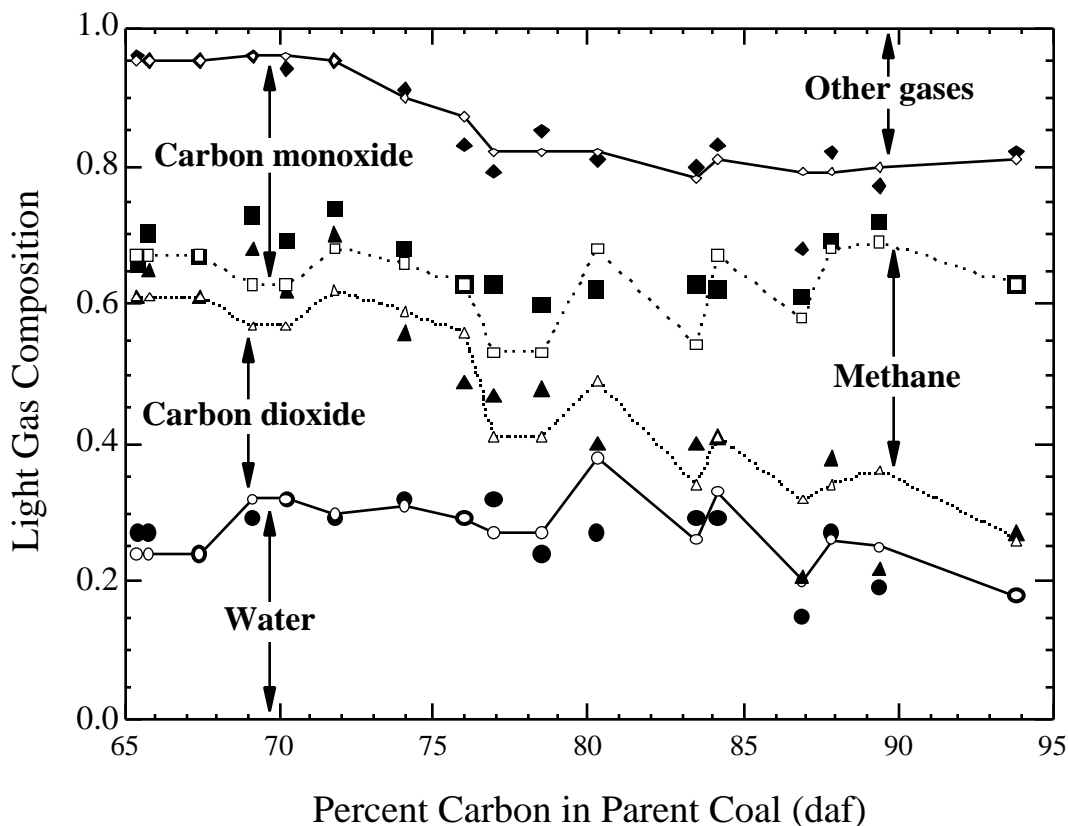


Figure 6.2. Comparison of CPD model predictions of light gas composition using the correlation with the light gas composition measured by Xu and Tomita.²⁸ The solid symbols represent the measured data and the open symbols represent the CPD model estimations.

Burnham et al.⁶⁰ conducted slow heating rate pyrolysis experiments (about 60 K/sec) on the Argonne premium coal suite using a Rock-eval apparatus. Based on the heating rate and peak temperature reported by Burnham, a particle temperature profile was estimated and used in the CPD model to predict tar and light gas yields. The coal samples studied by Burnham are identical to those examined by Solomon et al.³¹ using TG-FTIR analyses (coals 1-8, Tables 4.1, 4.2, and 4.3). The measured NMR parameters listed in Table 4.3 were used in the CPD model. CPD model predictions of light gas

composition are compared with the measured compositions in Figure 6.3. With the exceptions of Upper Freeport and Pocahontas no. 3, model predictions of the gas composition compare well with the measured data.

Burnham reports that the light gases released from Upper Freeport and Pocahontas no. 3 are 4.5 percent and 2.1 percent water (dry-ash-free), respectively. As seen in Figure 6.3, the CPD model estimates much higher water content in the light gas. This is interesting since the CPD model predictions for these two coals are based on the TG-FTIR data on the same Argonne Premium coals. The correlation, therefore, is an interesting tool in comparing the light gas composition reported by different investigators for the same coals pyrolyzed under similar conditions.

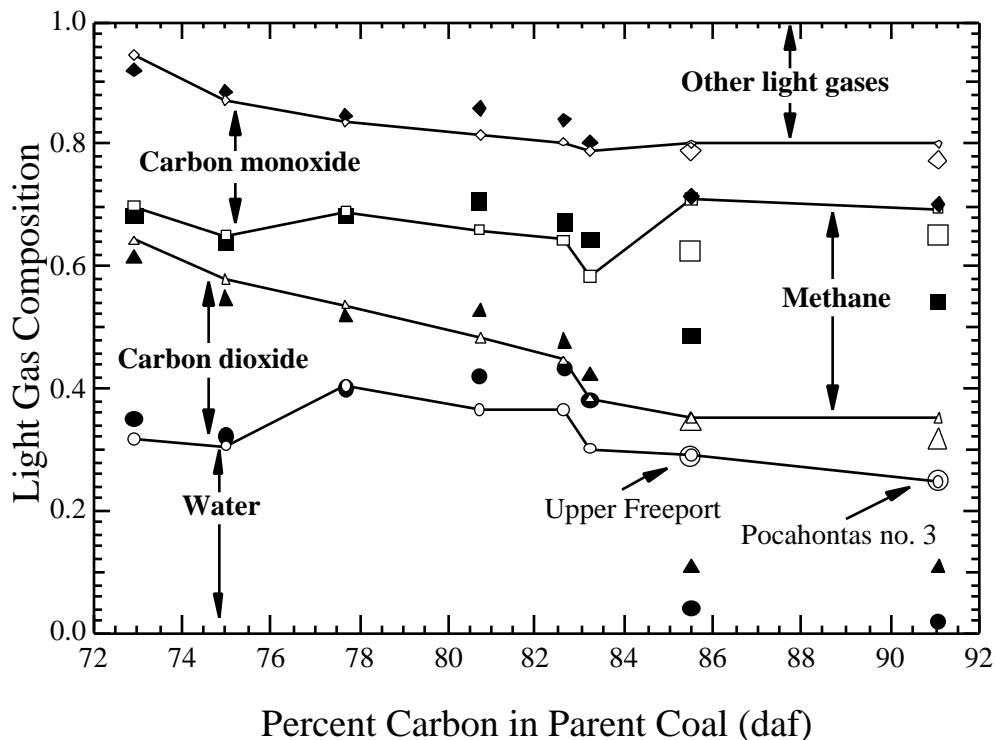


Figure 6.3. Comparison of CPD model predictions of light gas composition using the correlation with the light gas composition measured by Burnham et al.⁶⁰ The solid symbols represent the measured data and the small open symbols represent the CPD model estimations. The large open symbols represent the measured light gas composition of Upper Freeport and Pocahontas no. 3 corrected to the water content measured in TG-FTIR experiments.

The compositions of the light gas pyrolysis products of Upper Freeport and Pocahontas no. 3 reported by Burnham and coworkers were corrected to the water content determined by the TG-FTIR experiments conducted by Solomon and coworkers. This correction cannot be completely justified; however, light gas data from similar coals generated by various investigators is consistent with the TG-FTIR water content data^{25, 28, 30} and may indicate experimental error in the Rock-eval process. This correction is represented in Figure 6.3 by the large open symbols. With this correction, the relative content of CO₂, CO, CH₄, and other gases reported by Burnham compare well with the TG-FTIR data. The correction makes it evident that the only large discrepancy between the light gas data reported by Burnham and by Solomon is in the light gas water content of the pyrolysis products of Upper Freeport and Pocahontas no. 3.

Discussion of Light Gas Correlation

Experimental data collected during the pyrolysis experiments conducted by Solomon et al.,³¹ Chen and Niksa,³⁰ and Burnham et al.⁶⁰ suggest that the composition of light gas released during coal pyrolysis is insensitive to heating rate but varies with the extent of light gas release and coal type. Therefore a correlation of light gas composition based on coal type and the extent of light gas release was developed in this study. This is a viable alternative to using a large set of differential rate equations to describe the evolution of each light gas species. Since no numerical solutions to differential equations must be performed when using the correlation, the correlation is expected to be a very rapid method of estimating the light gas composition of pyrolysis products. It is anticipated that the correlation can be implemented in comprehensive coal combustion codes such as PCGC-3 without a significant increase in run time.

As mentioned previously, the maximum yield of each light gas species must be specified in the FG submodel of the FG-DVC model. This is the equivalent of the light gas composition when X_{gas} equals one in the light gas correlation developed in this study.

The maximum yields are estimated in the FG-DVC model using the two-dimensional triangular interpolation technique based on Argonne Premium coals analyzed by TG-FTIR. Therefore, the accuracy (or inaccuracy) of the two approaches are similar.

The light gas composition correlation presented here offers several additional advantages over the differential equation approach used in the FG-DVC model. Estimations of light gas composition are interpolated directly from experimental data as a function of X_{gas} as opposed to using differential rate equations. The empirically derived rate constants used in the FG-DVC model to solve for the yields of each species as a function of time likely introduce additional error. Also, the light gas data reported by Chen was used in this study to expand the triangular mesh of reference coals so that the correlation will be applicable to a larger range of coals. Another advantage of the look-up table approach is that the light gas submodel can be used as a post-processing device to estimate the composition of light gas after complete devolatilization (or as it enters and leaves a grid cell) instead of calculating the composition at each time step.

Chapter 7. Conclusions

The primary objective of this project was to develop a primary volatile nitrogen release model based on the chemical structure of coal, and to incorporate the model into the CPD model. A secondary, but equally important, objective of this project was to increase the industrial usefulness of the CPD model. These objectives were successfully achieved through the following accomplishments:

- A reasonable correlation was developed to estimate the chemical structure of coal based on elemental composition and volatile matter content.
- A volatile nitrogen release model was developed based on the chemical structure of coal, and evaluated using gas, char, and tar nitrogen release yields.
- The volatile nitrogen release model developed in this study was further evaluated in a novel manner by comparing model predictions to the chemical structure of char as determined by ^{13}C NMR spectral analyses.
- A submodel was developed and coupled with the CPD model to estimate the composition of light gas released during devolatilization.

Correlations to Estimate Coal Structure

Non-linear correlations were developed to model the average structural characteristics of coal as a function of elemental composition and ASTM volatile matter content. Reasonable estimations of ^{13}C NMR structural parameters for most coals can be

expected using the correlation. However, it is expected that these correlations, just like any correlation, will not work well for some unusual coals.

The *non-linear* modified quadratic correlation of ^{13}C NMR measurements of coal structure with ultimate analysis and volatile matter content seems to be an appropriate method to estimate the coal structure input parameters for network devolatilization models, such as the CPD model. The correlation, combined with the CPD model, appears to work well in predicting total volatiles and tar yields for low to high rank coals. Although one of the principal motives for this study was the estimation of the input parameters for the CPD model, the estimated structural parameters should be useful in other applications, and a similar approach could be used to develop predictive models for other structural parameters.

The accuracy of CPD model predictions of tar and light gas were enhanced by developing a correlation to estimate the initial fraction of stable bridges, c_0 , based on the elemental composition of coal. The correlation seems to give reasonable estimates of c_0 for a wide range of coals.

Volatile Nitrogen Release Model

A volatile nitrogen release model was developed in this study by (1) modeling the release of nitrogen from the char as HCN with a first order rate expression with a distributed activation energy model, (2) modifying the CPD model to calculate the quantity of nitrogen released with the tar at each time step, and (3) evaluating the model by comparing model predictions of nitrogen release to experimental data not included in the regression of model parameters. Model predictions of nitrogen release compared well with experimental nitrogen release data for most coals and pyrolysis conditions. The model, therefore, seems to represent an appropriate and accurate method of predicting volatile nitrogen release for most coals during pyrolysis.

In order to satisfy the shortage of available nitrogen release data for low volatile coals, six high rank coals were pyrolyzed in a flat-flame burner as part of this study. Comparison of volatile nitrogen release predictions with the measured nitrogen release data obtained for the six high rank coals confirmed that the volatile nitrogen release model developed in this study over-predicts nitrogen release from some low volatile coals pyrolyzed under severe pyrolysis conditions. The experimental data collected in this study on high rank coals will be very important in developing and evaluating advanced nitrogen release models in the future.

The volatile nitrogen release model developed in this work represents the first volatile nitrogen release model evaluated by comparing model predictions with the chemical structure of char (as measured by ^{13}C NMR analyses). Model predictions of N_{site} were compared to measured values of N_{site} (determined from ^{13}C NMR spectral analyses of the chars) determined from the pyrolysis experiments conducted by Fletcher and coworkers^{1, 14, 55-57, 48} and by Hambly.¹⁶ Predictions of N_{site} compared well with measured values for most coals.

Evaluation of the model based on the chemical structure of the char is significant because (i) it confirms that nitrogen is released not only with the tar, but also as HCN from the char due to the thermal rupture of pyrrolic and pyridinic nitrogen forms; and (ii) it quantifies the accuracy of the predicted distribution of nitrogen between char, tar, and HCN (as opposed to only comparing model predictions with total nitrogen release). Other models have primarily been evaluated based on comparing model predictions with measured total nitrogen release. The evaluation based on the chemical structure of char seems to indicate that the volatile nitrogen release model developed in this study not only accurately predicts total nitrogen release for most coals and conditions, but also accurately describes the distribution of nitrogen between char, tar, and HCN which may be important in developing advanced low NO_x technology.

Light Gas Submodel

A submodel was created and coupled with the CPD model that estimates the composition of light gas evolved during pyrolysis. The model includes a look-up table of measured light gas composition for 12 coals of various rank as a function of the extent of devolatilization. A double interpolation method was developed in order to estimate the composition of light gas pyrolysis products of an unknown coal. CPD model predictions of light gas composition compared well with experimental data collected in low and high heating rate pyrolysis experiments that were not included in the look-up table. It is anticipated that the look-up table approach used in this modeling effort will not add any significant run-time when coupled with comprehensive coal combustion codes such as PCGC-3. It seems, therefore, that the look-up table approach to estimating light gas composition is a valuable alternative to solving a continuity equation for each species.

Impact of This Work

The modifications made in this study to the CPD model enhance its industrial usefulness. The volatile nitrogen release model is an important step toward more accurately modeling the formation of NO_x precursors in comprehensive coal combustion codes which provide an important screening tool of new low NO_x technology. Due to the reliable method of estimating the chemical structure input parameters of any coal developed in this study, and the creation of a computationally simple method to estimate light gas pyrolysis product compositions, the CPD model will be a more useful addition to comprehensive combustion models. It is anticipated that the modified CPD model will be coupled with PCGC-3 in the near future, and therefore will significantly increase the accuracy and applicability of PCGC-3, including improving the accuracy of NO_x predictions.

Chapter 8. Recommendations for Future Work

Significant progress in modeling volatile nitrogen release and enhancing the industrial usefulness of the CPD Model has been made in this thesis project. Like most research, however, this project represents a work in progress. During the course of this project, a number of ideas to further improve this work were conceived. Recommendations regarding work that might be conducted to continue this project are given below.

NMR Correlation

It is not known why the correlations between the chemical structural parameters and the elemental composition and volatile matter content exist. It was suggested in Chapter 4 that perhaps the correlations exist because there is a relationship between the elemental composition and the maceral content that the quadratic correlations are able to describe. It would be useful to examine the elemental composition and volatile matter content of macerals at various stages of maturation in order to confirm or discount this hypothesis. Such a study of maceral content would not only be useful in improving the NMR correlations, but may also be helpful in improving CPD Model predictions of tar and light gas release.

Volatile Nitrogen Modeling

The actual mechanism of light gas nitrogen release during pyrolysis is still unknown. Further studies of the chemical structure of pyrolysis products from a wide variety of coals and conditions using ^{13}C NMR spectroscopy will be necessary to more fully understand the mechanism of light gas nitrogen release. Determining the actual

mechanism of light gas nitrogen release will undoubtedly lead to a more accurate model. It may also be possible to continue improving the model using an empirical approach. For example, perhaps two individual rate expressions could be used to describe the decay of the stable nitrogen and the less stable nitrogen. Another possibility would be to correlate f_{st} with pyrolysis conditions such as temperature and heating rate. These approaches may help to model N_{site} decay in low volatile coals during severe pyrolysis.

Light Gas Correlation

It would be interesting to do a mass balance on coal using the light gas correlation and compare the predicted elemental composition of chars with measured compositions. Being able to determine the composition of char would be useful in determining char burnout rates in coal combustion models. A mass balance on coal was not conducted in this study because the composition of the fraction of light gas called “other” light gas is not known. In the future, perhaps a correlation could be developed between the composition of “other” light gases (thought to be olefins and paraffins) and coal rank. Such a correlation would be useful in closing a mass balance.

References

1. Baxter, L. L., R. E. Mitchell, T. H. Fletcher and R. H. Hurt, *Energy & Fuels*, **10**, 188-196 (1996).
2. Cai, H. Y., A. J. Guell, D. R. Dugwell and R. Kandiyoto, *Fuel*, **72**, 321-327 (1993).
3. Smoot, L. D. and P. J. Smith, *Coal Combustion and Gasification*, Plenum Press, New York (1985).
4. Fletcher, T. H., A. R. Kerstein, R. J. Pugmire and D. M. Grant, *Energy and Fuels*, **6**, 414-431 (1992).
5. Smith, K. L., L. D. Smoot, T. H. Fletcher and R. J. Pugmire, *The Structure and Reaction Processes of Coal*, Plenum Press, New York (1994).
6. Krevelen, D. W. v., *Coal: Typology, Chemistry, Physics, and Constitution*, Elsevier, New York (1981).
7. Spiro, C. L. and P. G. Kosky, *Fuel*, **61**, 1080-1084 (1982).
8. Solomon, P. R., *Coal Structure and Thermal Decomposition*, In New Approaches in Coal Chemistry, B. D. Blaustein, B. C. Bockrath and S. Friedman, Ed., American Chemical Society, Washington, D.C., Vol. 169, pp 61-71 (1981).
9. Marzec, A. and H. R. Schulten, *Preprint, American Chemical Society, Division of Fuel Chemistry*, **34**, 3, 668-675 (1989).
10. Given, P. H., A. Marzec, W. A. Barton, L. J. Lynch and B. C. Gerstein, *Fuel*, **65**, 155-163 (1986).
11. Solomon, P. R., D. G. Hamblen, R. M. Carangelo, M. A. Serio and G. V. Deshpande, *Energy and Fuels*, **2**, 405-422 (1988).
12. Solum, M. S., R. J. Pugmire and D. M. Grant, *Energy and Fuels*, **3**, 187-193 (1989).
13. Orendt, A. M., M. S. Solum, N. K. Sethi, R. J. Pugmire and D. M. Grant, *¹³C NMR Techniques for Structural Studies of Coals and Coal Chars*, In Advances in Coal Spectroscopy, H. L. C. Meuzelaar, Ed., Plenum Press, New York, pp 215-254 (1992).

14. Fletcher, T. H., M. S. Solum, D. M. Grant, S. Critchfield and R. J. Pugmire, *23rd Symposium (Int.) on Combustion*; The Combustion Institute, Pittsburgh, PA, pp 1231 (1990).
15. Watt, M., "The Chemical Structure of Coal Tar and Char During Devolatilization," M.S. Thesis, Chemical Engineering Department, Brigham Young University (1996).
16. Hambly, E., "The Chemical Structure of Coal Tar and Char During Devolatilization," M.S. Thesis, Chemical Engineering Department, Brigham Young University (1998).
17. Niksa, S., *Energy and Fuels*, **9**, 467-478 (1995).
18. Burchill, P. and L. S. Welch, *Fuel*, **68**, 100 (1989).
19. Bartle, K. D., D. L. Perry and S. Wallace, *Fuel Processing Technology*, **15**, 351-361 (1987).
20. Wojtowicz, M. A., J. R. Pels and J. A. Moulijn, *Fuel*, **74**, 507-515 (1995).
21. Kelemen, S. R., M. L. Gorbaty and P. J. Kwiatek, *Energy & Fuels*, **8**, 896 (1994).
22. Wallace, S., K. D. Bartle and D. L. Perry, *Fuel*, **68**, 1450-1455 (1989).
23. Kelemen, S. R., M. L. Gorbaty, S. N. Vaughn and P. J. Kwiatek, *ACS Division of Fuel Chemistry Preprints*, **38**, 2, 384 (1993).
24. Anthony, D. B., J. B. Howard, H. C. Hottel and H. P. Meissner, *15th Symposium (Int.) on Combustion*; The Combustion Institute, Pittsburgh, PA, pp 1303-1317 (1974).
25. Suuberg, E. M., W. A. Peters and J. B. Howard, *17th Symposium (Int.) on Combustion*; The Combustion Institute, Pittsburgh, PA, pp 117-130 (1978).
26. Gibbins, J. and R. Kandiyoti, *Energy & Fuels*, **3**, 670-677 (1989).
27. Saxena, S. C., *Progress in Energy and Combustion Sciences*, **16**, 55-94 (1990).
28. Xu, W. and A. Tomita, *Fuel*, **66**, 627-631 (1987).
29. Serio, M. A., D. G. Hamblen, J. R. Markham and P. R. Solomon, *Energy & Fuels*, **1**, 138-52 (1987).
30. Chen, J. C. and S. Niksa, *Energy & Fuels*, **6**, 254-264 (1992).
31. Solomon, P. R., M. A. Serio, R. M. Carangelo and R. Bassilakis, *Energy & Fuels*, **4**, 319-333 (1990).

32. Blair, D. W., J. O. L. Wendt and W. Bartok, *16th Symposium (Int.) on Combustion*; The Combustion Institute, Pittsburgh, PA, pp 475 (1977).
33. Solomon, P. R. and M. B. Colket, *Fuel*, **57**, 749-755 (1978).
34. Solomon, P. R. and T. H. Fletcher, *25th Symposium (Int.) on Combustion*; The Combustion Institute, Pittsburgh, PA, pp 463 (1994).
35. Mitchell, R. E., R. H. Hurt, L. L. Baxter and D. R. Hardesty, *Milestone Report, Sandia Report SAND92-8208*, (1992).
36. Freihaut, J. D., W. Proscia, N. Knight, A. Vranos, H. Kollick and K. Wicks "Combustion Properties of Micronized Coal for High Intensity Combustion Applications," Final Report for DOE/PETC Contract DE-AC22-85PC80263 (1989).
37. Freihaut, J. D., W. M. Proscia and J. C. Mackie, *Combustion Science and Technology*, **93**, 323 (1993).
38. Howard, J. B., *Fundamentals of Coal Pyrolysis and Hydrolysis*, In Chemistry of Coal Utilization, M. A. Elliot, Ed., Wiley, New York, pp 665-784 (1981).
39. Ko, G. H., W. A. Peters and J. B. Howard, *Fuel*, **66**, 1118-1122 (1987).
40. Solomon, P. R., D. G. Hamblen, M. A. Serio, Z.-Z. Yu and S. Charpenay, *Fuel*, **72**, 4, 469-488 (1993).
41. Niksa, S., *Energy and Fuels*, **5**, 673-683 (1991).
42. Serio, M., A., P. R. Solomon and Y. Zhao, *25th Symposium (Int.) on Combustion*; The Combustion Institute, Pittsburgh, PA, pp 553-560 (1994).
43. Niksa, S., *Energy and Fuels*, **8**, 659-670 (1994).
44. Gerstien, B. C. M., P. D.; and Ryan, L. M., *Coal Structure*, Academic Press, New York, (1982).
45. Bassilakis, R., Y. Zhao, P. R. Solomon and M. A. Serio, *Energy & Fuels*, **7**, 710-720 (1993).
46. Genetti, D. B., T. H. Fletcher and R. J. Pugmire, *Coal Science: Proceedings of the 8th International Conference on Coal Science*; Elsevier, Oviedo, Spain, (1995).
47. Hintze, J., NCSS Statistical Software, Kaysville, UT, pp (1997).
48. Fletcher, T. H. and D. R. Hardesty "Milestone Report for DOE's Pittsburgh Energy Technology Center," contract FWP 0709, Sandia Report No. SAND92-8209, available NTIS (1992).

49. LECO, *CHNS-932 Elemental Analyzer Instruction Manual*, (1993).
50. Nash, J. C., *Nonlinear Parameter Estimation*, Marcel Dekker, Inc., New York, NY, (1987).
51. Carr, A. D. and J. E. Williamson, *Organic Geochemistry*, **16**, 313-330 (1983).
52. Chen, J. C. "Effect of Secondary Reactions on Product Distribution and Nitrogen Evolution from Rapid Coal Pyrolysis," Ph.D. Dissertation, Stanford University (1991).
53. Perry, S., "Modeling Nitrogen Release During Devolatilization Based on the Chemical Structure of Coal", Ph.D. Dissertation in Progress, Brigham Young University (1998).
54. Hill, S., Research Professor, Brigham Young University, Personal Communication (1998).
55. Fletcher, T. H., *Combustion and Flame*, **78**, 223 (1989).
56. Pugmire, R. J., M. S. Solum, D. M. Grant, S. Critchfield and T. H. Fletcher, *Fuel*, **70**, 414 (1991).
57. Fletcher, T. H., M. S. Solum, D. M. Grant and R. J. Pugmire, *Energy and Fuels*, **6**, 643-650 (1992).
58. Ma, J., "Soot Formation During Coal Pyrolysis," Ph. D. Dissertation, Chemical Engineering Department, Brigham Young University (1996).
59. Solomon, P. R. and M. B. Colket, *17th Symposium (Int.) on Combustion*; The Combustion Institute, Pittsburgh, PA, 131-143 (1978).
60. Burnham, A. K., S. O. Myongsook and R. W. Crawford, *Energy & Fuels*, **3**, 42-55 (1988).

Appendices

Appendix A: Correlated Structural Parameters

Table A.1

Structural Parameters for Coals in Data base Calculated Using the Correlation

#	Source	Seam	M	M_{cl}	p_0	+ 1	c_0
1	PSOC 1507 (AR)	Beulah-Zap	42	326	0.60	5.0	0.11
2	PSOC-1520 (AR)	Wyodak	41	357	0.54	5.0	0.08
3	PSOC-1502 (AR)	Blind Canyon	36	386	0.46	5.0	0.00
4	PSOC-1493 (AR)	Illinois #6	37	334	0.54	5.2	0.01
5	PSOC-1451 (AR)	Pittsburgh #8	31	330	0.53	4.9	0.00
6	ANL (AR)	Stockton	31	329	0.55	5.0	0.00
7	ANL (AR)	Upper Freeport	25	277	0.63	4.8	0.00
8	PSOC-1508 (AR)	Pocahontas #3	16	230	0.75	4.1	0.36
9	PSOC-1443 (ACERC)	Lower Wilcox	36	281	0.61	4.8	0.11
10	PSOC-1488 (ACERC)	Dietz	40	347	0.55	5.0	0.07
11	PSOC-1468 (ACERC)	Buck Mountain	14	616	0.90	4.6	0.36
12	PSOC-1445D (Sandia)	Blue #1	40	348	0.54	5.0	0.07
13	PSOC-1451D (Sandia)	Pittsburg #8	30	353	0.51	4.8	0.00
14	PSOC-1493D (Sandia)	Illinois #6	42	383	0.51	5.2	0.01
15	PSOC-1507D (Sandia)	Beulah-Zap	50	348	0.66	4.4	0.15
16	PSOC-1508D (Sandia)	Pocahontas #3	18	242	0.76	4.4	0.36
17	Goudey A (AFR)	not named	21	276	0.66	5.1	0.27
18	Goudey B (AFR)	not named	17	299	0.67	4.8	0.34
19	DECS-1 (BYU)	Bottom	50	436	0.48	4.5	0.12
20	DECS-7 (BYU)	Adaville #1	44	365	0.56	4.8	0.11
21	DECS-11 (BYU)	Beulah-Zap	46	320	0.63	4.5	0.15
22	DECS-13 (BYU)	Sewell	26	288	0.61	4.8	0.00
23	DECS-18 (BYU)	Kentucky #9	36	416	0.44	5.3	0.00
24	DECS-20 (BYU)	Elkhorn #3	33	387	0.48	4.9	0.00
25	DECS-21 (BYU)	Lykens Valley #2	9	321	0.94	4.0	0.36
26	DECS-27 (BYU)	Deadman	39	357	0.55	5.0	0.05
27	PSOC-1515 (BYU)	Penna. Semian. C	16	251	0.82	4.6	0.33
28	PSOC-1516 (BYU)	Lower Kittanning	21	301	0.66	4.9	0.08
29	PSOC-1520 (BYU)	Smith-Roland	52	386	0.56	4.2	0.15
30	PSOC-1521 (BYU)	Lower Hartshorne	16	237	0.71	4.1	0.36

Appendix B: Sample CPD Model Input Files

In order to predict tar and total volatiles yields reported by Fletcher and Hardesty using the CPD model, the chemical structure, elemental composition, gas velocity history, and gas temperature history had to be specified. Three input files were used to specify this information: (i) a main input file where the coal properties were specified, (ii) a velocity profile, and (iii) a temperature profile. Based on the temperature and velocity profiles, and the composition of the coal, the CPD model solves the energy equation to determine the particle temperature history. Sample input files for the Pittsburgh no. 8 coal are given below.

Main Input File

```
sandia_ffb.vel      !velocity profile from sandia flat-flame-burner
sandia_ffb.temp     !temperature profile from sandia flat-flame-burner
out.1451.nmr        !specify output file
1.                 TIMAX      !maximum time (seconds)
300                TG0
72.               VG0 !cm/s
0.7               RHOP !G/CM**3
1.06e-2           DP !CM
0.0              swell !(df-d0)/d0
-100.            DELHV !CAL/G (- MEANS ENDOTHERMIC)
.015             Omegaw
.153            OMEGAA
.7              EMIS
500.            TWALL
1700.           THTR (1700 for high T, 1200 for Low T)
300.            TTUBE
5.e-5,1.e-4,10   dt,dtmax,iprint

0.48            !p0
0.0             !c0
4.8            !sig+1
```

329	!mw(solum)
33	!mdel(solum)
2.602e15	!ab
55400	!eb
1800	!ebsig
0.9	!ac=rho
0	!ec
3.e15	!ag
69000	!eg
8100	!egsig
3.e15	!Acr (pre-exponential factor for crosslinking rate)
65000	!Ecr (Activation energy for crosslinking rate)
1.0	!pressure (atm)

.8423	%Carbon (DAF)
.0554	%H
.0165	%N
.0756	%O
.0101	%S

Velocity Profile

c velocity profile of sandia flat-flame burner

c z(mm) vp (cm/s)

0	38
2.5	71
5	104
7.5	137
13	176
25	189
38	199
64	216

Temperature Profile

c Temperature profile of sandia flat-flame burner

c z(mm) Tg (K)

00.0	300
2.5	557
5	815
7.5	1072
13	1608
25	1583
38	1568
64	1545

Appendix C: Sample CPD Model Input File

The NMR correlation was used to estimate the chemical structure of 17 coals studied by Xu and Tomita. The CPD model was then used to predict tar and total volatiles yields based on the estimated chemical structure. Because a velocity profile was not reported by Xu and Tomita, a particle temperature history was estimated based on the reported heating rate and peak temperature. A sample input file for a Yallourn coal is given below. The same particle temperature profile was used for each coal.

Sample Input File

```
0.68      !p0
.15       !c0
4.1       !sig+1
340       !mw
50        !mdel

2.602e15  !ab
55400     !eb
1800      !ebsig
0.9       !ac=rho
0         !ec
3.e15     !ag
69000     !eg
8100      !egsig
3.e15     !Acr (pre-exponential factor for crosslinking rate)
65000     !Ecr (Activation energy for crosslinking rate)

1.0       !pressure (atm)

6         !number of time points
0,300    !time(ms),particle temp(K)
100,600
200,900
```

246,1037
300,1037
4246,103

Appendix D: Tabulated Mass and Tar Release

Table D.1

Predicted and Measured Mass and Tar Yields Reported by Xu and Tomita

coal	% mass release		% tar yield	
	experimental	CPD	experimental	CPD
Yallourn	51.0	51.2	19.9	15.8
Rhein Braun	52.5	48.6	22.1	18.4
Morwell	55.5	51.1	25.6	14.8
Velva	48.5	53.0	17.9	15.0
Soyakoishi	49.0	50.5	20.9	16.6
South Beulah	47.0	54.2	16.8	17.0
Colowyo	41.5	50.2	19.3	16.2
Taiheiyo	53.0	47.7	29.6	24.6
Millmerran	51.5	46.4	29.8	24.4
Wandoan	52.0	51.0	27.9	25.5
Hunter Valley	38.0	50.1	21.9	22.0
Liddell	39.5	47.5	22.2	26.0
Newvale	35.5	46.8	19.4	24.2
Yubari Shinko	38.0	37.6	22	20.8
Vicary Creek	24.5	23.5	11.7	8.0
Keystone	17.0	12.8	8.1	3.7
Hongay	6.0	4.4	2.6	2.1

Appendix E: Nitrogen Release Comparisons

Comparisons of CPD model predictions of N_{site} , N_{char} , fractional nitrogen release, and mass release that were not included in chapter 5 are given in this appendix. For reference, Table 5.3 is also repeated below.

Table 5.3.

Description of Sets of Test Cases Used in Model Evaluation

Set	Researcher(s)	Coals (rank)	Reactor; residence time; peak gas temp; approximate heating rate
1	Fletcher and Hardesty ⁴⁸	Beulah Zap (lig), Blue #1 (subB), Illinois #6 (hvbB), Pittsburgh #8 (hvaB), Pocahontas #3 (lvbB)	^a drop tube; 250 ms; 1050 K; 10^4 K/s. ^b drop tube; 240 ms; 1250 K; 10^4 K/s. ^c FFB (flat-flame burner); 47 ms; 1600 K; 10^5 K/s.
2	Chen ⁵²	Dietz (subB), Illinois #6 (hvaB), Pittsburgh #8 (hvaB), Lower Kittanning (lvB)	drop tube; 56, 61, 66, 72, 77, 83, 86.5, and 89 ms; radiantly heated particles (1840 K wall temperature); 10^4 K/s.
3	Hambly ¹⁶	Beulah Zap (lig), Blue #1 (subB), Illinois #6 (hvbB), Pittsburgh #8 (hvaB), Pocahontas #3 (lvbB)	^a drop tube; 170 ms; 820 K; 10^4 K/s. ^b drop tube; 280 ms; 1080 K; 10^4 K/s. ^c drop tube; 410 ms; 1220 K; 10^4 K/s. ^d FFB; 18 ms; 1560 K, 10^5 K/s.

N_{site} and N_{char} Comparisons

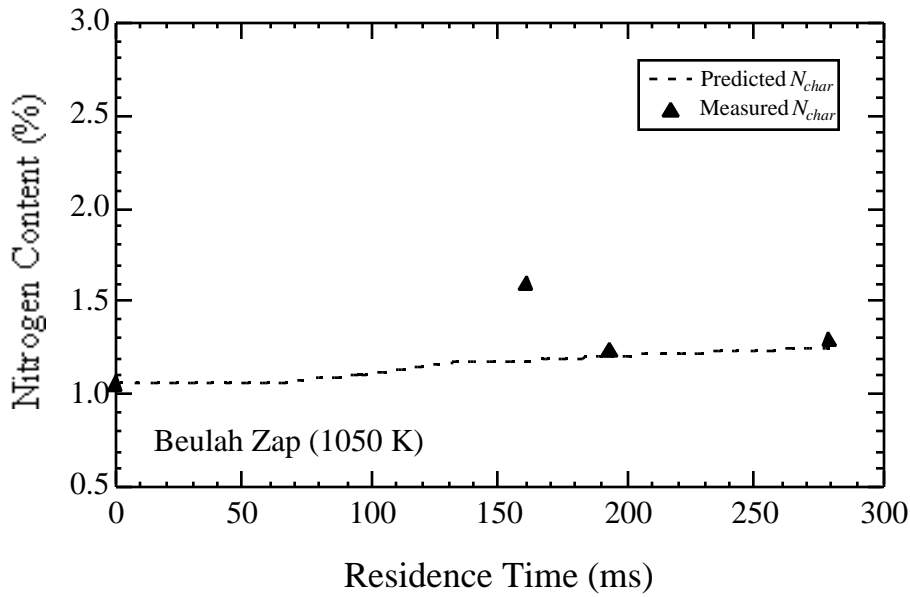


Figure E.1. Comparison of predicted and measured N_{char} values of a Beulah Zap lignite. Beulah Zap was pyrolyzed in a drop tube reactor with a peak temperature of 1050 K and a residence time of 280 ms (Set 1a).

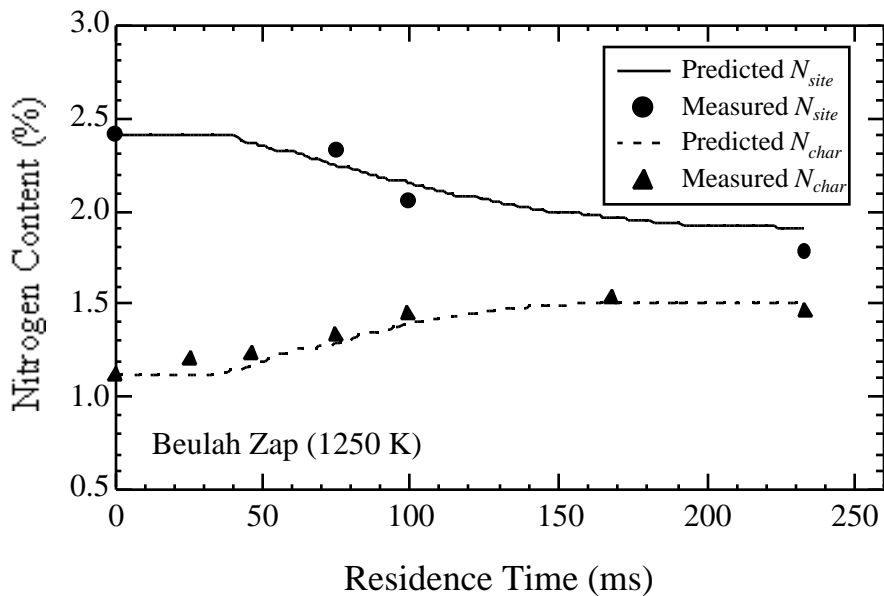


Figure E.2. Comparison of predicted and measured N_{char} values of a Beulah Zap lignite. Beulah Zap was pyrolyzed in a drop tube reactor with a peak temperature of 1250 K and a residence time of about 240 ms (Set 1b).

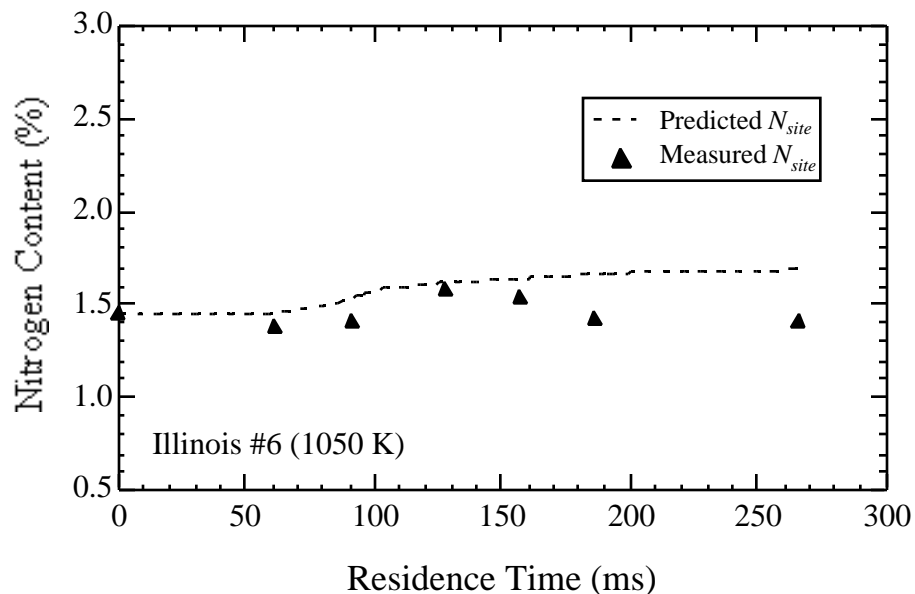


Figure E.3. Comparison of predicted and measured N_{char} values of a Illinois no. 6 high volatile bituminous coal. Illinois no. 6 was pyrolyzed in a drop tube reactor with a peak temperature of 1050 K and a residence time of about 260 ms (Set 1a).

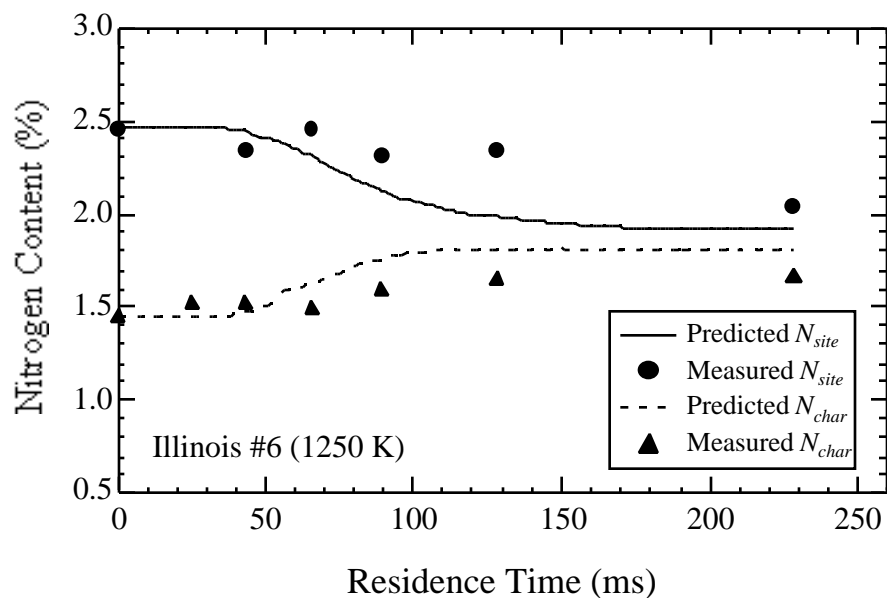


Figure E.4. Comparison of predicted and measured N_{char} values of a Illinois no. 6 high volatile bituminous coal. Illinois no. 6 was pyrolyzed in a drop tube reactor with a peak temperature of 1250 K and a residence time of about 240 ms (Set 1b).

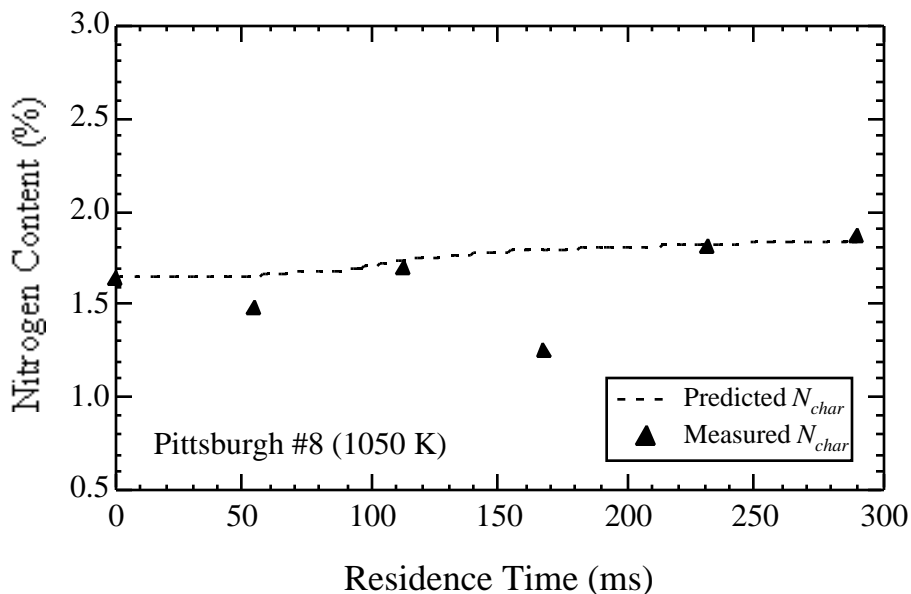


Figure E.5. Comparison of predicted and measured N_{char} values of a Pittsburgh no. 8 high volatile bituminous coal. Pittsburgh no. 8 was pyrolyzed in a drop tube reactor with a peak temperature of 1050 K and a residence time of about 290 ms (Set 1a).

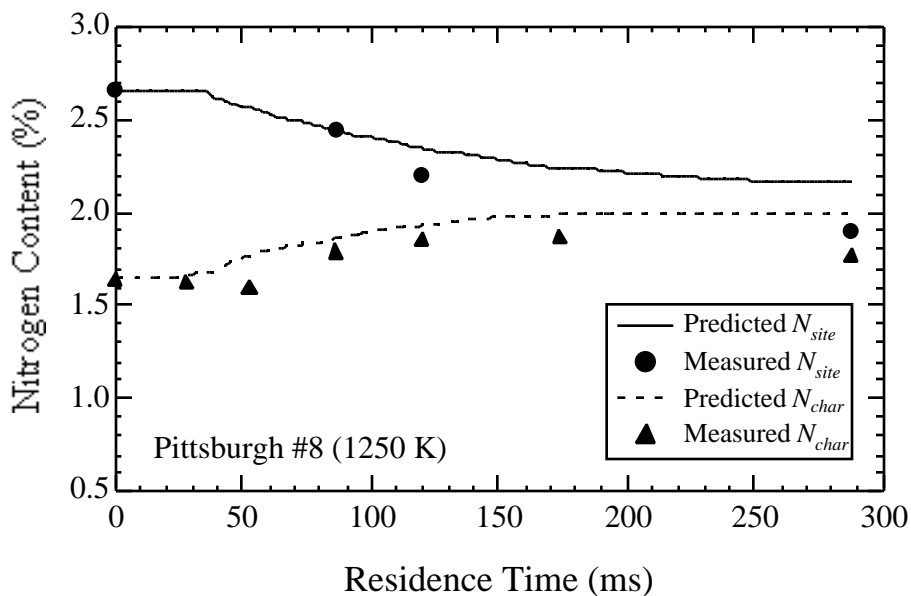


Figure E.6. Comparison of predicted and measured N_{char} values of a Pittsburgh no. 8 high volatile bituminous coal. Pittsburgh no. 8 was pyrolyzed in a drop tube reactor with a peak temperature of 1250 K and a residence time of about 290 ms (Set 1b).

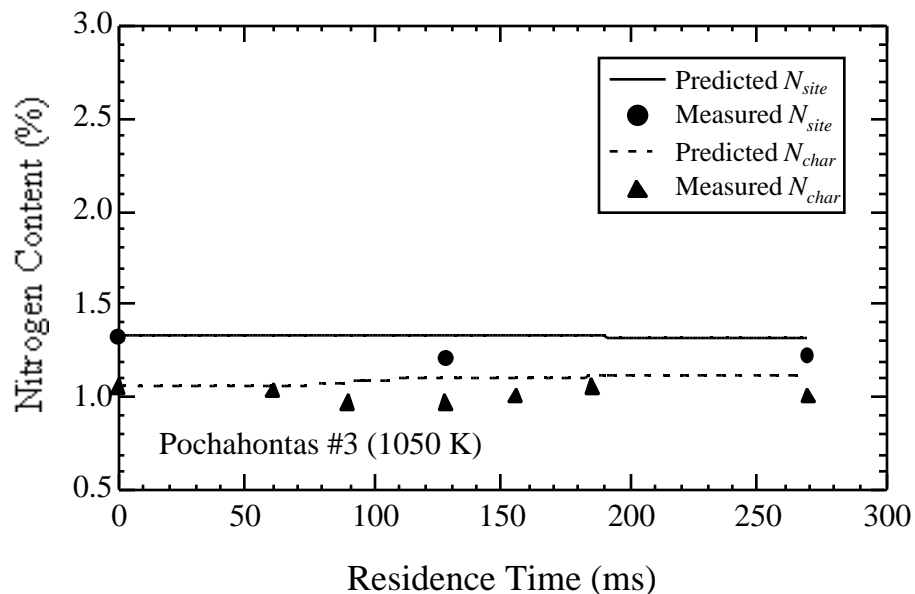


Figure E.7. Comparison of predicted and measured N_{char} values of a Pocahontas no. 3 low volatile bituminous coal. Pocahontas no. 3 was pyrolyzed in a drop tube reactor with a peak temperature of 1050 K and a residence time of about 270 ms (Set 1a).

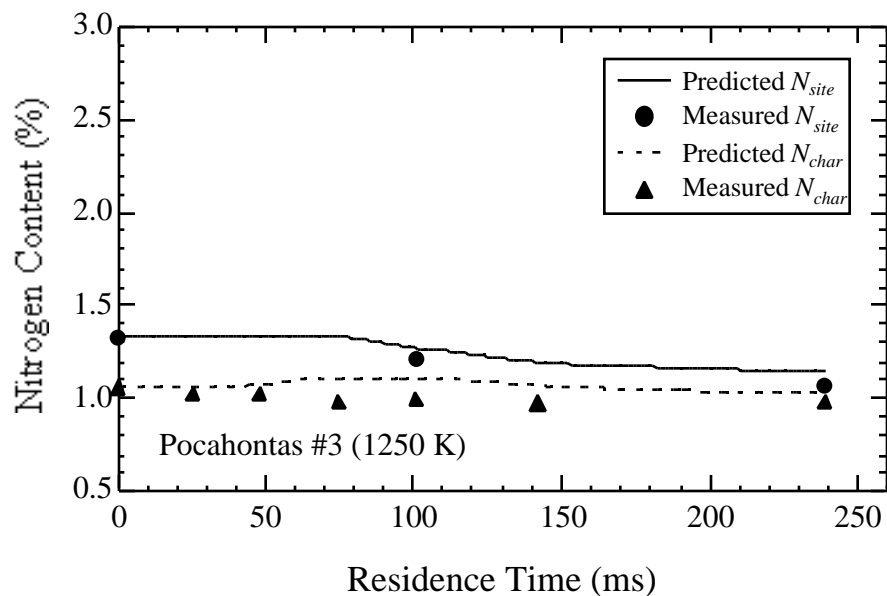


Figure E.8. Comparison of predicted and measured N_{char} values of a Pocahontas no. 3 low volatile bituminous coal. Pocahontas no. 3 was pyrolyzed in a drop tube reactor with a peak temperature of 1250 K and a residence time of about 240 ms (Set 1b).

Mass and Nitrogen Release Comparisons

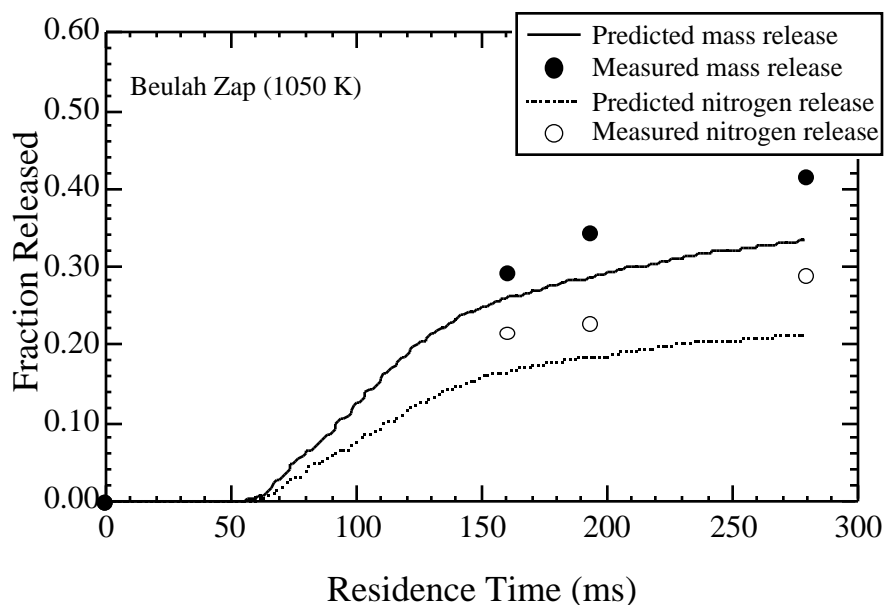


Figure E.9. Comparison of predicted and measured mass and nitrogen release of a Beulah Zap coal. Beulah Zap was pyrolyzed in a drop tube reactor with a peak temperature of 1050 K and a residence time of 280 ms (Set 1a).

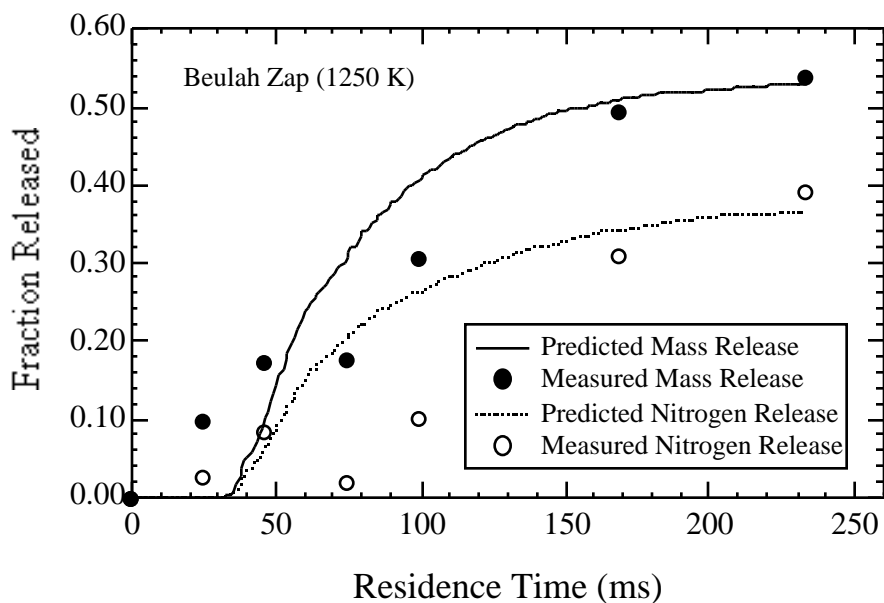


Figure E.10. Comparison of predicted and measured mass and nitrogen release of a Beulah Zap coal. Beulah Zap was pyrolyzed in a drop tube reactor with a peak temperature of 1250 K and a residence time of 240 ms (Set 1b).

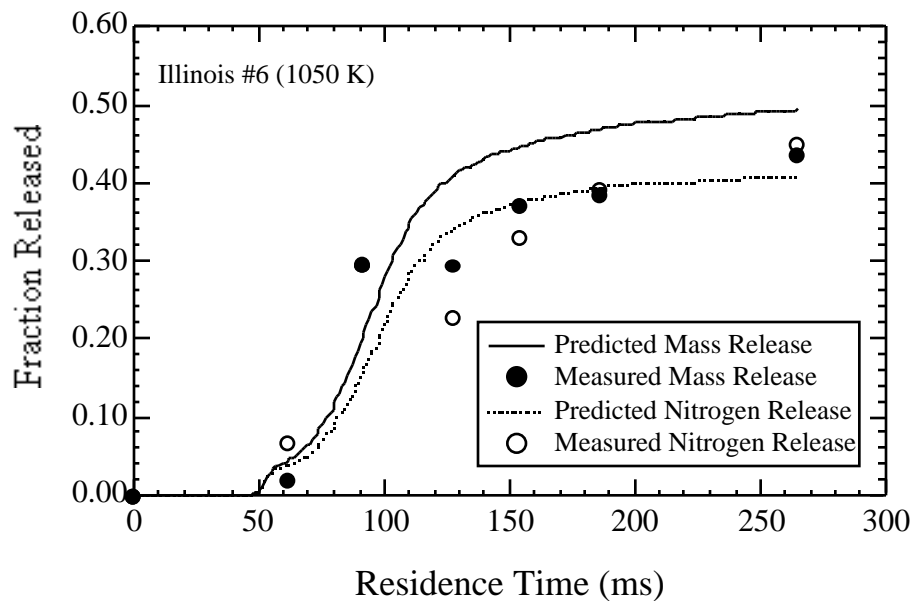


Figure E.11. Comparison of predicted and measured mass and nitrogen release of a Illinois no. 6 coal. Illinois no. 6 was pyrolyzed in a drop tube reactor with a peak temperature of 1050 K and a residence time of 260 ms (Set 1a).

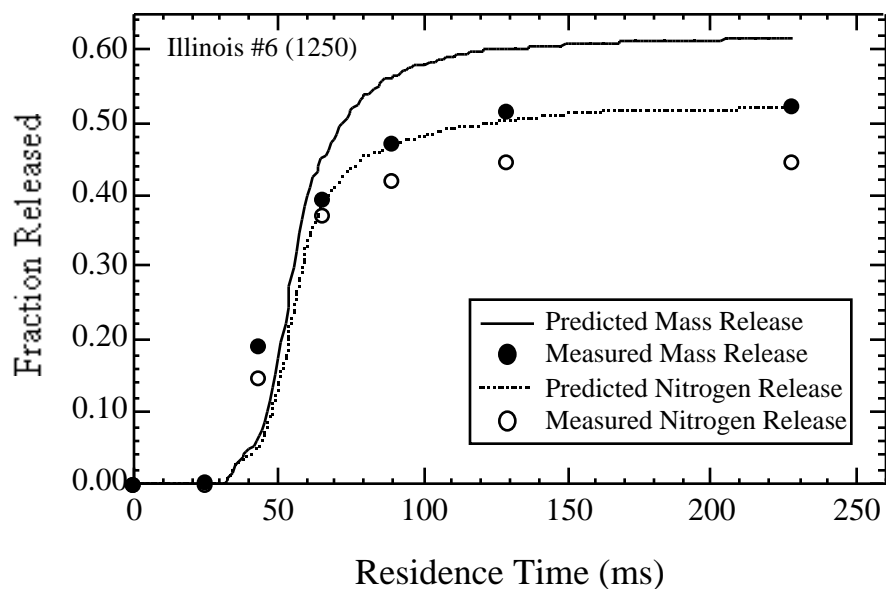


Figure E.12. Comparison of predicted and measured mass and nitrogen release of a Illinois no. 6 coal. Illinois no. 6 was pyrolyzed in a drop tube reactor with a peak temperature of 1250 K and a residence time of 240 ms (Set 1b).

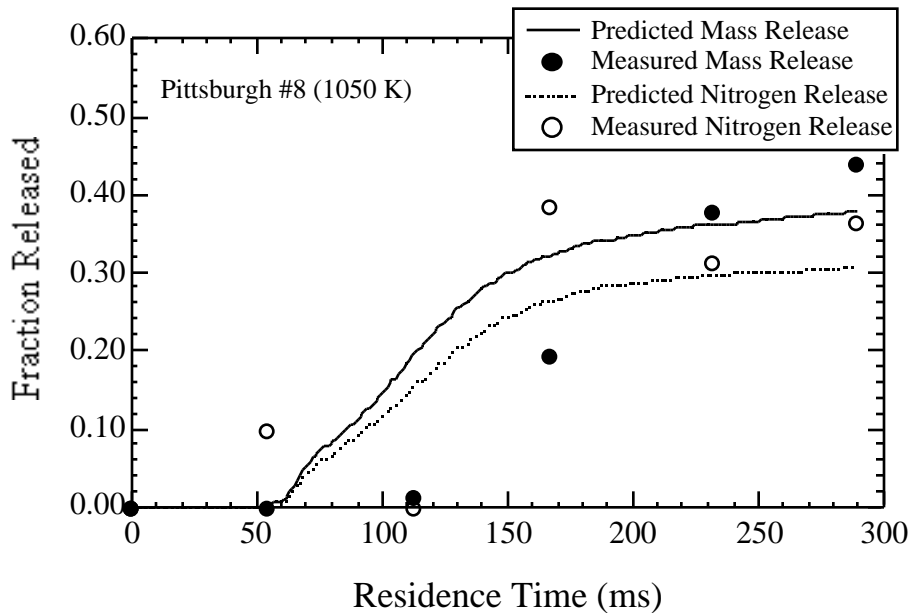


Figure E.13. Comparison of predicted and measured mass and nitrogen release of a Pittsburgh no. 8 coal. The coal was pyrolyzed in a drop tube reactor with a peak temperature of 1050 K and a residence time of 290 ms (Set 1a).

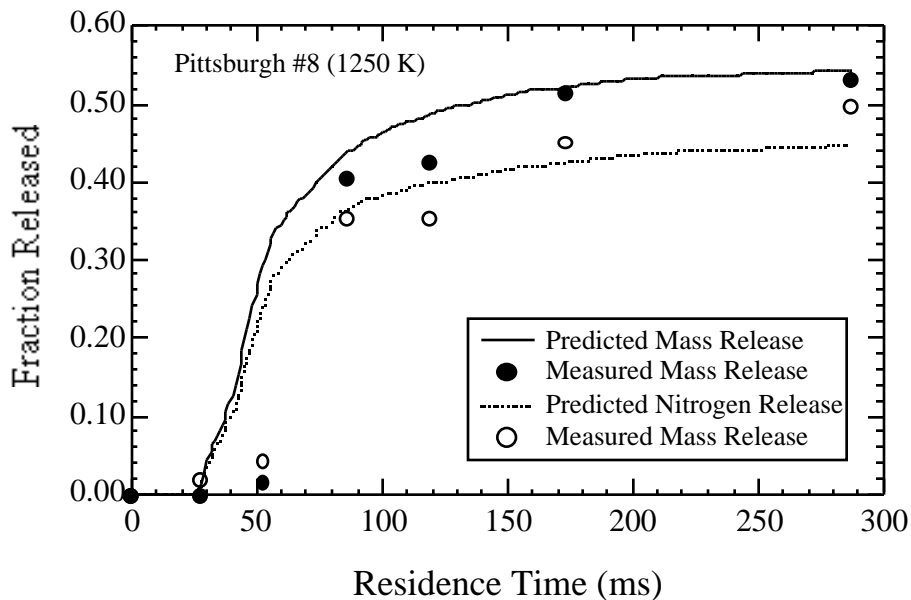


Figure E.14. Comparison of predicted and measured mass and nitrogen release of a Pittsburgh no. 8 coal. The coal was pyrolyzed in a drop tube reactor with a peak temperature of 1250 K and a residence time of 290 ms (Set 1b).

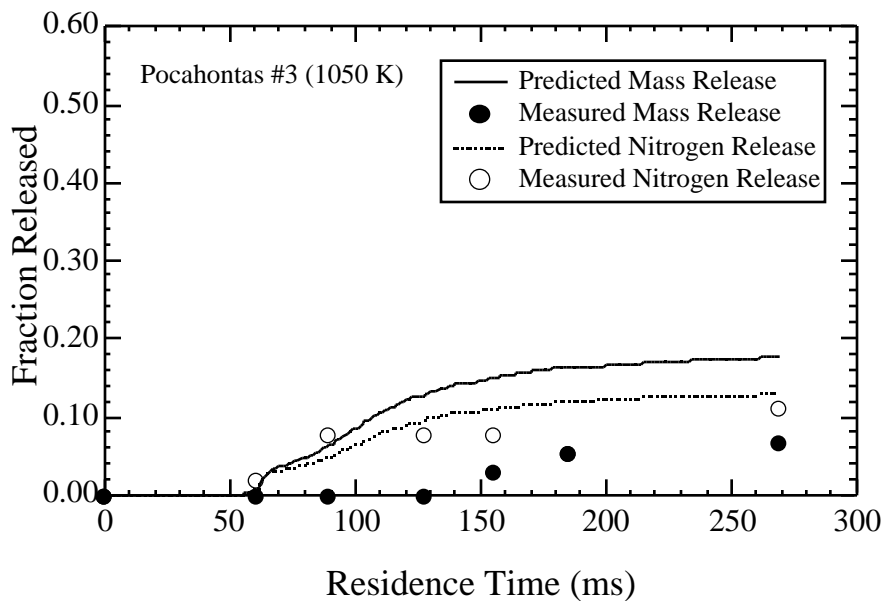


Figure E.15. Comparison of predicted and measured fractional mass and nitrogen release of a Pocahontas no. 3 coal. The coal was pyrolyzed in a drop tube reactor with a peak temperature of 1050 K and a residence time of 270 ms (Set 1a).

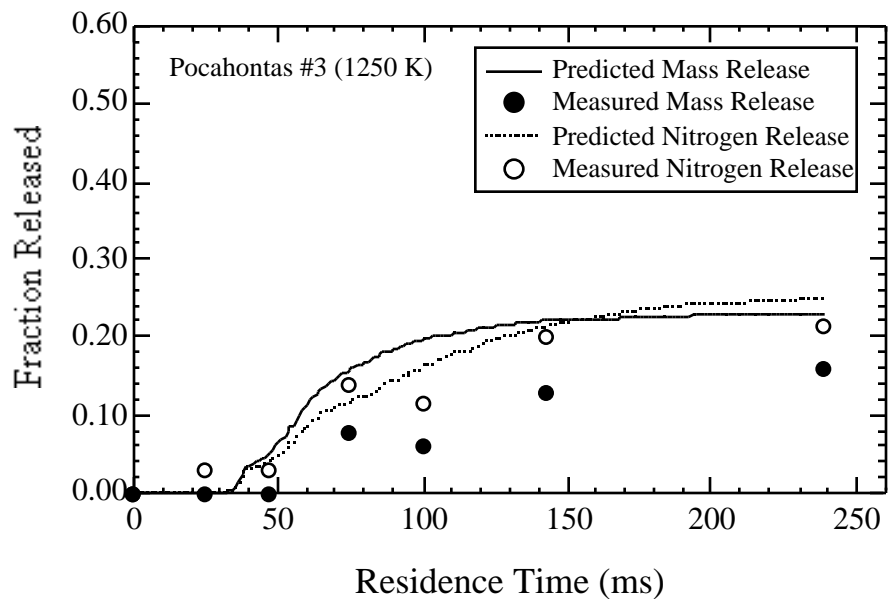


Figure E.16. Comparison of predicted and measured fractional mass and nitrogen release of a Pocahontas no. 3 coal. The coal was pyrolyzed in a drop tube reactor with a peak temperature of 1250 K and a residence time of 240 ms (Set 1b).

Due to wall effects in the drop tube reactor used to conduct the pyrolysis experiments of sets 5, 6, and 7, the reported centerline gas temperature profiles reported by Eric Hambly and used in the CPD model likely under-estimate the severity of the 820 K and 1080 K pyrolysis conditions. This may explain some of the large discrepancies between predicted and measured mass release as shown in Figures D.17 and D.18.

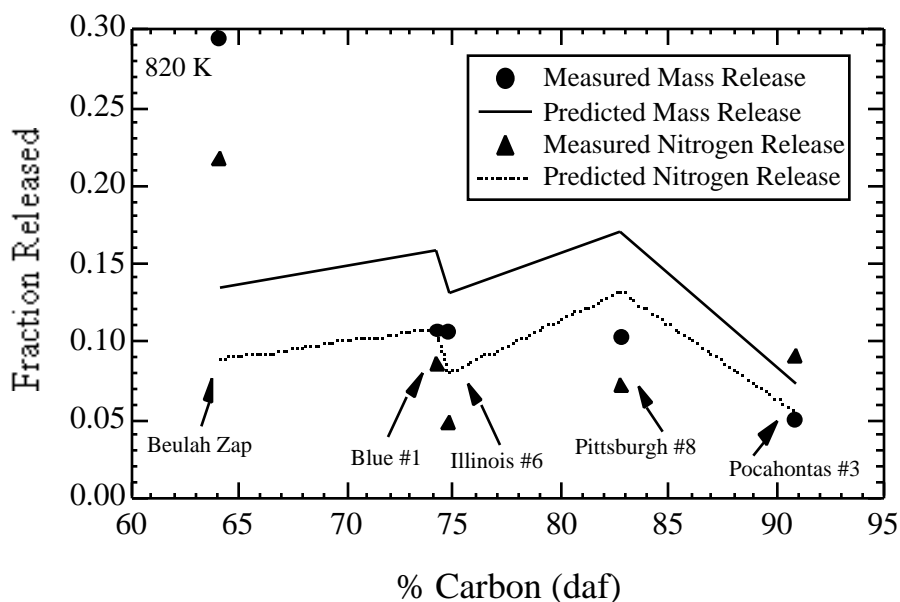


Figure E.17 Comparison of predicted and measured mass and nitrogen release of five coals pyrolyzed by Hambly at the 820 K drop tube condition (Set 3a).

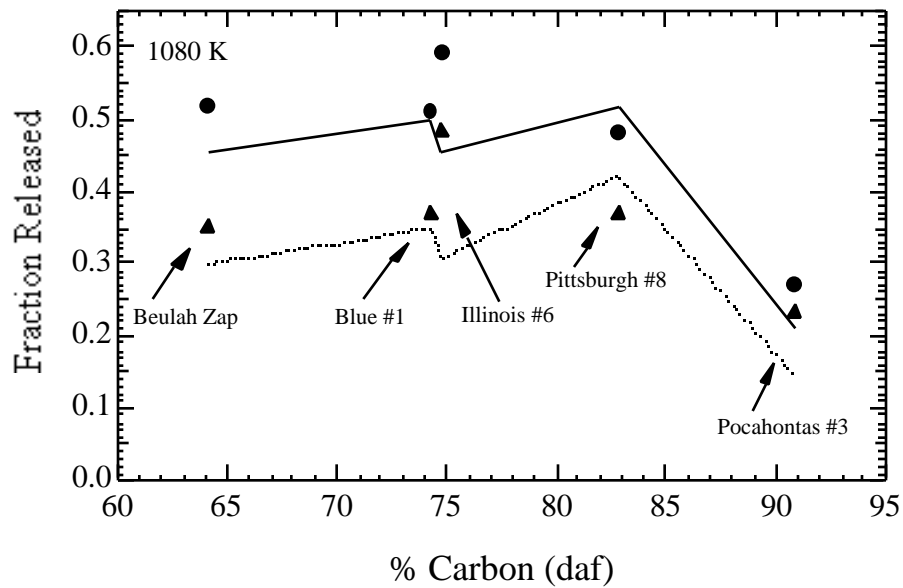


Figure E.18 Comparison of predicted and measured mass and nitrogen release of five coals pyrolyzed by Hamby at the 1080 K drop tube condition (Set 3b).

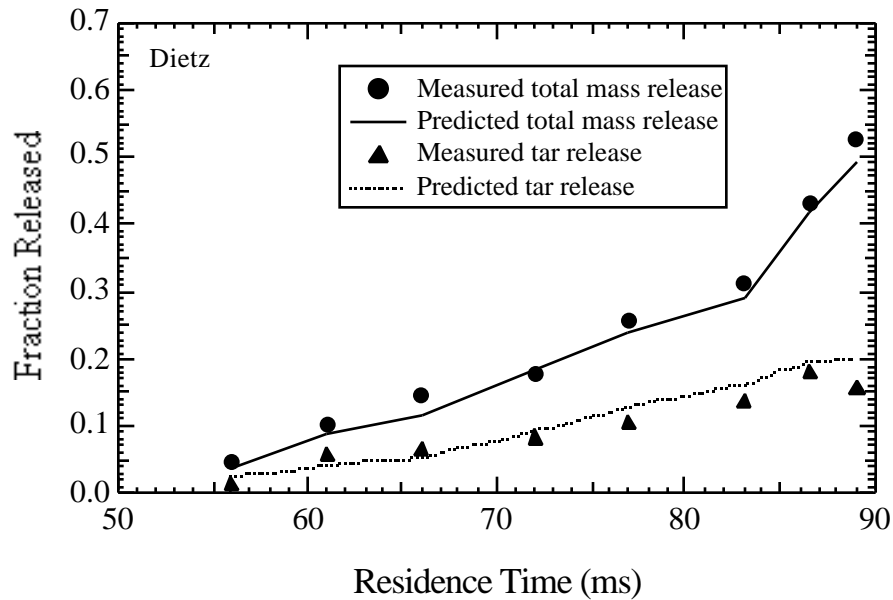


Figure E.19. Comparison of predictions of total mass and tar release with experimental data from experiments conducted by Chen on a Dietz subbituminous coal. Particles were radiatively heated in a drop tube reactor with a wall temperature of 1800 K (Set 2).

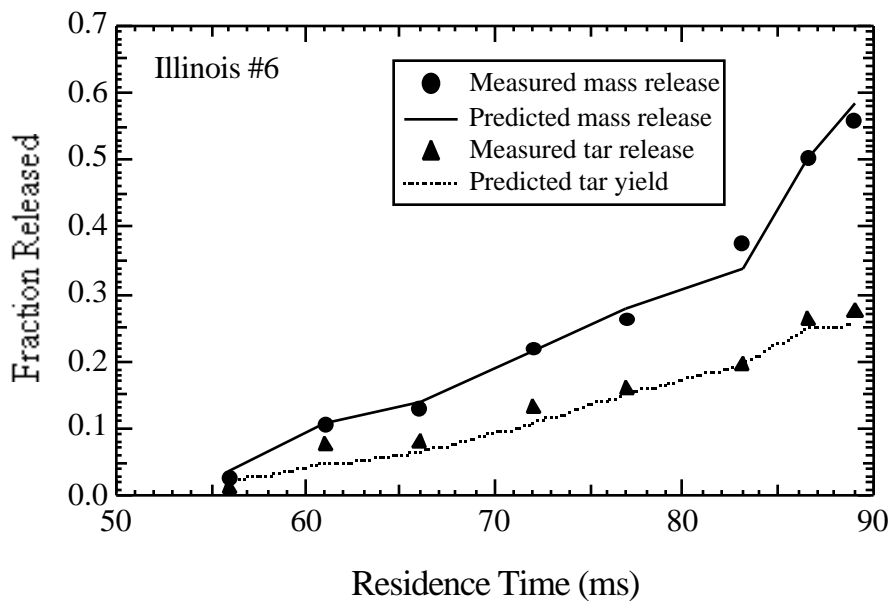


Figure E.20. Comparison of predictions of total mass and tar release with experimental data from experiments conducted by Chen on a Illinois no. 6 bituminous coal. Particles were radiatively heated in a drop tube reactor with a wall temperature of 1800 K (Set 2).

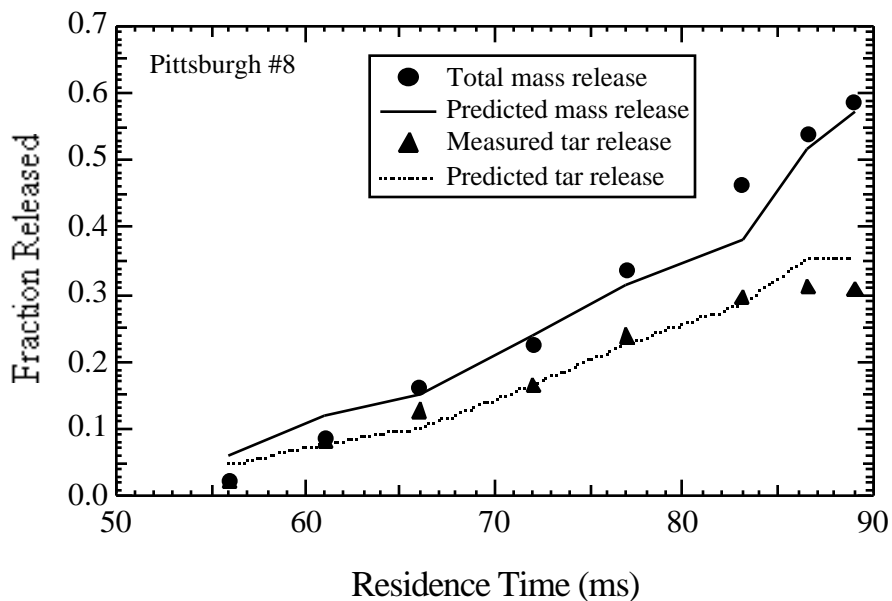


Figure E.21. Comparison of predictions of total mass and tar release with experimental data from experiments conducted by Chen on a Pittsburgh no. 8 bituminous coal. Particles were radiatively heated in a drop tube reactor with a wall temperature of 1800 K (Set 2).

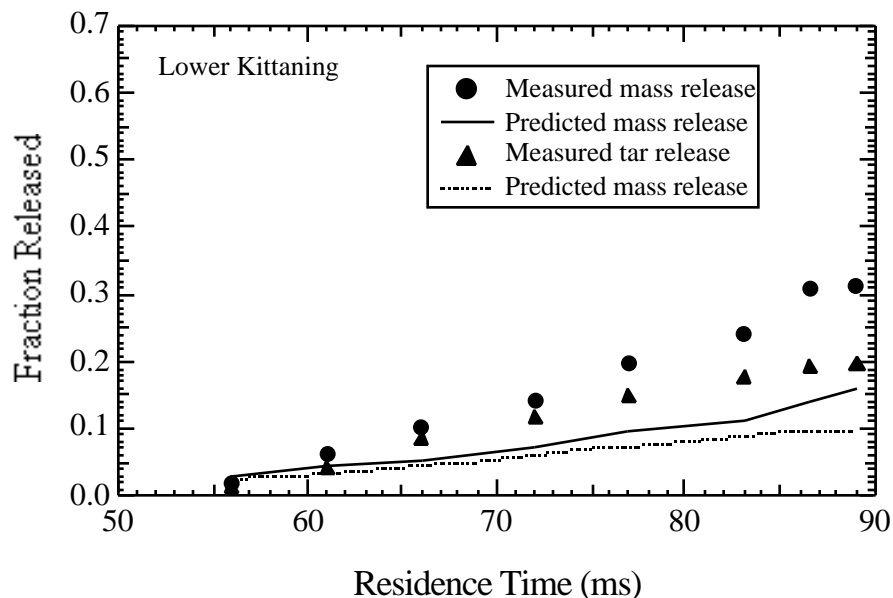


Figure E.22. Comparison of predictions of total mass and tar release with experimental data from experiments conducted by Chen on a Lower Kittanning low volatile coal. Particles were radiatively heated in a drop tube reactor with a wall temperature of 1800 K (Set 2).

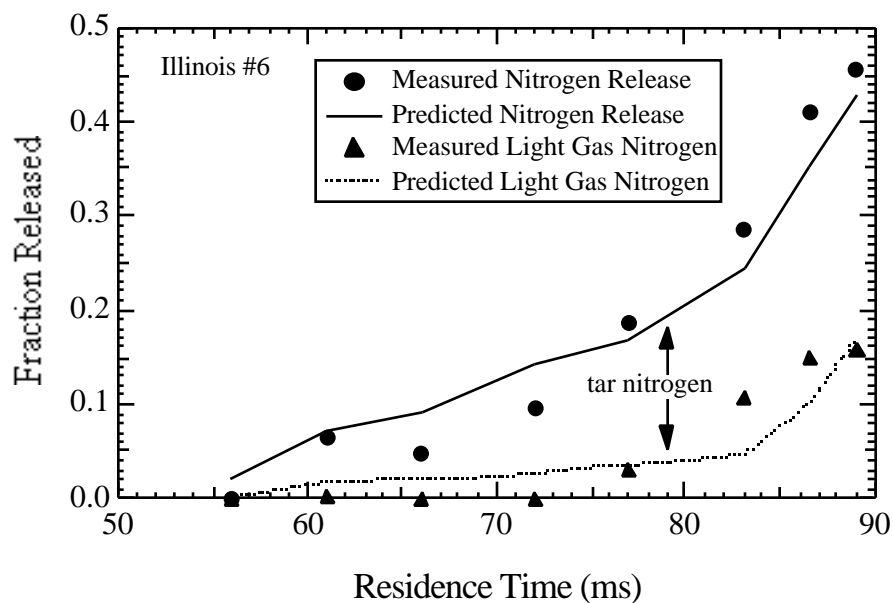


Figure E.23. Comparison of predictions of total, tar, and light gas nitrogen with experimental data from experiments conducted by Chen on a Illinois no. 6 bituminous coal. Particles were radiatively heated in a drop tube reactor with a wall temperature of 1800 K (Set 2).

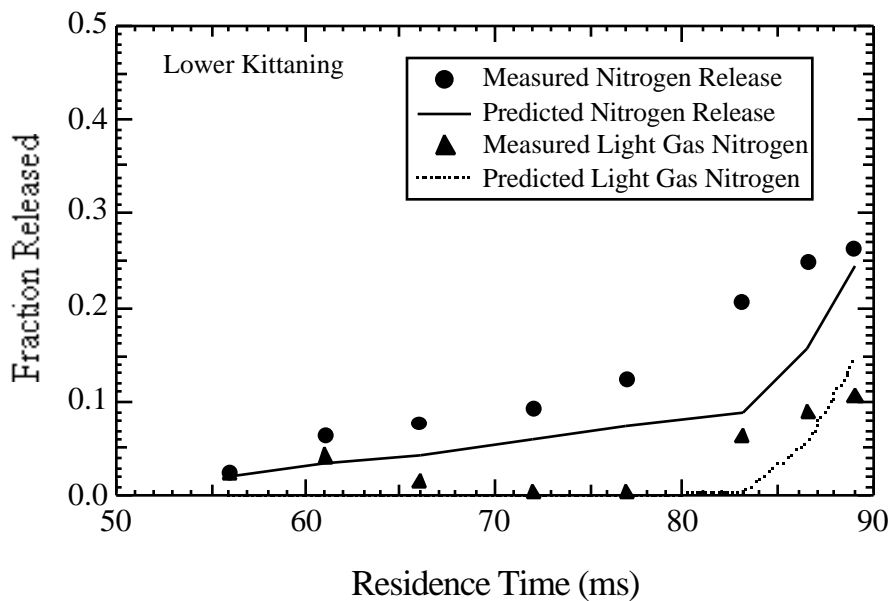


Figure E.24. Comparison of predictions of total, tar, and light gas nitrogen with experimental data from experiments conducted by Chen on a Lower Kittaning low volatile coal. Particles were radiatively heated in a drop tube reactor with a wall temperature of 1800 K (Set 2).

Appendix F: Particle Temperature Profiles of Radiantly Heated Reactor

Particle temperature profiles were fit to match the total mass and tar yields of Chen's pyrolysis experiments on a Dietz subbituminous coal. The particle temperature profiles estimated in this manner and used in the CPD model for each of Chen's pyrolysis conditions are given in this appendix. The format of the input files were similar to the input file shown in Appendix C.

Table F.1
56 ms Condition

Time (ms)	Particle Temperature (K)
0	300
6	315
12	335
18	400
24	480
30	640
36	740
42	775
48	770
56	760

Table F.2

61 ms Condition

Time (ms)	Particle Temperature (K)
0	300
6	315
12	335
18	400
24	500
30	670
36	820
42	835
48	835
54	810
61	760

Table F.3

66 ms Condition

Time (ms)	Particle Temperature (K)
0	300
6	315
12	335
18	400
24	500
30	605
36	710
42	770
48	830
54	875
60	840
66	740

Table F.4

72 ms Condition

Time (ms)	Particle Temperature (K)
0	300
10	330
20	345
30	425
40	560
50	770
58	910
70	870
72	735

Table F.5

77 ms Condition

Time (ms)	Particle Temperature (K)
0	300
10	335
20	350
30	430
40	555
50	770
60	950
70	890
77	770

Table F.6

83 ms Condition

Time (ms)	Particle Temperature (K)
0	300
10	335
20	360
30	450
40	580
50	800
60	980
70	960
80	820
83	790

Table F.7

87 ms Condition

Time (ms)	Particle Temperature (K)
0	300
10	335
20	380
30	415
40	610
50	800
60	1050
70	1140
80	1040
86.5	940

Table F.8
89 ms Condition

Time (ms)	Particle Temperature (K)
0	300
10	340
20	400
30	460
40	660
50	700
60	1130
70	1270
80	1170
89	1070

Appendix G: Coals Pyrolyzed in BYU FFB

A list of the coals pyrolyzed in the BYU flat-flame burner by Hambly and in this study is given this appendix. The coals listed here correspond to coals 19 to 30 given in Tables 4.1, 4.2, and 4.3. The chemical structure input parameters were taken directly from the ^{13}C NMR data listed in Table 4.3 except for the Lykens Valley #2 coal. The correlation described in Chapter 4 was used to estimate the structural parameters for the Lykens Valley #2 coal.

Table G.1
Elemental Composition of Coals Pyrolyzed in FFB

Seam	ASTM Rank	% C (daf)	% H (daf)	% O (daf)	% N (daf)	% S (daf)
Smith-Roland	subC	67.4	5.37	24.39	1.00	1.84
Beulah-Zap	ligA	68.5	4.94	24.96	1.00	0.64
Bottom	subC	70.7	5.83	20.83	1.47	1.18
Adaville #1	hvCb	72.5	5.22	20.09	1.17	1.04
Deadman	subA	76.5	5.24	15.95	1.53	0.76
Kentucky #9	hvBb	79.4	5.62	8.57	1.74	4.71
Elkhorn #3	hvAb	82.7	5.73	8.76	1.78	0.99
Sewell	m vb	85.5	4.91	7.12	1.72	0.72
Lower Kittanning	lvb	86.2	4.86	4.64	1.81	2.45
Penna. Semian. C	sa	88.4	4.02	5.47	1.24	0.86
Lower Hartshorne	lvb	91.2	4.56	1.53	1.82	0.89
Lykens Valley #2	an	93.8	2.72	1.96	0.92	0.62

Appendix H: Velocity and Temperature Profiles of FFB

The velocity and temperature profiles of the flat-flame burner experiments conducted by Hambly (18 ms) and in this Study (78 ms) are given in this appendix.

Table H.1

Gas Velocity Profile for 18 ms FFB Condition

Position (mm)	Gas Velocity (cm/s)
0	3.4
0.02	13
0.33	49
1.04	88
2.33	128
4.66	168
7.56	197
10.01	212
13.07	223
18.8	233
25.4	233
33	233

Table H.2

Gas Temperature Profile for 18 ms FFB Condition

Position (mm)	Gas Temperature (K)
0	300
6.4	1591
12.7	1625
19.1	1636
25.4	1641
31.8	1641
33	1639

Table H.3

Gas Velocity Profile for 78 ms FFB Condition

Position (mm)	Gas Velocity (cm/s)
0	23
6.4	183
12.7	210
19.1	224
25.4	250
31.8	250
38.1	250
50.8	250
63.5	250
76.2	250
88.9	250
102	250
127	250
152	250
178	250

Table H.4

Gas Temperature Profile for 78 ms FFB Condition

Position (mm)	Gas Temperature (K)
0	300
6.4	1591
12.7	1625
19.1	1636
25.4	1641
31.8	1641
38.1	1638
50.8	1633
63.5	1624
76.2	1619
88.9	1609
102	1598
127	1579
152	1552
178	1528

Appendix I: Analysis of Light Gas Data

Introduction

The devolatilization of coal results in tar and light gas release.⁵ Light gas release results from the cleavage of aliphatic bridge and side chain material. Light gas in general is mainly composed of the following species: (i) H₂O; (ii) CO₂; (iv) CO; (v) CH₄; and (iv) other light hydrocarbons. The distribution of the species depends on the functional group content of the coal. In general, light gas release is a function of coal rank. Low rank coals release the largest relative amount of light gas, and light gas release decreases with higher rank coals. The distribution of light gas species is also a function of rank. Since the release of light gas is the result of a chemical rupture of aliphatic bridge and side chain material, the kinetics of light gas release are also a function of residence time, particle temperature, and aliphatic concentration.

TG-FTIR spectroscopy was used to analyze the devolatilization products of the Arrgone coals to determine the kinetics of the evolution of light gas species.³¹ The FG model of the FG-DVC is based on these kinetics.¹¹ The FG model determines the quantity and distribution of light gas evolved during devolatilization using first order kinetics with distributed activation energy. One of the difficulties with the approach used by the FG-DVC model is that it requires extensive knowledge about the function group content of the coal (generally through FTIR spectroscopy), which is not generally known for most coals.

A simpler approach would be to develop a look up table based on coal rank and the extent of light gas release. The purpose of this study is to evaluate available light gas release data to determine whether or not the “look-up” approach is feasible.

TG-FTIR Analysis of Pyrolysis Products

Solomon et. al. developed a TG-FTIR instrument that combines thermogravimetric analysis with evolved gaseous product analysis by Fourier transform infrared spectroscopy.³¹ This instrument was used to analyze the devolatilization products of the eight Argonne premium coals. The analysis gave the relative amounts of the following species evolved during pyrolysis: tar, H₂O, CO, CO₂, CH₄, SO₂, NH₃, C₂H₄, and COS. The samples were heated up to 900 °C at a heating rate of 30 °C/min, and then immediately cooled to 250 °C over a period of 20 minutes.

Eight coals were selected for the Argonne National Laboratory's Premium Coal Sample Program. The coals selected were well characterized and represented a large variation on coal rank. The elemental composition and the chemical structure parameters derived from ¹³C NMR analyses of the Argonne Premium Coals are given in Tables 4.1, 4.2, and 4.3. The Argonne suite of coals vary from a lignite to a low volatile bituminous coal.

Figure H.1 compares the light gas release of the Argonne suite of coals during Solomon's experiments as a function of residence time (temperature profiles were nearly identical for each coal pyrolyzed). The light gas release data illustrate several important trends. First and foremost, Figure H.1 shows that coals close in rank release light gas at nearly the same rate. This is an important trend because it shows that modeling of total light gas release can likely be accomplished based on rank without knowing the functional group composition of each coal. Also, the data show that the initial fraction of light gas released is water which correlates directly with moisture content of the unpyrolyzed coal (Table E.1). Furthermore, it appears that additional light gas release begins to occur between 15 and 18 minutes regardless of coal rank.

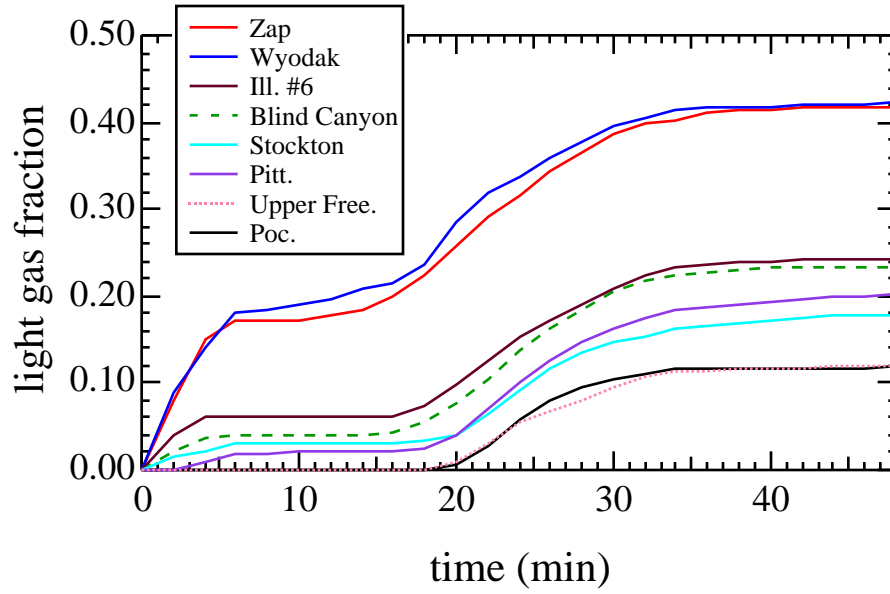


Figure I.1. Comparison of the light gas release of Argonne suite of coals studied using TG-FTIR analysis.

Table I.1

As-Received Moisture Content of Argonne Suite of Coals*

Coal	Moisture (% as recieved)
Beulah Zap	32.24
Wyodak	28.09
Illinois #6	7.97
Blind Canyon	4.63
Lewis Stockton	2.42
Pittsburgh	1.65
Upper Freeport	1.13
Pocahontas #3	0.65

* data obtained from Smith⁵

Figures H.2 through H.6 compare the fractional release (fraction of light gas released) on a dry basis of H₂O, CO₂, CO, CH₄, and C₂H₄, respectively. As with total gas release, coals, two of which are lower rank coals (Illinois #6 and Lewis Stockton) and two of which are high rank coals (Upper Freeport and Pocahontas #3) is has an H₂O content of about 70%, then the H₂O content gradually decreases as further light gas is evolved reaching a content of about 30% in the last stages of devolatilization. There is not a clear correlation between the H₂O content of the light gas and coal rank. As light gas release increases, however, one trend is apparent. The H₂O content of all the light gases converges to a value between 35 and 45% by the end of devolatilization.

The CO₂ content of the lowest rank coals (Beulah Zap and is initially very high, and then gradually decreases to about 30% by the end of devolatilization (Figure H.3). The rest of the coals have a wide variety of CO₂ contents initial, but by the time 30% of light gas has been released, it is observed that the CO₂ contents converge to similar values. The variation in CO₂ content of the initial light gas does not seem to follow any particular trend with rank.

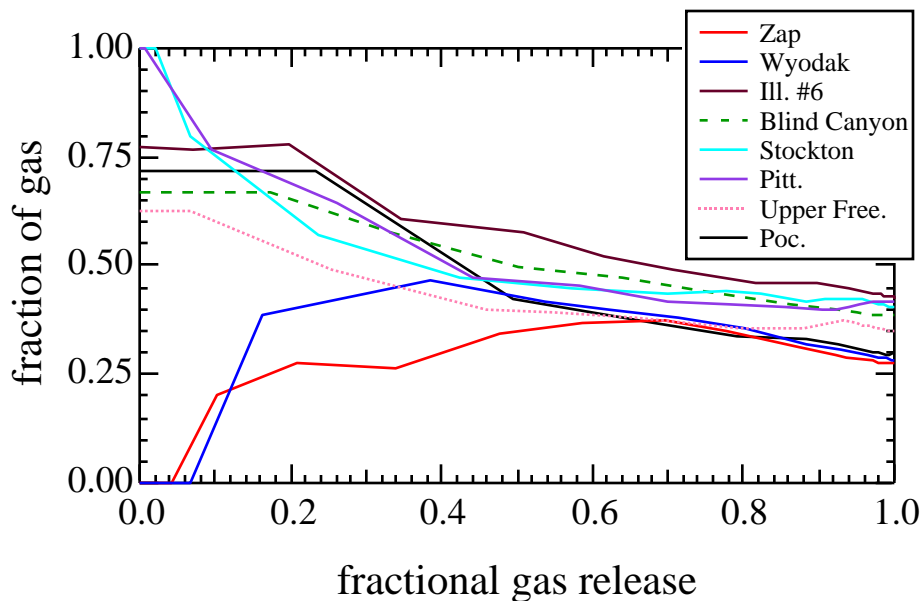


Figure I.2. Fractional release of H₂O of Argonne suite of coals studied using TG-FTIR analysis.

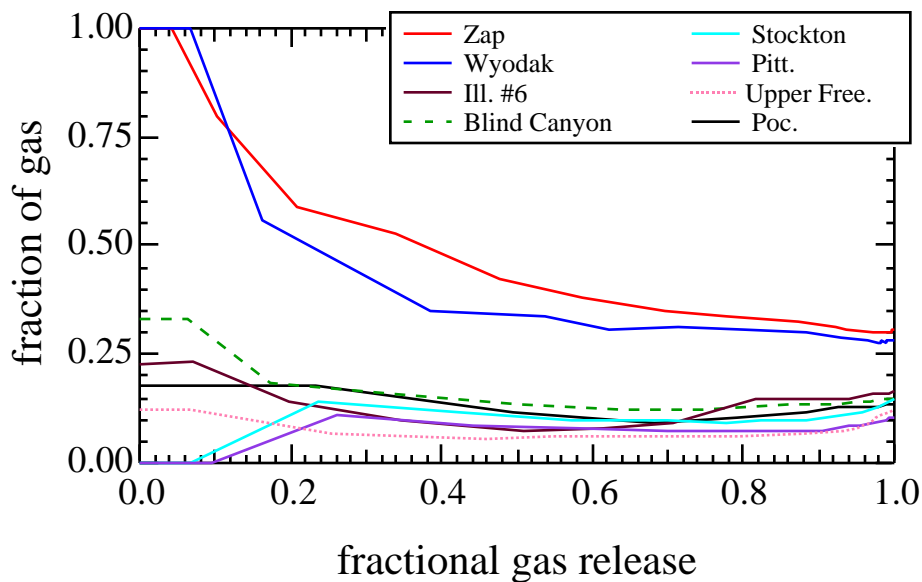


Figure I.3. Fractional release of CO₂ of Argonne suite of coals studied using TG-FTIR analysis.

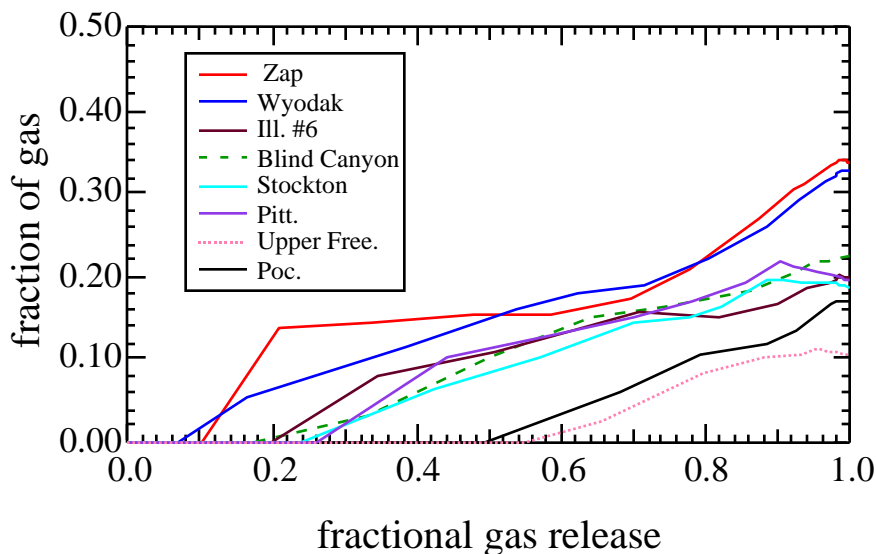


Figure I.4. Fractional release of CO of Argonne suite of coals studied using TG-FTIR analysis.

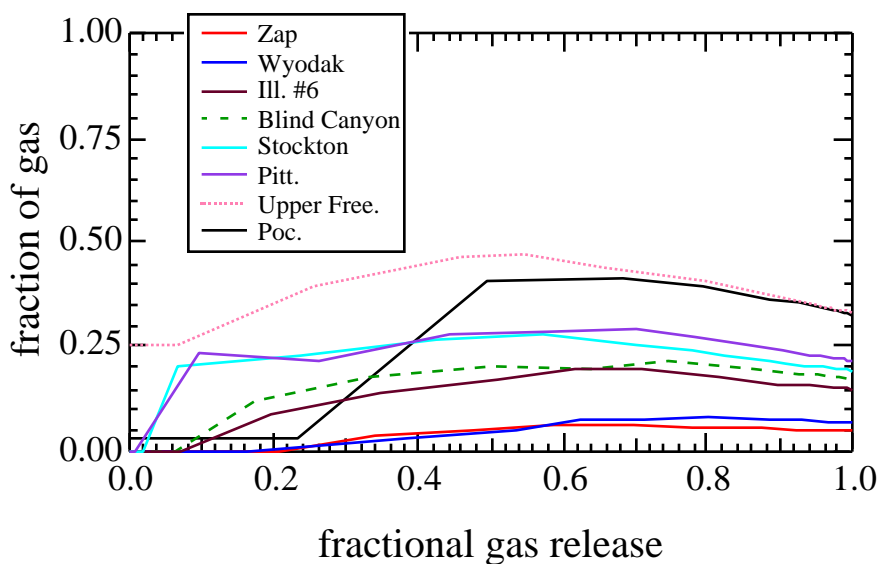


Figure I.5. Fractional release of CH₄ of Argonne suite of coals studied using TG-FTIR analysis.

The initial quantity of light gas released from each of the coals did not contain any CO (Figure H.4). CO began to be released from the low rank coals (Zap and Wyodak) when about 10% of the light gas had been released. The CO content then increased linearly to about 33% by the end of devolatilization. The mid-rank coals (Ill #6, Blind

Canyon, Stockton, and Pittsburgh) began to release CO after about 25% of the total light gas had been released. The CO content of the light gas from the mid-rank coals also increased linearly to 20% at the final stage of devolatilization. Upper Freeport and Pocahontas #3 did not begin to release CO until more than 50% of the total light gas had been released. The CO content of the light gas in each case increased linearly with about the same slope. However, the delay in CO release differed with coal rank, with high rank coals having the greatest delay.

The CH₄ content of light gas in general seems to follow a parabolic pattern (Figure H.5). At the onset of light gas release the CH₄ content is low, reaches a maximum when about 50% of the light gas has been released, then declines as light gas release comes to completion. The CH₄ content of light gas also appears to follow a definite trend in relation to coal rank. Low rank coals have the lowest relative CH₄ content, and CH₄ content increases with coal rank. The CH₄ content ranged from 5% in the light gas of the lowest rank coal to nearly 35% in the light gas of the highest rank coal at the end of light gas release.

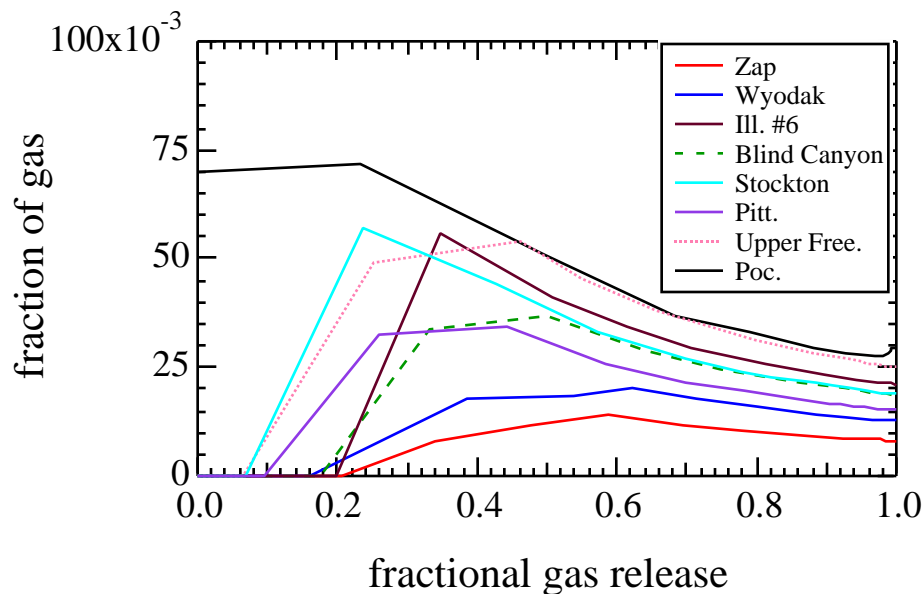


Figure I.6. Fractional release of C₂H₄ of Argonne suite of coals studied using TG-FTIR analysis.

C_2H_4 content of light gas has a rank dependence similar to that of CH_4 . That is, low rank coals have a lower relative C_2H_4 content than do higher rank coals. For most of the coals tested, C_2H_4 release is delayed until 10 to 20% of the light gas has been released. Then, the C_2H_4 content increases sharply after which it begins to gradually decline. The C_2H_4 content ranged from 0.7% in the light gas of the lowest rank coal to 3.0% in the light gas of the highest rank coal at the end of light gas release.

Conclusions based on TG-FTIR data. A light gas distribution model would be feasible based on the data given by Solomon. For most light gas species, a rank and degree of light gas release is readily evident. For the H_2O and CO_2 light gas content, two of the main constituents of light gas, a trend with rank is not readily evident. However, the light gas contents of these two species seem to follow similar patterns for similar coals which makes the look up table idea feasible.

Light Gas Data From a Radiantly Heated Reactor

Chen conducted pyrolysis experiments on four PETC coals using a radiant coal flow reactor (Table H.2).⁵² In the radiant flow reactor, the coal particles were heated to temperatures of 600 to 1300 K without significant heating of the carrier gas. This eliminated secondary reactions from occurring. Different particle temperature profiles were obtained by varying particle residence time. A weakness of the experiments conducted by Chen is that particle temperatures were not measured directly, but rather estimated using an energy balance. Therefore, it is expected that there is significant error in Chen's reported particle temperature histories.

Table I.2**Ultimate Analysis of Coals Used by Chen***

Coal	Volatile Matter Content (dry wt.%)	Ash (dry wt.%)	% C (daf)	% H (daf)	% N (daf)	% S (daf)	% O (daf)
Dietz	39.90	3.90	69.50	5.00	0.97	0.40	24.10
Illinois #6	37.50	12.90	74.10	5.30	1.52	5.70	13.40
Pittsburg #8	34.70	12.60	82.50	5.60	1.77	1.60	8.50
Lower Kittaning	17.10	19.30	88.70	5.00	1.72	2.50	2.10

* Adapted From Chen⁵²

Chen performed 8 pyrolysis runs on each coal with a wall temperature of 1840 K and a heating rate of $\sim 10^4$ K/s.⁵² Each run was conducted at a different residence time to achieve different particle temperatures. Appendix E contains tables listing the residence time and estimated particle temperature history of each condition. Effluent Non-condensable (light gas) gases were quantified by non-dispersive infrared (NDIR) and chemiluminescence analyses, and gas chromatography as described in Chen's thesis.

Figure H.7 illustrates the light gas release trends of the 4 PETC coals. Notice that Figure H.7 differs from Figure H.1 since Chen's data is on a *dry ash free* basis. Figure H.1 includes the initial release of moisture. Furthermore, the pyrolysis experiments of Chen and Solomon differ in that Solomon used TG-FTIR technology while Chen ran a separate experiment for each residence time. In light of the differences in the experimental conditions of Solomon's and Chen's experiments, the rank dependence of light gas release is remarkably similar. Figure H.7 shows clearly that light gas release decreases with increasing coal rank. At is also evident from figure H.7 that the ultimate light gas yield has not yet been reached in Chen's experiments. This conclusion is drawn from the fact that light gas release appears to be increasing rapidly as residence time (or temperature) increases, particularly between the 87 and 89 millisecond conditions.

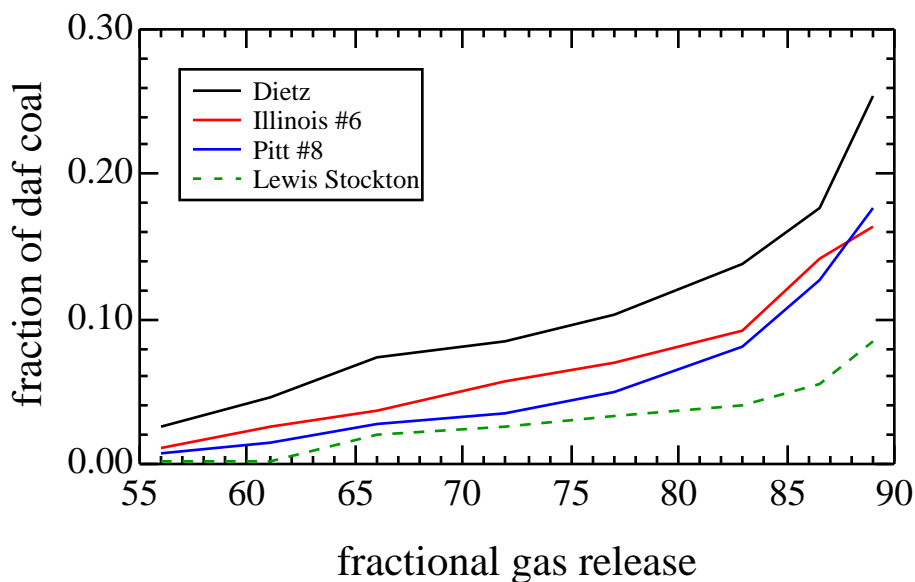


Figure I.7. Comparison of the light gas release of PETC coals studied by Chen.

Figure H.8 compares the H_2O content of the light gas released from the four PETC coals as a function of the fraction of total light gas released at the maximum residence time. The H_2O content of light gas appears to be inversely proportional to rank in this data set. This somewhat contradicts the trends found in Solomon's light gas data which did not appear to exhibit a strong rank dependence. The convergence of the coals to a common fractional H_2O light gas release in Chen's data is similar to that of Solomon.

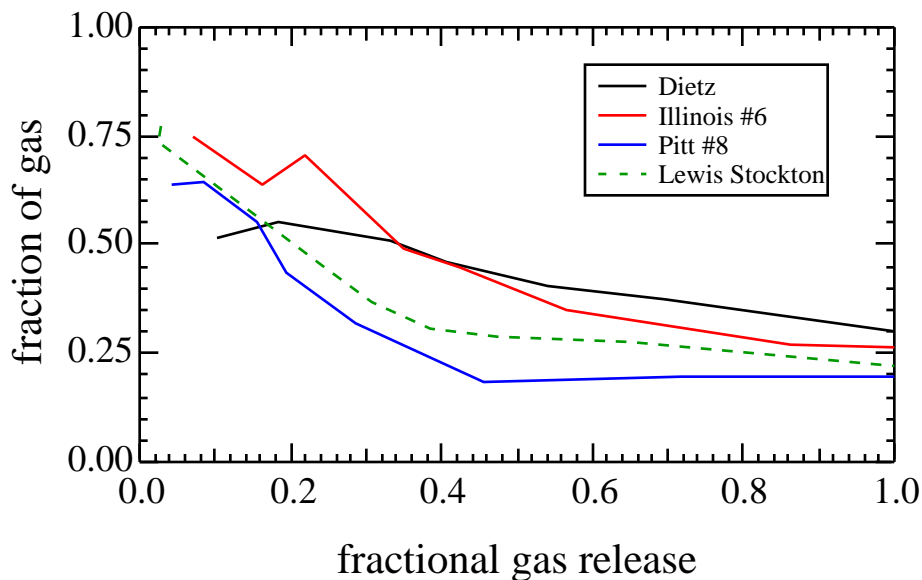


Figure I.8. Fractional release of H₂O of PETC coals studied by Chen.

Figure H.9 compares the fractional release of CO₂ of the PETC coals. The PETC suite exhibits the same trend as Arrgone premium coals. Fractional CO₂ release decreases with increasing coal rank. Also, the fractional CO₂ release appears to diminish slightly at higher residence times, as did the Argonne premium coals.

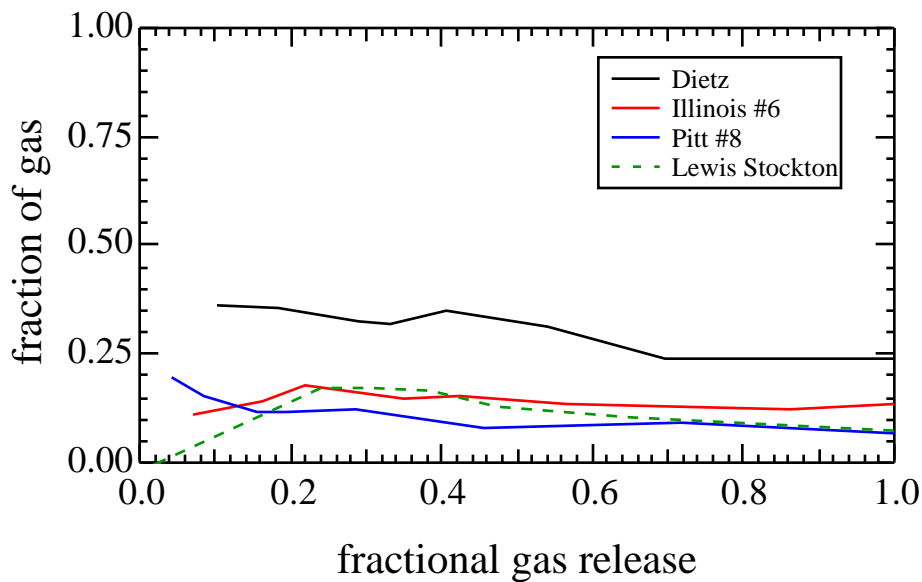


Figure I.9. Fractional release of CO₂ of PETC coals Studied by Chen.

Figure H.10 is a comparison of the fractional light gas release of CO. Fractional CO release generally appears to decrease with increasing coals rank as it did in the experiments conducted by Solomon on the Argonne premium coal suite. Fractional CO release generally increases with increasing light gas yield, but reaches a maximum at when reaching 65% of the light gas yield at the maximum residence time.

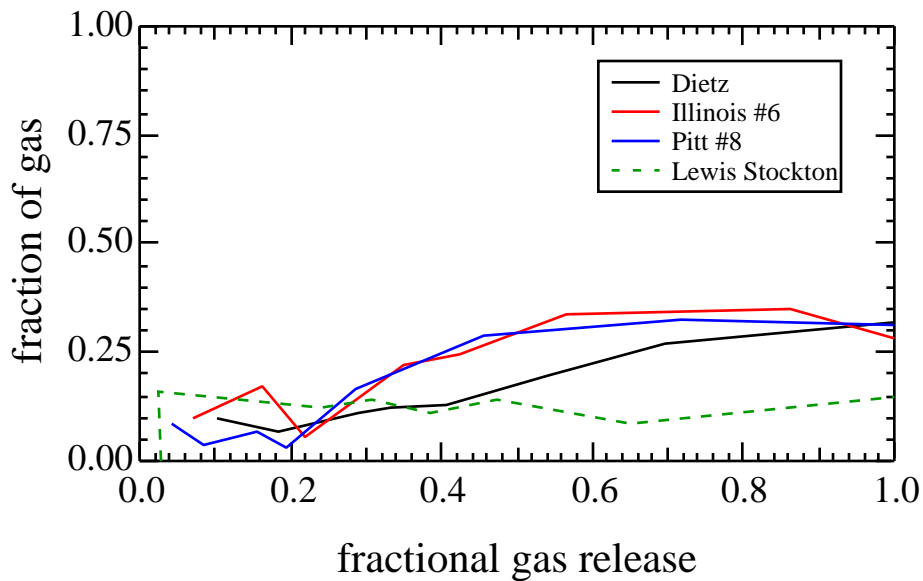


Figure I.10. Fractional release of CO of PETC coals studied by Chen.

The trend illustrated in Figure H.11 for the fractional release of CH₄ is remarkably similar to that of fractial CH₄ release of the Argonne premium coals (Figure H.5). Fractional CH₄ release increases with increasing coal rank.

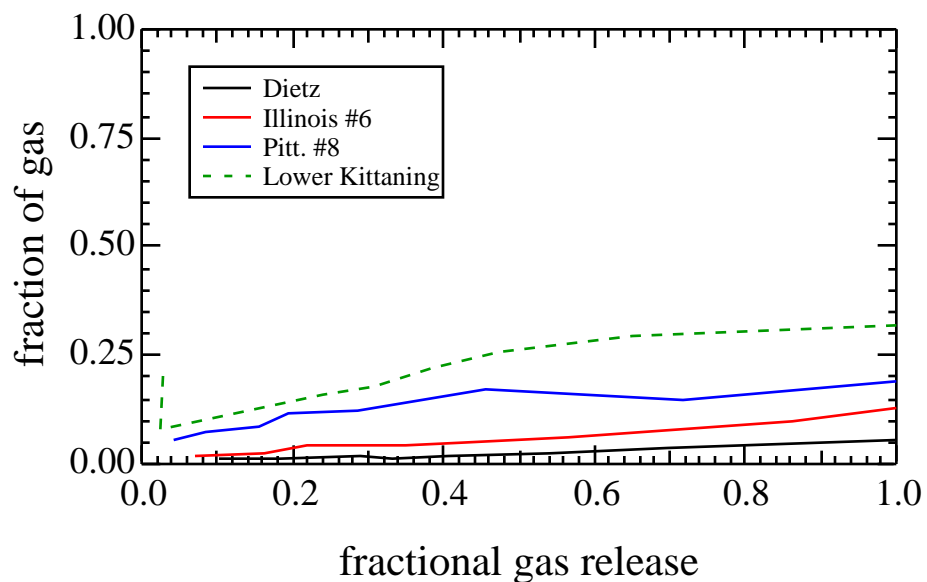


Figure I.11. Fractional release of CH_4 of PETC coals studied by Chen.

Figure H.12 compares the fractional release of C_2H_4 of the 4 PETC coals. Although the fractional release of C_2H_4 of the PETC coals exhibited the same rank dependence as the Argonne coals (higher rank, higher C_2H_4), an order of magnitude larger fractional release of C_2H_4 was observed in the pyrolysis experiments conducted on the PETC coals.

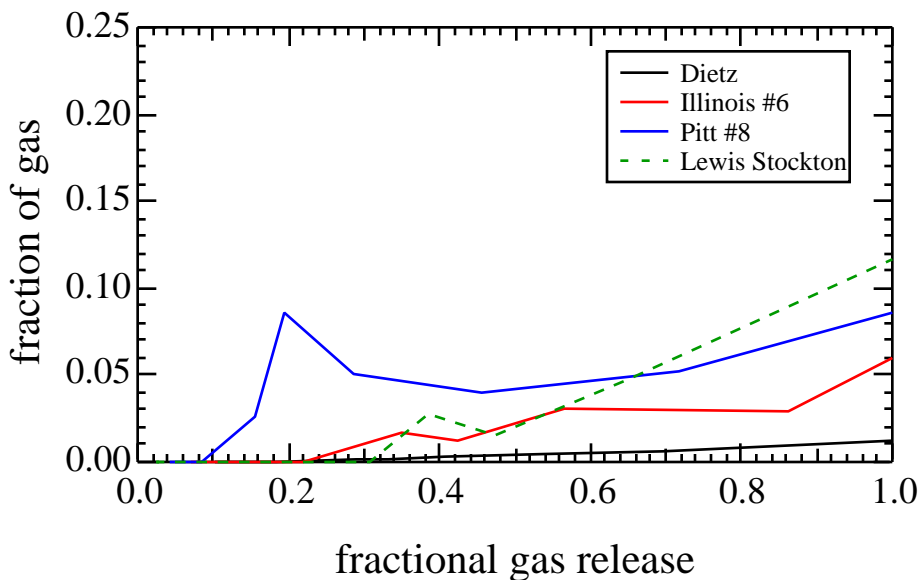


Figure I.12. Fractional release of C_2H_4 of PETC coals studied by Chen.

Small amounts of other light hydrocarbons gases are also released during devolatilization. The fractional release of the other light hydrocarbons is compared in Figure 13. It appears that a light gas released from higher rank coals contains a larger fraction of “other light hydrocarbons” than lower rank coals.

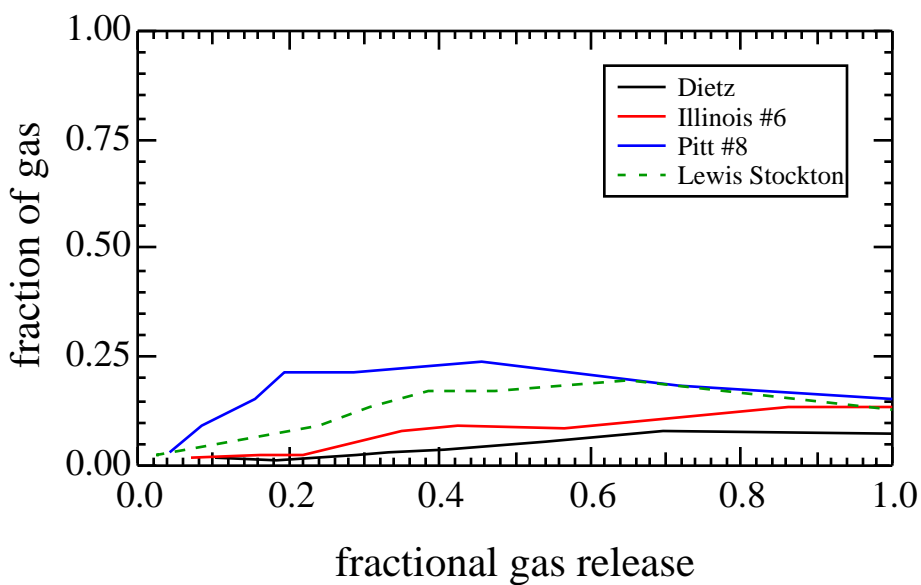


Figure I.13. Fractional release of other light hydrocarbons of PETC coals Studied by Chen.

Light gas Data from Currie Point Pyrolyzer

Xu and Tomita conducted pyrolysis experiments of 17 coals of varying ranks in a Currie Point pyrolyzer.²⁸ The coal samples were rapidly heated to 1037 K and held at that temperature for 4 seconds. The procedure used was very similar to the method used in determining ASTM volatile matter content. The elemental composition and ASTM volatile matter contents of the coals studied by Xu and Tomita are given in Table 4.7. The overall mass release results of the coals pyrolyzed by Xu and Tomita are very similar to the ASTM volatile matter content. Figure H.14 illustrates the rank dependence of total light gas release.

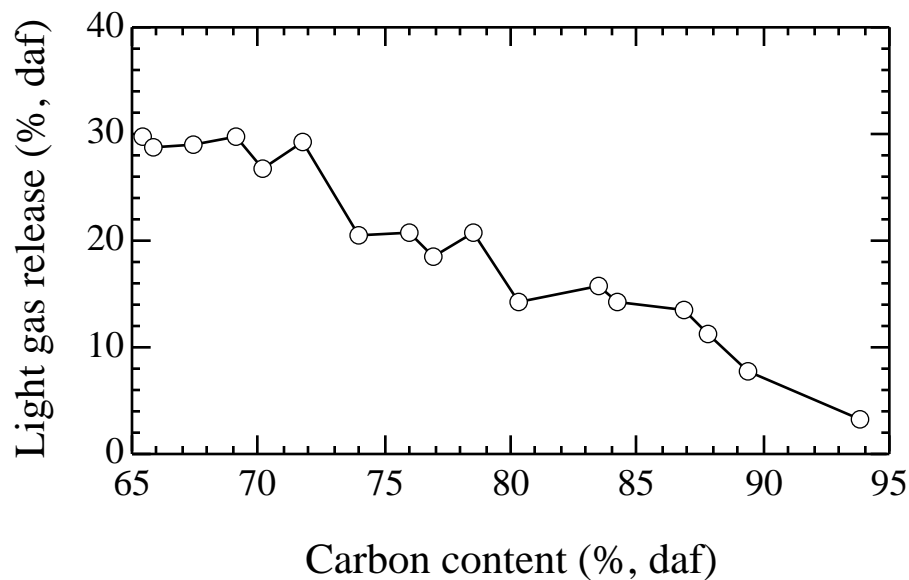


Figure I.14. Light gas release versus the carbon content of the parent coal.

Figures H.15 to H.19 show the rank dependence of the composition the light gas released during Xu and Tomita's pyrolysis experiments.

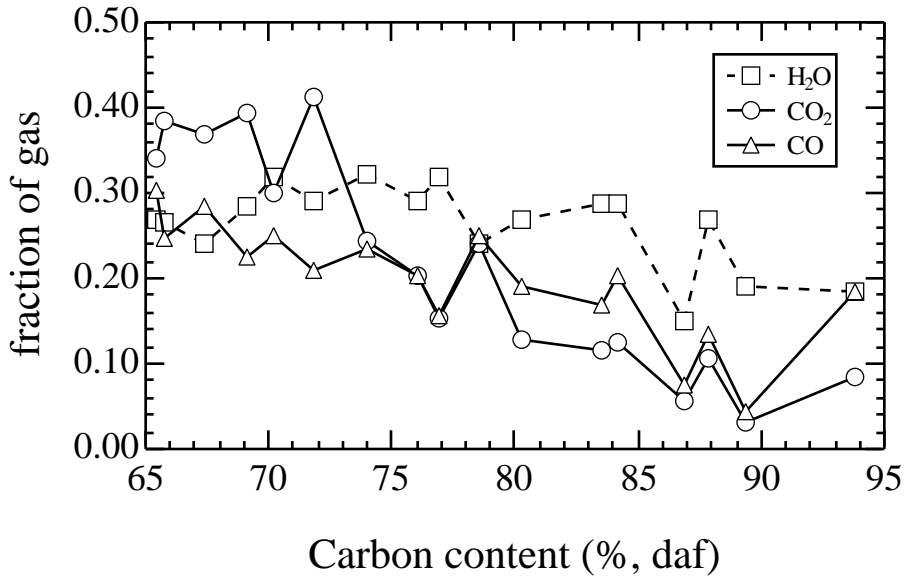


Figure I.15. Comparison of H₂O, CO₂, and CO fractional light gas release of coals studied by Xu and Tomita.

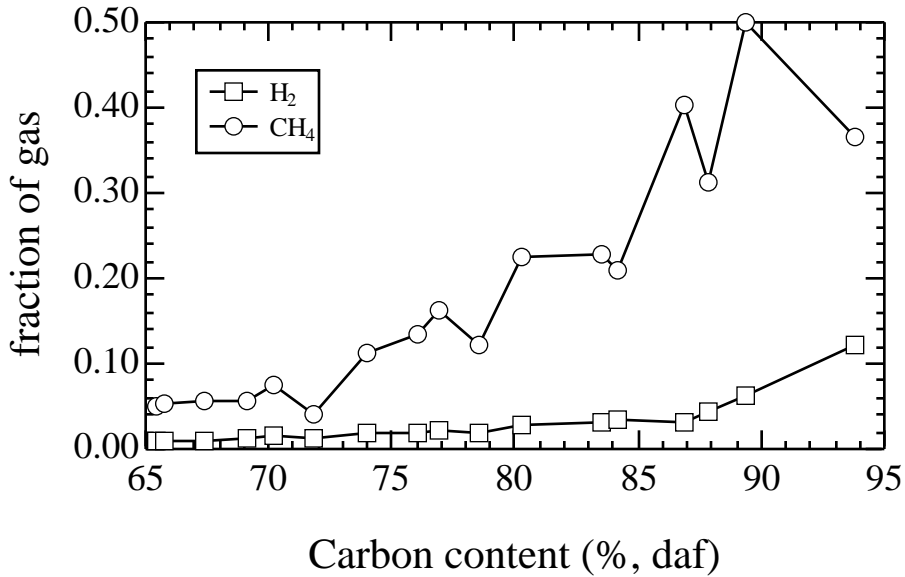


Figure I.16. Comparison of H₂ and CH₄ fractional light gas release of coals of various rank.

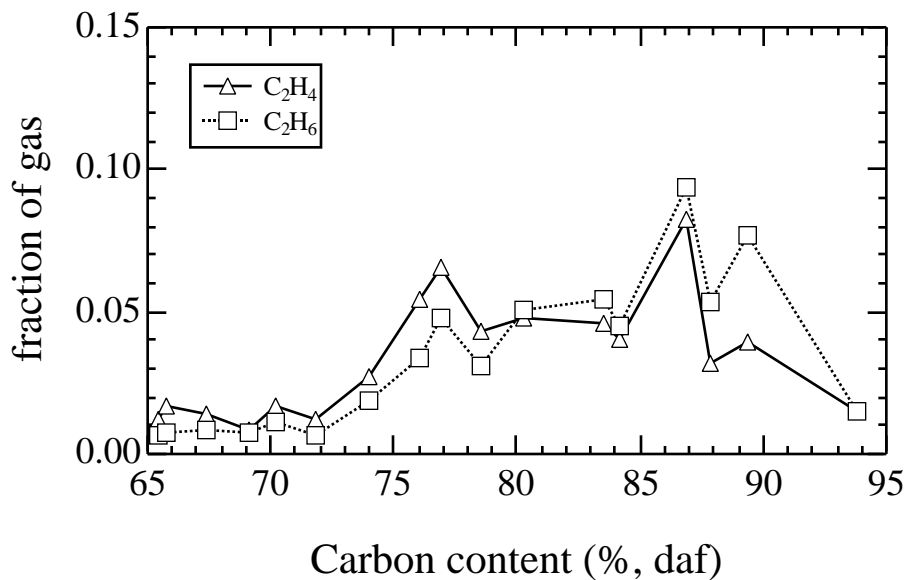


Figure I.17. Comparison of C₂ hydrocarbon fractional light gas release of coals of various rank.

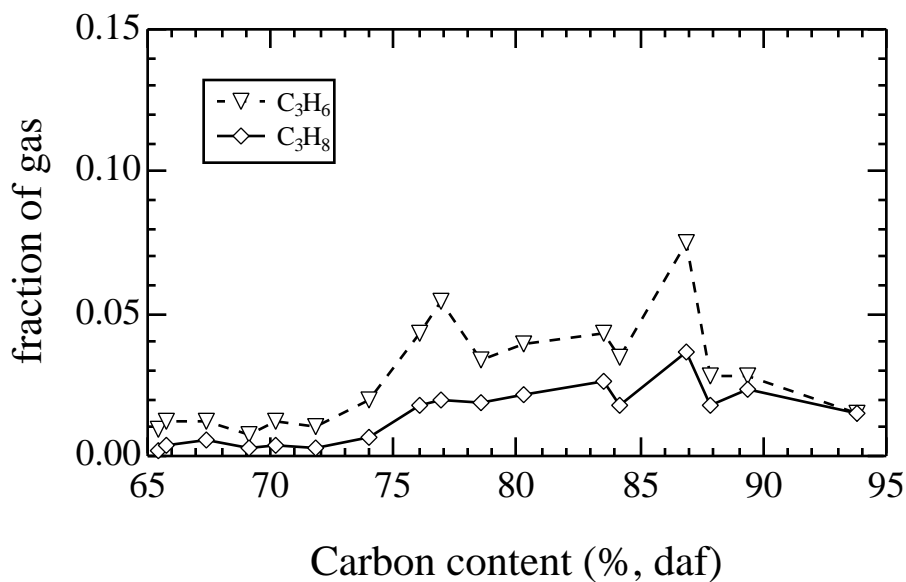


Figure I.18. Comparison of C₃ hydrocarbon fractional light gas release of coals of various rank

In general, the light gas composition of pyrolysis products of Xu and Tomita's experiments compare well with the final light gas composition of the experiments conducted by Chen and Solomon. A few discrepancies exist between Xu's results and

Somolon's work. The same discrepancies exist between the work of Chen and Solomon as well. Two possible explanation for the discrepancies are: (i) Solomon's data have not been corrected appropriately to a dry, ash, free basis; (ii) the Argonne premium coals used by Solomon have never been exposed to oxygen as the other coal suites have.

Conclusions

The following important conclusions were drawn from this analysis: (i) light gas is primarily composed of water, carbon dioxide, carbon monoxide, and methane; (ii) other minor constituents include hydrogen, nitrogen and sulfur containing gases, and low molecular weight olifins and parrifins; (iii) the composition of light gas is a function of rank (low rank coals contain more carbon oxides while high rank coal contain more hydrocarbons); (iv) the evolution rates of individual species are relatively insensitive to coal type; and (v) the composition of light gas seems to correlate well with the extent of light gas release, and is relatively insensitive to heating rate. Based on these conclusions, it appears that using a look-up table to estimate light gas composition would be appropriate.

Appendix J: Light Gas Look-Up Table

A look-up table is used in the light gas submodel to determine the composition of the light gas released from a coal as a function of the extent of light gas release. Table J.1 lists the reference coals by number. Table J.2 lists the measured extent of total light gas release for each coal (the x values of the ordered pairs). Tables J.3 - J.6 list the measured mass fractions of H₂O, CO₂, CH₄, and CO (the y values of the ordered pairs) which correspond to extent of light gas release given in Table J.2.

Table J.1
Reference Coals Used in Look-Up Table

Reference No.	Coal
1	Lower Kittaning (Chen)
2	Pocahontas no. 3 (ANL)
3	Upper Freeport (ANL)
4	Pittsburgh (Chen)
5	Lewis Stockton (ANL)
6	Utah Blind Canyon (ANL)
7	Illinois no. 6 (ANL)
8	Illinois no. 6 (Chen)
9	Wyodak (ANL)
10	Beulah Zap (ANL)
11	Dietz (Chen)
12	PSOC 1448 (Serio and Coworkers)

Table J.2
Extent of Total Light Gas Release

Ref. No.	1	2	3	4	5	6	7	8	9	10	11	12
1	0.000	0.040	0.110	0.140	0.210	0.270	0.340	0.675	0.900	1.000	0.000	0.000
2	0.000	0.161	0.442	0.663	0.777	0.874	0.921	0.967	1.000	0.000	0.000	0.000
3	0.000	0.022	0.200	0.430	0.526	0.640	0.787	0.875	0.927	0.955	1.000	0.000
4	0.000	0.040	0.120	0.150	0.230	0.290	0.360	0.680	0.900	1.000	0.000	0.000
5	0.000	0.018	0.058	0.210	0.417	0.572	0.696	0.778	0.821	0.883	0.932	1.000
6	0.000	0.052	0.144	0.291	0.498	0.639	0.746	0.859	0.925	0.949	0.966	1.000
7	0.000	0.063	0.178	0.330	0.506	0.612	0.706	0.813	0.895	0.940	1.000	0.000
8	0.000	0.040	0.120	0.150	0.230	0.290	0.360	0.680	0.900	1.000	0.000	0.000
9	0.000	0.061	0.146	0.374	0.535	0.622	0.714	0.800	0.883	0.931	0.964	1.000
10	0.000	0.034	0.087	0.179	0.316	0.472	0.585	0.694	0.777	0.872	0.935	1.000
11	0.000	0.040	0.120	0.160	0.250	0.310	0.370	0.680	0.900	1.000	0.000	0.000
12	0.000	0.020	0.055	0.170	0.313	0.434	0.546	0.716	0.874	0.935	0.973	1.000

Table J.3
Mass Fraction H₂O

Ref. No.	1	2	3	4	5	6	7	8	9	10	11	12
1	0.772	0.772	0.738	0.455	0.371	0.304	0.290	0.273	0.218	0.218	0.000	0.000
2	0.699	0.632	0.299	0.269	0.247	0.249	0.236	0.225	0.226	0.000	0.000	0.000
3	0.000	0.000	0.350	0.297	0.301	0.299	0.284	0.291	0.306	0.297	0.283	0.000
4	0.636	0.636	0.646	0.550	0.436	0.320	0.186	0.199	0.195	0.195	0.000	0.000
5	1.000	0.983	0.754	0.488	0.413	0.385	0.373	0.382	0.377	0.362	0.367	0.348
6	0.665	0.636	0.604	0.508	0.435	0.409	0.383	0.362	0.351	0.343	0.342	0.339
7	0.763	0.737	0.698	0.572	0.527	0.470	0.438	0.411	0.411	0.396	0.378	0.000
8	0.748	0.748	0.637	0.704	0.490	0.446	0.348	0.268	0.266	0.266	0.000	0.000
9	0.000	0.000	0.385	0.461	0.396	0.369	0.344	0.323	0.292	0.277	0.266	0.257
10	0.000	0.000	0.197	0.267	0.260	0.333	0.361	0.369	0.346	0.306	0.285	0.267
11	0.521	0.521	0.550	0.523	0.511	0.460	0.414	0.388	0.313	0.313	0.000	0.000
12	0.000	0.000	0.291	0.335	0.264	0.271	0.261	0.211	0.171	0.160	0.153	0.149

Table J.4
Mass Fraction CO₂

Ref. No.	1	2	3	4	5	6	7	8	9	10	11	12
1	0.000	0.000	0.000	0.174	0.174	0.167	0.129	0.102	0.071	0.071	0.000	0.000
2	0.259	0.234	0.113	0.086	0.097	0.109	0.116	0.118	0.122	0.000	0.000	0.000
3	0.333	0.327	0.070	0.052	0.057	0.060	0.059	0.062	0.066	0.080	0.115	0.000
4	0.194	0.194	0.152	0.117	0.116	0.122	0.081	0.092	0.065	0.065	0.000	0.000
5	0.000	0.000	0.000	0.122	0.103	0.086	0.083	0.082	0.085	0.086	0.093	0.128
6	0.332	0.318	0.165	0.141	0.120	0.108	0.105	0.119	0.120	0.122	0.125	0.130
7	0.229	0.221	0.125	0.090	0.070	0.073	0.083	0.133	0.132	0.130	0.147	0.000
8	0.111	0.111	0.142	0.175	0.149	0.155	0.136	0.122	0.133	0.133	0.000	0.000
9	0.980	0.984	0.550	0.345	0.317	0.285	0.286	0.277	0.273	0.264	0.254	0.255
10	0.993	0.989	0.786	0.572	0.519	0.416	0.375	0.345	0.335	0.320	0.303	0.299
11	0.363	0.363	0.353	0.325	0.321	0.350	0.318	0.251	0.249	0.249	0.000	0.000
12	1.000	0.983	0.448	0.179	0.104	0.090	0.104	0.151	0.166	0.160	0.158	0.154

Table J.5
Mass Fraction CH₄

Ref. No.	1	2	3	4	5	6	7	8	9	10	11	12
1	0.203	0.203	0.078	0.160	0.180	0.219	0.258	0.294	0.320	0.320	0.000	0.000
2	0.041	0.037	0.388	0.389	0.359	0.332	0.323	0.307	0.299	0.000	0.000	0.000
3	0.667	0.655	0.420	0.454	0.444	0.419	0.382	0.353	0.331	0.321	0.306	0.000
4	0.055	0.055	0.073	0.088	0.116	0.124	0.170	0.150	0.189	0.189	0.000	0.000
5	0.000	0.000	0.188	0.195	0.234	0.243	0.224	0.210	0.200	0.186	0.177	0.167
6	0.000	0.000	0.110	0.155	0.176	0.172	0.185	0.173	0.163	0.159	0.156	0.151
7	0.000	0.000	0.075	0.136	0.159	0.178	0.174	0.157	0.143	0.141	0.132	0.000
8	0.020	0.020	0.026	0.042	0.045	0.049	0.064	0.100	0.128	0.128	0.000	0.000
9	0.000	0.000	0.000	0.029	0.048	0.067	0.069	0.072	0.069	0.066	0.063	0.061
10	0.000	0.000	0.000	0.000	0.035	0.050	0.061	0.058	0.057	0.053	0.049	0.046
11	0.010	0.010	0.011	0.016	0.011	0.021	0.023	0.035	0.060	0.060	0.000	0.000
12	0.000	0.000	0.216	0.262	0.362	0.327	0.307	0.250	0.203	0.189	0.182	0.177

Table J.6
Mass Fraction CO

Ref. No.	1	2	3	4	5	6	7	8	9	10	11	12
1	0.000	0.000	0.157	0.121	0.141	0.112	0.139	0.085	0.145	0.145	0.000	0.000
2	0.000	0.000	0.000	0.057	0.097	0.109	0.124	0.150	0.153	0.000	0.000	0.000
3	0.000	0.000	0.000	0.000	0.000	0.024	0.078	0.097	0.099	0.104	0.099	0.000
4	0.083	0.083	0.038	0.066	0.032	0.168	0.286	0.324	0.313	0.313	0.000	0.000
5	0.000	0.000	0.000	0.000	0.055	0.091	0.124	0.131	0.142	0.171	0.168	0.162
6	0.000	0.000	0.000	0.028	0.093	0.129	0.142	0.162	0.181	0.191	0.193	0.195
7	0.000	0.000	0.000	0.075	0.099	0.122	0.139	0.133	0.148	0.167	0.177	0.000
8	0.101	0.101	0.173	0.054	0.219	0.247	0.335	0.349	0.280	0.280	0.000	0.000
9	0.000	0.000	0.055	0.115	0.151	0.168	0.172	0.200	0.236	0.264	0.287	0.298
10	0.000	0.000	0.000	0.133	0.142	0.150	0.150	0.173	0.206	0.265	0.307	0.331
11	0.096	0.096	0.066	0.113	0.123	0.130	0.200	0.281	0.334	0.334	0.000	0.000
12	0.000	0.000	0.000	0.084	0.078	0.115	0.130	0.191	0.262	0.294	0.311	0.322

